A Deterministic Discrete Stage-Structured SIR Model with Indirect Transmission

by
Abby Anderson

A Thesis
presented to
The University of Guelph

In partial fulfilment of requirements
for the degree of
Master of Science
in
Mathematics & Statistics

Guelph, Ontario, Canada

ABSTRACT

A DETERMINISTIC DISCRETE STAGE STRUCTURED
SIR MODEL WITH INDIRECT TRANSMISSION

Abby Anderson
University of Guelph, 2023

Advisor:
Dr. Hermann Eberl

In this thesis we propose a deterministic discrete stage-structured SIR model with indirect transmission. We show that the model is well-posed using fundamental Ordinary Differential Equations (ODE) theory. We derive a sufficient but not necessary condition for stability of the disease-free equilibrium (DFE) using Gershgorin's Theorem. We calculate the basic reproduction number, $\mathcal{R}_0$, using the Next Generation Method. In our numerical simulations, we further explore the stability of the DFE via Gershgorin's Theorem and the eigenvalues of the Jacobian matrix evaluated at the DFE. Additionally, we establish $\mathcal{R}_0$ as a sharp criterion for disease persistence and establish a relationship between the model's transience and $\mathcal{R}_0$. We compare the stage-structured SIR model against its non-stage-structured counterpart, demonstrating that the latter gives a more refined description of disease dynamics. We conclude by proposing a model for the spread of *Nosema ceranae* in the Western honey bee which includes discrete stage-structure and indirect transmission.

Acknowledgements

I offer my personal thanks to Michael Pupulin, Nasim Muhammad, and Alysha Cooper for their advice and consultation on various aspects of my thesis.

Contents

List of Tables

List of Figures

Chapter 1

Introduction

In this chapter we provide the necessary background for this research. We begin by discussing the motivation for this work, highlighting the relevant biological information for the problem being studied. Then, we discuss the mathematical modelling concepts used in our model. We use this background to develop inclusion and exclusion criteria for a subsequent literature review. Drawing from the results of the literature review, we clearly define the objective of our research. The introduction concludes with an outline of this thesis.

1.1 Motivation

The motivation for this research began with the Western honey bee, *Apis mellifera*. Humanity has a vested interest in protecting Western honey bee populations. In 2018, honey sales contributed $ 278 million dollars to Canadian agriculture, a record-breaking high in this industry [6]. *A. mellifera* play important roles in global crop production and trade, variety and nutritional value of the human diet, and sustaining biodiversity of wild flowering plants [7]. The Western honey bee is categorized as an "eusocial insect", meaning their colonies demonstrate an advanced level of social organization in which only one female (the queen) produces all other bees in the colony (the offspring) which do not reproduce, but rather, cooperate in caring for the younger individuals (called brood). In a colony, individuals are categorized through a caste system, with the three castes of a colony comprising the queen, the workers, and the drones. For worker bees, the division of labor (which involves tasks such as food/water collection, building hive combs, caring for the queen, brood-rearing, etc.) is correlated to an individual's age, a phenomenon referred to as temporal polyethism [50]. As explained in [50], "young workers perform brood-nest associated tasks...middle-aged bees

typically perform food processing, nest construction, and guarding...older bees progress to foraging outside the nest for food".

In 2006 large numbers of colony losses were reported by beekeepers worldwide [28]. There are many factors for such drastic losses, including disease, viruses, mites, pesticides, stress from hive management, and habitat loss. The cause of these losses likely involves a convergence of these factors. One pathogen of concern is *Nosema ceranae*, the pathogen responsible for the spread of nosema disease, called nosemosis, in *A. mellifera*. Detection of *N. ceranae* was first reported in Europe, in 2006 [15]. Since then, *N. ceranae* infection has spread throughout the world, becoming increasingly virulent in some areas [11, 12]. *N. ceranae* is an obligate intracellular spore forming parasite that infects the midgut epithelial cells of *A. mellifera*. Most agree that infection impairs digestion, nutrient absorption, and induces energetic stress in worker bees [12, 15, 29, 56]. Some reports argue that infection with *N. ceranae* increases honey bee mortality, but if it does and to what degree is highly contested [5, 43]. Most agree that transmission occurs indirectly through comb cleaning and directly through trophallaxis (food exchange between individuals via the exchange of regurgitated liquids) [15, 51]. While multiple transmission routes have been considered when modelling *N ceranae* [40], there is literature that supports indirect transmission as the primary route for Nosemosis [29, 56]. However, there is still much uncertainty surrounding the degree to which *N. ceranae* proliferates in its host. Proliferation of *N. ceranae* in *A. mellifera* depends on a multitude of factors, including nutritional availability, initial dosage of spore inoculum, and days post inoculation (dpi) [5]. Studies have found much variation in spore counts of individual bees infected with *N. ceranae*, with a proliferation plateau range spanning from 10 to 25 million spores per bee [5]. Due to the amount of variation across observational studies, some suggest the level of infection at which *N. ceranae* proliferation attains a maximum is different between individual bees, colonies, apiaries, or geographical regions of the world [5]. Current treatment strategies for Canadian beekeepers include the use of the antibiotic fumagillin (Fumidil B), disinfection of combs and equipment with acetic acid vapors [19, 27]. As a relatively new pathogen of study, there is much to be learned on aspects of its biology, pathology, and disease dynamics [12]. With so many questions surrounding *N. ceranae*, innovative modeling is of the utmost importance.

Viewing nosemosis as a disease that spreads throughout a population, we turn to Susceptible-Infected-Recovered (SIR) models for innovation. We will incorporate indirect disease transmission since individual bees in a colony need not come in direct contact with each other for the disease to spread. There are many SIR models for sexually transmitted diseases and

general disease structure [16, 30, 32, 34], but very few regarding *N. ceranae*. In a recent review article of honey bee disease modeling [4], there were four SIR *N. ceranae* models [2, 5, 40, 43]. All these models have honey bee polyethism and further subdivision into infected and susceptible groups. The difference in these models lies in the transmission routes. Betti et. al uses direct transmission [2], in both Comper & Eberl and Petric et. al indirect transmission is used [5, 43], Muhammad & Eberl use both direct and indirect tranmission [40]. One thing these studies do not incorporate is the spore count variation across individual bees. Thus, we take a new approach by including variations in the level of infection in the model structure, which we call stage-structured transmission. In doing this, we hope to gain a deeper understanding of nosemosis spread in *A. mellifera* colonies. In combination with a SIR framework, this leads to a SIR compartmental model which uses indirect transmission and stage-structure. While our original research question was: "What is known about modelling *N. ceranae* spread in *A. mellifera* using SIR model structure?", we learned that the more basic question "What is known about SIR modelling with indirect transmission *and* stage structure?" was also lacking in answers. Thus, while the motivation for this thesis is modelling *N. ceranae* in the Western honey bee, the research presented is primarily concerned with an innovative structure for SIR models. In this thesis we aim to develop this building block so that this structure could be applied to modelling a multitude of diseases.

In the next section we outline the mathematical concepts related to the derivation of our model. These concepts are necessary in clearly comparing and contrasting our model framework with other research.

1.2 Background

This thesis introduces a deterministic discrete stage-structured SIR model with indirect transmission. In this section, we will cover what each of these terms means in the context of this research.

The core principle of compartmental modelling is rather self explanatory; individuals in a population are divided into distinct groups or classes, called compartments. Also important are the "assumptions about the nature and time rate of transfer from one compartment to another" [3]. In an SIR model, individuals are divided across three such compartments, labelled as susceptible (S), infected (I), and recovered (R). In each SIR compartment, one typically assumes individuals are identical in their status with respect to the disease being

studied [3]. Generally, one can think of susceptible individuals as those who lack immunity to the infectious agent and are likely to be infected if exposed [3]. Infected individuals are then those who are currently infected and can spread this infection to susceptible individuals [3]. Recovered individuals are those who have passed through both the susceptible and infectious compartments and thus have immunity to the infection (which may or may not be temporary), during which time they do not affect transmission dynamics when coming into contact with susceptible or infected individuals [3]. Note that in some models, the recovered compartment also includes individuals that are removed from the population as a result of death, natural or otherwise. The movement of an individual in a SIR system is typically starting in S, then moving from S to I, and ending by moving from I to R. This movement is visualized in Figure 1.1.

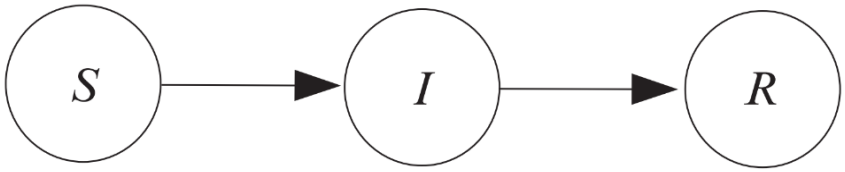

Figure 1.1: A flow diagram for a basic SIR model as illustrated in [3]. The compartments S, I, and R denote susceptible, infected, and recovered individuals, respectively. The movement is from S to I then to R.

The two main types of compartmental models are deterministic and stochastic. As it relates to the epidemic process, a deterministic model assumes "the behaviour of a population is determined completely by its history and by the rules which describe the model" [3]. In comparison, stochastic models [as it relates to the epidemic process] use probabilistic concepts which give way to a distribution of possible behaviours [3]. Mathematically, deterministic models are often formulated as differential equations, but can also be formulated as difference equations if time is discrete [3]. Depending on the model assumptions, SIR models may have equations for each S, I, and R compartment, or may only need equations for compartments S and I. The latter is typically a result of assuming that individuals only leave the population through death. This means the R equation is decoupled from the S and I equations present in the model, and can therefore be removed as it does not affect the dynamics of the S or I compartments [3]. There are many variations in SIR modelling. Before introducing our modifications of the basic SIR model, we must clearly outline how diseases spread.

Generally an infectious disease is the result of interactions between agent, host, and

environment [13]. The CDC clarifies that in epidemiology, a chain of infection occurs, "when the agent leaves its reservoir or [a] host through a portal of exit, is conveyed by some mode of transmission, and enters through an appropriate portal of entry to infect a susceptible host" [13]. A reservoir is defined as the "habitat in which the agent normally lives, grows, and multiplies", a portal of exit is defined as the "path by which a pathogen leaves its host", and a portal of entry is defined as the "manner in which a pathogen enters a susceptible host" [13]. The mode of transmission involves a more thorough definition since there are multiple forms. In their article, the CDC outlines indirect transmission as including transfer from reservoir to host via either suspended air particles, vehicles, or vectors [13]. The first of the three methods, airborne, is straightforward, indicating an infectious agent is carried, by dust or droplet nuclei, which are suspended in air [13]. The second, vehicular transmission, involves inanimate objects that can either passively carry a pathogen or provide an environment allowing for the growth of the pathogen/toxin [13]. Finally the third, vector-borne, indicates a vector (typically a pest such as mosquitoes, fleas, ticks, etc.) has carried the infectious agent via purely mechanical means [13].

We will begin by defining indirect transmission. While both direct and indirect modes of transmission have been studied in *N. ceranae* modelling (see Section 1.1), we only consider indirect transmission. The main source of indirect transmission for *N. ceranae* is from comb cleaning. Following the definition from the CDC above, for *N. ceranae*, the agent is the *N. ceranae* spores. The reservoir is the contaminated (via the presence of feces laden with *N. ceranae* spores) hive combs. The portal of exit of the spores from the reservoir to a new uninfected bee is ingestion by said bee. In *N. ceranae*, transmission is vehicular, since the pathogen simply exists in the contaminated feces, which sits on the surface of the inside of the hive. Due to the cyclical nature of *N. ceranae*'s indirect transmission, the chain of infection as defined by the CDC can be more confusing than enlightening. Typically in mathematical modelling of indirectly transmitted diseases, the environmental reservoir is taken to be the inanimate source from which susceptible individuals come into contact with the pathogen. Examples of such sources include (but are not limited to) water, food, soil, and objects (like straws, toothbrushes, clothing, etc.) that have been contaminated by the presence of the pathogen. Note that in this mathematical framework, the disease is not necessarily growing in its reservoir in a biological sense. That is, the pathogen which causes the infection may or may not be going through biological processes such as mitosis to grow. For example, in diseases such as nosemosis and COVID-19, the pathogen multiplies in the reservoir because individuals deposit more pathogens as more of the population becomes

infected. The pathogens are not able to proliferate without a host. In this sense, the pathogen is deposited into the reservoir and then remains there, possibly losing viability. Hence, the pathogen is "growing" in the sense that the amount of bacteria in the environmental reservoir is increasing in size, but not in the sense that biological processes are at play. While the model presented in this thesis was motivated by *N. ceranae*, it is not technically an nosemosis disease model. The essence of what indirect transmission means in our model is that there are pathogens existing in the environment with which a susceptible individual comes into contact. Thus, while the CDC article in [13] defines indirect transmission as including airborne, vehicleborne, and vector-borne transmission, we only use vehicleborne in our definition of indirect transmission. In vector-borne transmission, the vector has an active role to play in disease spread and its dynamics must be taken into account in the model. We do not do this in our research. Additionally, for airborne transmission, one could argue that most airborne (viral at least) disease transmission requires susceptible and infected individuals to be in close proximity at the same time, which is more suitably modeled by direct transmission.

The last term needing clarification is stage-structure. By using stage-structure we attempt to refer to the multiple infected compartments in the model. That is, the infectious compartments of the model are stage-structured. These compartments arise from the assumption that an increase in an individual's infection is a result of increased pathogens in their system, typically due do the proliferation of pathogen cells inside the body. Thus, in our model, the stage-structure is based on the viral load of the disease, rather than any population dynamics of the species in question. Nomenclature for this assumption is complicated because it is not standardized. In HIV/AIDS modelling, stage structure models are also referred to as Markov chain, and/or staged-progression (SP) models. In this context, stage-structure is explained (in [22]) as meaning; "infected individuals progress through a series of infection stages, with the infectiousness of [an individual] depending upon [its] current disease stage". It is important to note however, that in HIV/AIDS modelling the infectiousness is not necessarily proportional to the current disease stage. That is, being in a higher stage does not always indicate that infectiousness has also increased. The progression is outlined in [22] as "[individuals are] highly infectious in the first few weeks after their own infection, then having low infectivity for many years, and finally becoming gradually more infectious as their immune system breaks down and they progress to AIDS". Thus in many HIV/AIDS models, the relationship between an individual's infectiousness and disease stage is inverted; the lowest/earliest disease stage has the greatest infectiousness, and the higher

(in compartmental number or elapsed time since infection) disease stages have lower infectiousness. There are many HIV/AIDS models that have this structure. Examples include [16, 17, 22, 32, 34]. However, in the context of ecological disease modelling, particularly models of predator-prey systems and/or pest control/management, stage-structure has a different meaning. In these contexts, the word stage often indicates the stage of life of the species in question, rather than the progression stage of the disease. For example, in many infectious predator-prey models, disease is introduced either in the predator or prey population, and stage-structure is included in the remaining population or multiple populations. Frequently this stage-structure is introduced as dividing a population into immature and mature individuals. Hence, such models would be more appropriately called age-structure models.

With a thorough understanding of the mathematical background for our model, we can now discuss the literature review.

1.3 Literature Review Set Up

In this thesis, scoping review methodology was modified to conduct a literature review. In this section, we first cover background information relating to scoping review methodology, then outline which part(s) of the methodology we changed to suit our research goals, and give a general overview of the reviewed literature.

A scoping literature review is a type of literature review which is most commonly used to either "explore the breadth or extent of the literature, map and summarize the evidence, and inform future research" [36]. Information relevant to the scoping review's methodology is preceded by a comprehensive introduction which covers all main elements of the topic under review [36]. However, scoping reviews are exploratory in nature, and thus it is unrealistic nor is it expected that the background covers the full extant of knowledge in the area under review [36]. Often for this type of literature review, one is interested in answering the question, "What is known about X?", where X is the topic of interest [36]. Typically, a scoping review is performed by at least two or more reviewers independently [36]. A scoping review will typically begin with development of a title which is informative and gives clear indication of the topic of the scoping review [36]. Next, the question of the scoping review is defined [36]. From the scoping review question, reviewers develop key words and phrases which are then turned into a search query [36]. This search query will be used in data bases which are relevant to the topic in question [36]. Before using a search query, reviewers outline

the inclusion and exclusion criteria used to screen sources retrieved from running the query [36]. Following the definition of inclusion and exclusion criteria, a search strategy must be developed [36]. The JBI Manual for Evidence Synthesis recommends a three step search strategy [36]. In the first step, the search query is used in at least two appropriate online databases relevant to the topic [36]. In the second step reviewers analyze of the words in the title and abstract of retrieved papers, as well as any key words used to describe the articles [36]. The third step is a full-text examination of articles deemed relevant in the title and abstract analysis [36]. The scoping review methodology finishes with the extraction of data, evidence analysis, and reporting of results [36].

In this thesis, our goal of the literature review was to identify whether SIR models with deterministic discrete stage-structure and indirect transmission had been posed before. A secondary goal was to understand the types of results obtained by such models, as well as how these results were obtained, so that we could use such knowledge to inform our model analysis. Thus, a scoping review framework suited such analysis. We adapted multiple aspects of the scoping review methodology so that the resulting literature review would satisfy time and resource constraints. The first change concerns the number of reviewers. In this review, only one reviewer (Abby Anderson) was required. Since we are adapting the methodology of a scoping review, it is unnecessary to develop an in-depth title, hence we simply use the phrase literature review. For this research, our review question is "What is known about deterministic discrete stage-structured compartmental disease models?". Based on the content covered in Section 1.2, inclusion criteria were the use of ordinary differential equations, deterministic structure, multiple (distinct) infective compartments, and mode of disease transmission characterized by airborne or vehicular. We also required articles be written in English. Exclusion criteria included models with stochastic structure, age-structure/age of infection or delay-structure, spatial or diffusive terms, and vector-borne transmission. The biggest modification comes from the changes made to the search strategy. The first change is that search queries were run only in one data base, MathSciNet. Doing this automatically streamlined sources such that they would only contain mathematical models. We also expect using MathSciNet will return all sources with theoretical results, rather than those demonstrating standard applications of such models to various diseases. Additionally, in the scoping review methodology, there is a "first round" of screening concerning the content of a source's title & abstract, which is then followed by a "second round" of screening concerning the content of the full text/PDF [36]. However, most of the titles and abstracts of the papers screened did not include enough details on model assumptions/structure. Thus,

rather than performing two separate rounds of screening, our search strategy was to analyze the content of the introduction, abstract, model formulation/equations. This information was sufficient to achieve the goals of the literature review (identify knowledge gaps). Some additional considerations were that papers from the International Journal of Biomathematics, Journal of Biological Systems,Acta Natura et Scientia, International Journal of Pure and Applied Mathematics, and Discrete and Continuous Dynamical Systems had limited PDF access. All searches in this review were run on November 8, 2022, with results being imported into the review software Covidence [23]. As described by their website, "Covidence is a web-based collaboration software platform that streamlines the production of systematic and other literature reviews" [23]. In this review, Covidence was used to keep records of inclusion and exclusion criteria, attach notes to articles pertaining details on why they were excluded or included, and keep track of how many and which articles passed screening. The first search query used in this review was created to answer the question, "What is known about deterministic discrete stage-structured compartmental disease models?". The query is as follows:

Query 1:

```
'Anywhere=(model OR models OR modelling) AND Anywhere=("indirect
    transmission" OR "indirectly transmitted" OR "contaminated
    environment" OR "environmental reservoir" ) AND Anywhere=("
    multi-staged infected progression" OR "staged progression" OR "
    staged disease progression" OR "stage structure" OR "stage-
    structure" OR "stage structured") '.
```

This search query gives a null result, indicating this type of model is original. To expand search results, this first query was split into the following two queries:

Query 2:

```
"Anywhere=(model OR models OR modelling) AND Anywhere=("multi-
    staged infected progression" OR "staged progression" OR "staged
     disease progression" OR "stage structure" OR "stage-structure"
    OR "stage structured") AND Anywhere=(disease OR diseases OR
    infectious OR infection OR illness OR epidemic)".
```

and

Query 3:

```
"Anywhere=(model OR models OR modelling) AND Anywhere=("indirect
```

transmission" OR "indirectly transmitted" OR "contaminated environment" OR "environmental reservoir")"

The reason for splitting query 1 into queries 2 and 3 is to ensure that all related content to our research question was also examined. This allows us to see the results and approaches in related literature, which could still be useful in informing our own research. Additionally, nomenclature for the model structure introduced in this thesis is not standardized. Thus queries 2 and 3 are also a way to ensure the null result in query 1 is truly an indication of original research, rather than a result of differences in phrasing. In the remainder of this section, we discuss the types of the model structures that arose in each query. In Section 1.4, we summarize the common results and approaches in the literature.

In the second query there were 166 results that went through the screening process. For the reasons discussed in 1.2, the inclusion criteria in title and abstract screening were models with ordinary differential equations, deterministic structure, and multiple (distinct) infective compartments. Furthermore, these infective stages must be determined by the viral load of the pathogen in the host rather than the age of the host. Generally, the model structure of results from this query were homogeneous. Many models fit into one of two categories: either the stage-structure was based on the age of infection, or stage-structure indicated the stage of the disease. Many models in the former category were predator-prey models, eco-epidemiological models, or pest management models. In papers such as [1, 49, 66] there are only disease/infectious compartments for the prey populations. In [1], stage-structure is only applied to predators, in [49] stage-structure is applied to prey, and in [66] stage-structure is used in both prey and predator populations. Conversely, papers such as [26, 60] introduce disease in the predator population only, with the prey population being divided into immature and mature populations. The latter category contained mostly HIV/AIDS models. This is because there is a clear disease progression beginning with HIV (which can continue for 8-10 years) before HIV develops into the clinical syndrome AIDS [17]. The distinct stages of this progression can be characterised by different $CD4^+$ T-cell counts and viral RNA levels [17]. The general pathway is written in [17] as "HIV-infected individuals are highly infectious in the first few weeks after infection [First infectious stage], then remain in an asymptotic stage of low infectiousness for many years [Second infectious stage], and become gradually more infectious as the immune system becomes compromised and they progress to AIDS [Final infectious stage]". Note that there may be any number of infected compartments in an HIV model depending on whether one investigates the entire progression from HIV to AIDS or a subset of this progression. For example, [22] derives multiple infected

compartments for a small, high-risk subset of a larger population, whereas [16, 17] derive multiple infected compartments spanning the entire HIV to AIDS disease progression for the whole population.

Query 3 resulted in 98 studies going through the screening process. For the reasons discussed in 1.2, the inclusion criteria in title and abstract screening were models with ordinary differential equations, deterministic structure, and mode of transmission characterized by airborne or vehicular. The types of models resulting from this query were much more varied than those of query 2. Not only did models include indirect transmission through a contaminated environment, but there were also models that used both direct and indirect transmission. There were also models that had multiple infected compartments. However, these models typically used age-structure or a multi-group/multi-patch structure in such compartments. As discussed above, age-structured models divide individuals into SIR classes based on age of/life cycle stage of infection. For multi-group/multi-patch models, the groups/patches of homogeneous groups (which are subgroups of a heterogeneous host population) are classified based on characteristics such as modes of transmission, contact patterns, or geographic distributions, allowing intra-group and inter-group interactions to be modeled separately [62]. One difficulty in reading multi-group model papers is that authors are not always clear on what criteria is being used in the formation of their groups. For example, in the multi-group cholera model proposed in [33], it's explicitly stated that groups are classified by their geographic location. However, while [62] briefly clarifies what a multi-group framework is, it's unclear what characteristic(s) (location, contact patterns, etc.) are used in the classification of groups.

While the types of models were more varied than in query 3, there were some common themes: cholera and COVID-19 modelling. Since cholera is a waterborne gastroenteric infection, indirect transmission via ingestion of contaminated water or feces is more common than casual human-human contact [33], thus such models were well represented by search query 2. These models typically have a SIR structure, with an additional compartment (commonly labelled with a B or W) to represent the pathogen concentration in the water, and can hence be dubbed SIWR models. Models such as [46] and [61] are representative of such simpler cholera models. However, while these models contained only 4 equations, the researchers incorporated direct and indirect transmission. There were models with multiple infected compartments, most often these were multi-group models such as [33, 62]. An example of a cholera model with multiple infected compartments that did not use the multi-group approach comes from [8]. However, these compartments represent symptomatic and

asymptomatic infected individuals [8].

As for COVID-19 models, indirect transmission typically manifests through inhaling infectious aerosols, or touching a contaminated surface [37, 67]. Such contaminated surfaces are thought of as the environmental reservoir in which the pathogen multiplies. Most COVID models that came up in the search results had an SEIR structure. The additional compartment E represents exposed individuals [3]. Exposed individuals are susceptible who have been exposed to the pathogen but are not yet infected [3]. However, there were many variations, such as SEIR models that included symptomatic and asymptomatic individuals, and SEIR model which included vaccination. Examples of COVID-19 models that included an equation for the environmental reservoir are [24, 35, 37, 67]. Generally, these models have several different pathways that individuals can progress through, meaning an individuals may not pass through every infected compartment before reaching recovery. Typically, this manifests when considering symptomatic and asymptomatic individuals in separate compartments, or considering confirmed and unconfirmed cases as separate compartments. An asymptomatic individual may or may not develop symptoms before recovery, just as an individual with an unconfirmed case of COVID may or may not need to go to a hospital (resulting in a confirmed case) before recovery. The latter can be seen in [37]; asymptomatic and undetected symptomatic individuals are considered as one infectious compartment, A, and detected symptomatic individuals are in a second infectious compartment, D. In this model, individuals in compartment A can either enter the recovered compartment directly, or they enter compartment D before reaching recovery [37]. These compartments and individual's movements between them can be seen in Figure 1.2. However, this is by no means the only form of multiple pathways in COVID models. For example, in [67], a susceptible individual moves into the asymptomatic or exposed compartment, not exposed then asymptomatic, and an asymptomatic individual may or may not enter the hospitalized compartment before entering the recovered compartment. These pathways are visualized in Figure 1.3 As well, COVID models may have individuals in only one or in multiple (distinct) infected classes contribute to the environmental reservoir. For example, in [35] and [37] individuals in only one infectious compartment contribute to the environmental reservoir, whereas in [24] and [67] individuals in multiple infectious compartments contribute to the environmental reservoir.

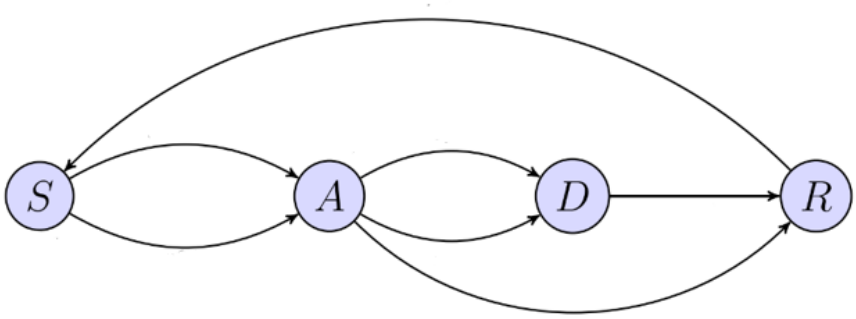

Figure 1.2: A simplified flow diagram for the movement of individuals in the model proposed by [37]. The compartments are defined as follows: S for susceptible individuals, A which consists of both asymptomatic infectious individuals and symptomatic individuals who have not been detected by the healthcare system, D for infected individuals have been detected by the healthcare system, and R for recovered individuals [37]. These compartments are represented by the circles with labels S, A, D, R. The movement of individuals from a given compartment is represented by arrows, with the arrowhead indicating the direction of movement from one compartment to another. For simplicity we omit the model terms written above the arrows that appear in the original diagram in [37]. Notably, in this model individuals from compartment S can progress through one of two pathways. First they enter compartment A, after which they can either enter R directly, or first pass through D before proceeding to R.

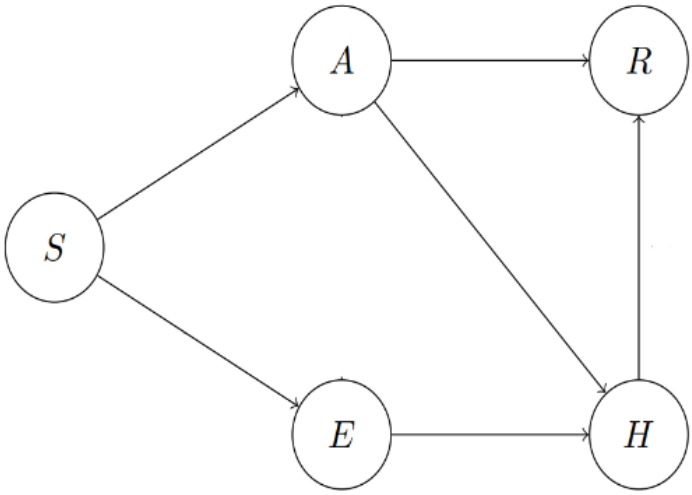

Figure 1.3: A simplified flow diagram for the movement of individuals in the model proposed by [67]. The compartments are defined as follows: S for susceptible individuals, A for asymptomatic infectious individuals, E for exposed individuals (whom are not yet infectious), H for hospitalized infectious individuals who are isolated from the rest of the population, and R for recovered individuals [67]. These compartments are represented by the circles with labels S, A, E, H, R. The movement of individuals from a given compartment is represented by arrows, with the arrowhead indicating the direction of movement from one compartment to another. For simplicity we omit the model terms written above the arrows that appear in the original diagram and remove visuals relating to the environmental reservoir. In contrast to [37], individuals from compartment S can progress through one of three pathways: first enter A then R, second enter A then H then R, or third enter E then H then R.

Before discussing the results of the review, we note that while none of the *N. ceranae* models discussed in Section 1.1 meet all the inclusion criteria of our review, some fall under concepts that we have discussed. For example, each of the *N. ceranae* models in [2, 5, 40, 43] distinguish between hive and forager bees. In our discussion of honey bee polyethism (see Section 1.1), we noted that there is often an age difference between these two categories, where hive bees are typically younger than their forager counter parts [50]. Hence, these could all be considered as models with population structure, as if one were distinguishing between younger and older individuals. This is similar to the aforementioned predator-prey models which divide individuals in the predator or prey sub-populations into susceptible mature and immature categories, which can then become infected. Another example comes from *N. ceranae* models such as [10, 39], which consider between-hive transmission. The hives in these

models each represent distinct geographical locations, and much like the aforementioned cholera models, modelling disease transmission thus results in a multi-patch model.

In the next section, we will discuss the findings of the literature review.

1.4 Results of the Literature Review

Finally, we discuss the standard results and approaches present in the literature. We begin by reporting the standard results, and then explore what methods are used to derive them. The first result most papers gave was the positivity and boundedness of model solutions. Some papers such as [1, 8, 49, 66] state both positivity and boundedness explicitly in its own Section/subsection. More commonly, papers such as [16, 17, 33, 37, 62, 61] include positivity and boundedness after the model equations, which may or may not be distinctly stated in a proposition, theorem, etc. Some papers such as [26] go a step further to not only include positivity and boundedness, but also that the model solutions are continuously differentiable. Sometimes researchers will also comment on the existence and uniqueness of model solutions, such as [60], but most see this as a trivial result not needing an explicit statement. However, there are papers such as [22, 24, 35, 46, 67] that do not comment on such results, likely viewing such results as trivial.

The next standard result is to derive the existence of equilibria, particularly the disease-free equilibrium (DFE). Depending on model equations, there may also be an endemic equilibrium. For example, [1] models a predator-prey system, and therefore derives 3 equilibria: trivial, the "axial state" - i.e. the DFE, and a predator-free - i.e. endemic equilibrium. Another predator-prey model described by [60] has similar results, with the three equilibria being described as trivial, predator-extinction, and disease-free. Such a result is typical of predator-prey models which also include disease in the predator/prey population. In models such as [33, 37] only the DFE is considered. In [16, 17] both disease-free and endemic equilibria are derived, with only the former having an explicit parameter-based expression for each component. In [22, 35, 62, 61], explicit expressions for the DFE are derived with only parameters describing each compartment, however, while there is an expression for each component of the endemic equilibrium, they are not all necessarily independent of compartments. A slightly different kind of result can be found in [8], which considers the effects of climate change on cholera spread. As a result, there are two variations of the same model: one without intra-annual climate variation, and one with. For the former, a DFE can be obtained, but for the latter, thresholds that guarantee disease extinction or uniform persis-

tence are derived [8]. Some papers such as [24, 46, 67] forgo traditional equilibria analysis. In the case of [24] focus was placed on deriving a relation for the final epidemic size of their SEIRV model. In [46] focus was placed on investigating heterogeneity in transmission pathways and the final outbreak size of the disease. In [67] emphasis was placed on the peak value of infection and final size of infection. Models such as [26, 49, 66] that consider time delays or periodicity investigate periodic solutions rather than equilibria, but are still likely to consider the equivalent equilibria types, i.e. periodic solutions with and/or without the source of disease.

Following derivation of equilibria, most researchers will investigate their stability. Most researchers first derive the basic reproduction number $\mathcal{R}_0$ (which we will define shortly) and then use it in their stability analysis of the DFE. However, not all epidemic models use $\mathcal{R}_0$. For [1], stability analysis was done with bifurcations of their model. For [60], Lyapunov functions and La Salle's invariance principle are used for sufficient stability results. For models with periodicity (such as [26, 49, 66]) $\mathcal{R}_0$ is not always needed. For papers that do use $\mathcal{R}_0$, we must first clarify the meaning of $\mathcal{R}_0$. There are many variations on the definition of $\mathcal{R}_0$ depending on the context [20]. We will use the definition of $\mathcal{R}_0$ in an epidemiological context, written by [20] as, "the number of individuals infected by a single infected individual during his or her entire infectious period, in a population which is entirely susceptible". From this definition, it follows that when $\mathcal{R}_0 < 1$, an infectious individual (on average) produces less than one new infectious individual, whereas when $\mathcal{R}_0 > 1$, an infectious individual (on average) produces more than one new infectious individual [20]. That is, when $\mathcal{R}_0 < 1$ we predict an infection doesn't persist in the population, and when $\mathcal{R}_0 > 1$ we predict an infection does persist. This so called threshold behaviour is the most important and useful aspect of $\mathcal{R}_0$ as a concept [20]. Furthermore, the magnitude of $\mathcal{R}_0$ can also be used when gauging the risk of an emerging infectious disease [20]. As it relates to stability of the DFE, the standard result one will find in the literature is some variation of "if $\mathcal{R}_0 < 1$, the DFE is stable, and if $\mathcal{R}_0 > 1$, the DFE is unstable". For example, in [8], local asymptotic stability is derived for $\mathcal{R}_0 < 1$, and instability is proven for $\mathcal{R}_0 \geq 1$. However, in [16, 17] the stability statement is slightly different. Global asymptotic stability is derived for $\mathcal{R}_0 \leq 1$, and instability is proven for $\mathcal{R}_0 > 1$ [16, 17]. Yet another variation can be found in [22], whose statement reads, "If $\mathcal{R}_0 < 1$, the infection-free equilibrium is locally asymptotically stable. If $\mathcal{R}_0 > 1$, the infection-free equilibrium is unstable, and an initial infection will spread". This set of inequalities are also present in [35, 37]. In [33], it is shown that global asymptotic stability exists for $\mathcal{R}_0 < 1$, but stability when $\mathcal{R}_0 > 1$ is not commented on. In

all these variations, $\mathcal{R}_0$ serves as a sharp criterion for the stability of the DFE.

We will now discuss the methods used in deriving the standard results. For positivity and boundedness, there are many different approaches one can take. We will give a brief sampling of methods here, but one should note that the specific approach taken is generally not important. For example, papers such as [8, 17, 16, 33, 62] use limits of the supremum of different state functions, such as the total population (which is the sum of all populations of SIR compartments) and environmental reservoir. Other papers such as [37] use properties of their differential equations like continuous differentiability. One can also use fundamental theory of differential equations, an approach taken by [60]. Papers with periodic solutions such as [26, 49] use impulsive differential equation theory. Another approach is to use the integrating factor on the total population size and environmental reservoir (if it is present), as seen in [48]. Deriving the DFE is trivial; simply set all state values other than those in uninfected compartments equal to 0, set the right-hand side of differential equations for uninfected compartments equal to zero, and solve this set of equations. To calculate the basic reproduction number, almost all researchers follow the Next Generation Matrix (NGM) approach described in [57]. Of more interest are the approaches used to relate the stability of the DFE to $\mathcal{R}_0$, thereby establishing $\mathcal{R}_0$ as a sharp criterion for stability. Note that there are cases such as [22, 37] where $\mathcal{R}_0$ is calculated but not needed in proving stability. For example, in [22] it is shown that the eigenvalues of the Jacobian matrix evaluated at the DFE have negative real parts. In [37] the Jacobian matrix evaluated at the DFE and a sub-matrix, B, have the same eigenvalues, thus, the Routh-Hurwitz criterion is used to show the trace of a sub-matrix B is negative. However, most papers use $\mathcal{R}_0$ directly or make use of assumptions in [57] related to the matrices in the NGM from which $\mathcal{R}_0$ is derived. For the former, the standard approach is to derive a Lypunov function which requires $\mathcal{R}_0 < 1$ in order to be asymptotically stable (see [17, 16, 62] for examples). For the latter, one can use assumptions A1-A5 and subsequent theorem(s) in [57] (see [33, 35] for examples).

Recall in the beginning of the literature review, we aimed to answer the following question: "What is known about deterministic discrete stage-structured compartmental disease models?" Our goal was to analyze knowledge gaps about the model structure created in this thesis, and understand what the standard results and methodologies are.

We can conclude that we know very little, if anything at all, about models with the structure posed in this thesis. Of all the papers screened in this review, none were able to satisfy exactly the criteria given in Section 1.2. Generally, models from search queries 2 and 3 fell into two categories: they had stage-structure based on the viral load/disease

progression of the pathogen inside the host but not indirect transmission, or they had indirect transmission (mainly via a contaminated environment) and no stage structure. In terms of differential equations, this would manifest in a model with an equation for each infected compartment, as well as an equation for an environmental reservoir. The small number of papers that did include both these did not satisfy key criteria outlined in 1.2. For example, in a hantavirus model proposed by [63], such a set up of equations can be found. However, in [63] individuals do not progress through multiple infective classes based on viral load; they are only categorized as "newly infectious with high viral titers and chronically infectious with low viral titers". This is fundamentally different from our model, in [63], the viral load of the pathogen has an inverse relationship with the duration an individual is infected. Another example can be found in a salmonellosis (in pigs) model proposed in [31]. Again there are multiple equations for infected individuals and an equation for the environmental reservoir, however, individuals are categorized based on the amount of pathogen they contribute to the environmental reservoir, not by the viral load of pathogen in their bodies [31]. It is differences in assumptions such as this that make such models separate from our own.

Many papers in the literature take the following approach: Derive the disease-free equilibrium and $\mathcal{R}_0$, then use $\mathcal{R}_0$ as a sharp criterion for the stability of the DFE by way of a Lyapunov function. If an endemic equilibrium is obtained, then its stability is similarly derived. Of the papers in search queries 2 and 3 very few, if any, called into question whether $\mathcal{R}_0$ is a suitable parameter for establishing a sharp criterion in the first place. As such, the focus of the literature is often on $\mathcal{R}_0$ in the context of its relationship with the DFE. Few papers investigate $\mathcal{R}_0$ in the context of general disease spread or model behaviour, yet many have explicit expressions for $\mathcal{R}_0$ which contain biologically meaningful parameters. We argue that this leaves much information about the dynamics of disease(s) unexplored. Given the importance of $\mathcal{R}_0$ on disease spread, there could be value in considering what biological processes have the greatest and least impact on $\mathcal{R}_0$. Understanding what processes increase $\mathcal{R}_0$, and subsequently increase the prevalence of disease in a population, could be vital for public health measures aiming to reduce disease spread.

This notion is also supported in research investigating transience of dynamic systems. Slightly different definitions of transience can be found depending on the context of the research. For example, in a disease model from [25], transient dynamics are defined as "non-permanent, short-term behaviors of the model, driven by stochasticity, small perturbations... Effectively, the behavior of the model when it is expressly not at equilibrium" [25]. Another definition written in an ecological context is given by [65], "A transient phase is the pattern

of change as a system moves from one equilibrium state to another". In a paper by [54], transience is examined across multiple fields including epidemiology, movement ecology, and parasitology, and excludes trajectories which attain equilibrium. We define transience as the short-term behaviour of model solutions that reach equilibrium. That is, we wish to measure how slowly or quickly our system reaches long-term behaviour. Regardless of how one defines transience, researchers are beginning to investigate its affects in a wide range of fields [21, 25, 54].

This concludes our discussion of the literature review. After considering the mathematical modelling background and the results of the literature review, we are ready to define the objective of this thesis.

1.5 Objective of Thesis

The objective of this thesis follows from the identified gaps in the literature. We essentially have one objective; formulate and analyze/explore a stage structured SIR model with indirect transmission.

1.6 Outline of Thesis

We can now provide an outline of the thesis, demonstrating how each of the remaining chapters relate to each other to achieve the stated objective.

In chapter 2 we first derive the model equations. These model equations are derived using some of the biological background on *N. ceranae* as well as the mathematical concepts discussed in Section 1.2. We explore the model analytically first. This includes establishing the model's well-posedness through fundamental ODE theory and deriving sufficient but not necessary conditions for the stability of the DFE. We also derive an expression for $\mathcal{R}_0$ using the NGM. We consider what biological processes in our model assumptions most impact the value of $\mathcal{R}_0$ by performing local sensitivity analysis on $\mathcal{R}_0$ with respect to model parameters. This leads to our numerical simulations.

In chapter 3 we use computational model simulation to address the identified knowledge gaps in both chapter 2 and Section 1.3. The former concerns investigating whether the sufficient conditions on DFE stability hold in model simulations. We also perform computational sensitivity analysis (of $\mathcal{R}_0$ with respect to parameters) for comparison against the results of the analytical sensitivity analysis. The latter primarily concerns answering the question,

"Does $\mathcal{R}_0$ serve as a sharp criterion for disease persistence in this model?" and investigating model transience as it relates to $\mathcal{R}_0$. Generally, we aim to gain a deeper understanding of the disease dynamics present in the derived system. With the completion of numerical simulations, we move to the discussion.

In our discussion (Ch.(4)), we place the results from previous chapters in the context of the literature. For each point brought up in our introduction we include a paragraph in our discussion. This results in answering the following list of questions: What is gained by adding discrete stage-structure to a SIR model with indirect transmission? How do the disease dynamics of our model compare to those in the literature? How would to proposed model be adapted to model *N. ceranae* in the Western honey bee? From our discussion, we draw final conclusions and future work in Ch.(5).

Chapter 2

Mathematical Model

In this chapter we derive a deterministic discrete stage-structured SIR model with indirect transmission. We begin by outlining the model assumptions. The resulting model equations are then defined, with a term-by-term analysis of each equation. We then derive mathematical results for the model, including well-posedness of the model, partial results for the stability of the DFE, and local sensitivity analysis of $\mathcal{R}_0$.

2.1 Model Assumptions

Before writing model equations we must clearly define the model assumptions. While this model is not a *Nosema ceranae* model, we will use some aspects of nosemosis disease transmission in our model assumptions. We also use assumptions typical of SIR modelling, in particular SIR models concerning indirect transmission, as well as assumptions that serve to simplify the modelling process. We write our model assumptions as follows:

A.1 We use a SIR model. We define our model compartments as follows: I_0 represents susceptible individuals who have not yet been infected, I_1 represents individuals who are in the lowest level of infection, I_2 represents individuals who are in the middle level of infection, and I_3 represents individuals who are in the highest level of infection. The total number of individuals in the population, N, is then the sum of compartments $I_{0,1,2,3}$, that is, $N(t) = I_0(t) + I_1(t) + I_2(t) + I_3(t)$. We use E to denote the development of the pathogen in the environmental reservoir. We assume disease progression is uninfected (I_0) $\rightarrow$ low infection (I_1) $\rightarrow$ medium infection (I_2) $\rightarrow$ high infection (I_3) $\rightarrow$ removed. Individuals are only removed from the system by death.

A.2 Individuals are brought into the population only by birth and do not carry the pathogen. Natural birth is represented by the parameter Λ. There is no vertical transmission of disease (i.e. disease is not transferred from parent to offspring during pregnancy).

A.3 Individuals are removed from the population in two ways: through natural death, which affects the population at all levels of infection (i.e. those in compartments $I_{0,1,2,3}$), and through disease-related death, which only occurs in those with the highest level of infection (i.e. those in compartment I_3 but not $I_{1,2}$). For simplicity, we assume infected and uninfected individuals have the same natural death rate; μ.

A.4 Since we are modelling indirect transmission, we assume that pathogens live in an environmental reservoir E.

A.5 The amount of spores that individuals remove from the environmental reservoir is negligible, as long as the environmental reservoir is sufficiently large. Hence the environmental reservoir is only decreased when spores lose viability, denoted by γ.

A.6 Infected individuals increase the environmental reservoir proportionally to their level of infection, denoted by α_i. We further assume that more infected individuals deposit more pathogens into the environmental reservoir than less infected individuals, hence $\alpha_1 \leq \alpha_2 \leq \alpha_3$.

A.7 Even with a high initial inoculum, many pathogens are voided. Hence, pathogen uptake rate plays a role in moving an uninfected individual into the first infected compartment (I_0 to I_1), but movement to higher infection compartments is a result of the pathogen's germination in the body, not ingesting more pathogens. For simplicity, we use a bilinear movement rate from I_0 to I_1, denoted cEI_0, and make all other movement rates constant, denoted by δ_i, $i = 1, 2$. As with assumption A.6 we assume recruitment into a higher level of infection is proportional to each class, i.e. $\delta_1 \leq \delta_2 \leq \delta_3$. Furthermore, we assume the rate at which an individual moves into a higher level of infection is proportional to their level of infection. That is, movement from I_1 to I_2 is a constant rate, denoted δ_1 which is different than that of I_2 to I_3, denoted δ_2.

With our model assumptions clearly defined, we can now derive ordinary differential equations representative of the biological process which we are modelling.

2.2 Model Equations

Below are the model equations. Note that the numbers located below each term indicate what assumption from section 2.1 is being used.

$$\frac{dI_0}{dt} = \underbrace{\Lambda}_{A.2} - \underbrace{cEI_0}_{A.7} - \underbrace{\mu I_0}_{A.3} \tag{2.1}$$

$$\frac{dI_1}{dt} = \underbrace{cEI_0}_{A.7} - \underbrace{\delta_1 I_1}_{A.7} - \underbrace{\mu I_1}_{A.3} \tag{2.2}$$

$$\frac{dI_2}{dt} = \underbrace{\delta_1 I_1}_{A.7} - \underbrace{\delta_2 I_2}_{A.7} - \underbrace{\mu I_2}_{A.3} \tag{2.3}$$

$$\frac{dI_3}{dt} = \underbrace{\delta_2 I_2}_{A.7} - \underbrace{\delta_3 I_3}_{A.3} - \underbrace{\mu I_3}_{A.3} \tag{2.4}$$

$$\frac{dE}{dt} = \underbrace{\alpha_1 I_1 + \alpha_2 I_2 + \alpha_3 I_3}_{A.6} - \underbrace{\gamma E}_{A.5} \tag{2.5}$$

We will interpret each term in the above equations to understand the underlying model assumptions. The first equation represents the change in the sub-population I_0 (susceptible individuals). Λ is the growth/birth term measured in units of individuals per unit time. In the term cEI_0, cE denotes the rate at which susceptible individuals transfer to the first infected compartment. The term cEI_0 has units individuals per time, with cE being measured in 1 per unit time, and the parameter c having units 1 per (unit time $\times$ spores). In μI_0 and all following terms μI_j, μ represents the natural death rate of individuals and is measured in units of 1 per unit time. Thus all terms μI_j are measured in units of individuals per unit time. Moving onto equations (2.2) and (2.3), δ_1 and δ_2 denote the rates at which individuals in the current infective class (I_i) move or are recruited to the next infective class (I_{i+1}), $i = 1, 2$. Each of $\delta_1, \delta_2, \delta_3$ has units 1 per unit time, thus each of $\delta_j I_j$ has units individuals per unit time. Moving to the fourth equation, δ_3 in the term $\delta_3 I_3$ is the rate at which the most infected individuals die from the disease, hence μI_3 has units individuals per unit time. Finally for the last equation, each α_i in $\alpha_1 I_1 + \alpha_2 I_2 + \alpha_3 I_3$ are the rates at which spores are deposited by each infective class, where α is measured in spores/(individual $\times$ unit time). Hence, each $\sum_{i=1}^{n} \alpha_i I_i$ is the contribution of spores from individuals to the environmental reservoir and are measured in (spores $\times$ individuals) per unit time. Lastly, γE is the rate

at which spores loose viability, where γ has units 1 per unit time, and γE is measured in spores per unit time. This information is summarized in Table 2.1, with the unit of time set to day(s).

Table 2.1: A summary of model parameters used in equations (2.1)-(2.5)

Symbol	Name/Interpretation	Units
Λ	Natural birth rate	individuals/day
c	Transfer from I_0 to I_1	1/(day $\times$ spores)
μ	Natural death rate	1/day
δ_1	Transfer from I_1 to I_2	1/day
δ_2	Transfer from I_2 to I_3	1/day
δ_3	Disease related death	1/day
α_1	Spore deposition of individuals in I_1	(spores $\times$ individuals)/day
α_2	Spore deposition of individuals in I_2	(spores $\times$ individuals)/day
α_3	Spore deposition of individuals in I_3	(spores $\times$ individuals)/day
γ	Spore decay	1/day

With our model equations defined, we will now aim to derive the standard results found in the literature. Recall from 1.3 such results include positivity/boundedness, existence of equilibria, and stability of said equilibria, and an expression for $\mathcal{R}_0$.

2.3 Well-posedness of the Model

In the following theorems, we will show that the model is globally well-posed. We use the definition of well-posedness from [59], stated as:

Definition 2.3.1 (Well-posed Problems)**.** A mathematical problem used to model a well-defined physical process that proceeds in a unique manner should satisfy three general requirements:

1. *Existence.* The problem has at least one solution.

2. *Uniqueness.* The problem has not more than one solution.

3. *Continuous Dependence.* The solution depends continuously on the data that are present. If the model results in an initial value problem (IVP), then the solution

depends continuously on the right hand side of the differential equation and on the initial values.

Theorem 2.3.1. [Local Existence Uniqueness and Dependence of Model] The IVP posed by equations (2.1)-(2.5) with initial conditions possesses a unique solution which is continuously dependent on its data (right hand side of the differential equation and initial conditions).

Proof. The right hand side of equations (2.1)-(2.5) are continuously differentiable with respect to their dependent/compartments $(I_{0,1,2,3}, E)$ and parameters $(c, \Lambda, \mu, \delta_{1,2,3}, \alpha_{1,2,3}, \gamma)$. Therefore, from the criterion on page 66 of [59], we have that the right hand side of equations (2.1)-(2.5) satisfies a local Lipschitz condition with respect to each compartment. By the Picard-Lindelöf theorem (See page 62, theorem 1 in [59]) the initial value problem given by equations (2.1)-(2.5) with nonegative initial conditions has a solution locally. By theorem 4 on page 145 of [59], we also have that the solution to our IVP depends continuously on the initial values and on the right hand side of equations (2.1)-(2.5) locally. Since the model parameters enter the system via the right hand side of equations (2.1)-(2.5), we also have local continuous dependence on model parameters.

□

Theorem 2.3.2. [Non-negativity] With nonegative initial conditions the solutions of system 2.1-2.5 are nonegative for all $t \geq 0$

Proof. We apply the tangent condition from [59] (See chapter 3, page 117, theorem 15). To simplify notation, we write a system of ODEs as:

$$\frac{dy}{dt} = f(y,t),\ y \in \mathbb{R}^n.$$

In our model, the vector y is given by $y = (I_0, I_1, I_2, I_3, E)$. The vector $f(y,t)$ then has components $f_i(y,t)$, $i = 1,2,3,4,5$, where $y = (I_0, I_1, I_2, I_3, E)$. We let $f_{1,2,3,4,5}$ denote the right-hand side of equations (2.1)-(2.5), respectively. For each $f_i(y,t)$, we set $y_i = 0$ for all $i = 1,2,3,4,5$, assuming $y_j \geq 0,\ i \neq j$. Recall in our model formulation, we assumed all model parameters are positive. We also have $y_i \geq 0$ for $t = 0$ from nonegative initial conditions. Thus for each vector component $f_i(y,t)$ we have:

$$
\begin{aligned}
f_1(0, I_1, I_2, I_3, E) &= \Lambda > 0 \\
f_2(I_0, 0, I_2, I_3, E) &= cEI_0 \geq 0 \\
f_3(I_0, I_1, 0, I_3, E) &= \delta_1 I_1 \geq 0 \\
f_4(I_0, I_1, I_2, 0, E) &= \delta_2 I_2 \geq 0 \\
f_5(I_0, I_1, I_2, I_3, 0) &= \alpha_1 I_1 + \alpha_2 I_2 + \alpha_3 I_3 \geq 0.
\end{aligned}
$$

Hence each vector component $f_i(y,t) \geq 0$ along the boundary of the positive orthant for all vector components $i \in [1,5]$. This implies the vector $f(y,t)$ points into the positive orthant from the boundary, regardless of the value of t. Therefore model solutions are nonegative for all $t \geq 0$. □

Theorem 2.3.3. [Boundedness] Assuming

$$N(0) \leq \frac{\Lambda}{\mu} \text{ and } E(0) \leq \frac{\alpha_3 \lambda}{\mu\gamma},$$

the set Ω as defined below is positively invariant.

$$
\begin{aligned}
\Omega = \Bigg\{ &(I_0(t), I_1(t), I_2(t), I_3(t), E(t)) \in \mathbb{R}^5_+ : \\
&0 \leq I_0(t) + I_1(t) + I_2(t) + I_3(t) \leq \frac{\Lambda}{\mu} \ , \ 0 \leq E(t) \leq \frac{\alpha_3 \lambda}{\mu\gamma} \Bigg\}
\end{aligned}
$$

Proof. The lower bound for $E(t)$ is proven in theorem (2.3.2). Also from theorem (2.3.2) we have that $N(t)$ is a sum of non-negative functions, thus $N(t) \geq 0$. To prove the upper bound(s) on $N(t)$ and $E(t)$ we use the integrating factor method.

We will begin with $N(t)$. Before applying the integrating factor, we note that the derivative of $N(t)$ is the sum of the derivatives of compartments $I_0(t), I_1(t), I_2(t), I_3(t)$, i.e. $\frac{dN(t)}{dt} = \frac{dI_0(t)}{dt} + \frac{dI_1(t)}{dt} + \frac{dI_2(t)}{dt} + \frac{dI_3(t)}{dt}$. Using model equations (2.1)-(2.5) we can replace the derivatives of $I_0(t), I_1(t), I_2(t), I_3(t)$, resulting in the equation $\frac{dN}{dt} = \Lambda - \delta_3 I_3 - \mu(I_0 + I_1 + I_2 + I_3)$. Since $N(t) = I_0(t) + I_1(t) + I_2(t) + I_3(t)$ the equation becomes $\frac{dN}{dt} = \Lambda - \delta_3 I_3 - \mu N$. The term $-\delta_3 I_3$ is negative, so we can bound this term from above, resulting in the following inequality:

$$\frac{dN}{dt} \leq \Lambda - \mu N$$

Multiplying both sides of the inequality by $e^{\mu t}$ gives $\frac{dN}{dt}e^{\mu t} + \mu e^{\mu t}N \leq e^{\mu t}\Lambda$. Using the chain rule, we rewrite the left-hand side to get $\frac{d}{dt}\left(e^{\mu t}N\right) \leq e^{\mu t}\Lambda$. Next, we take the definite integral from 0 to t of both sides, using the letter s as a place holder for the integration variable, i.e. we calculate $\int_0^t \frac{d}{ds}\left(e^{\mu s}N\right)\, ds \leq \int_0^t e^{\mu s}\Lambda\, ds$. Calculating the integrals results in the inequality $e^{\mu t}N(t) - N(0) \leq \frac{\Lambda}{\mu}\left(e^{\mu t} - 1\right)$, which we then multiply by $e^{-\mu t}$ to get the inequality $N(t) - e^{-\mu t}N(0) \leq \frac{\Lambda}{\mu}\left(1 - e^{-\mu t}\right)$. Isolating $N(t)$ on the left-hand side results in the final inequality $N(t) \leq \frac{\Lambda}{\mu} - \left(\frac{\Lambda}{\mu} - N(0)\right)e^{-\mu t}$. So for $N(t) \leq \frac{\Lambda}{\mu}$, we need $\left(\frac{\Lambda}{\mu} - N(0)\right)e^{-\mu t} \geq 0$. Since $e^{-\mu t} \geq 0\ \forall t$, we require $N(0) \leq \frac{\Lambda}{\mu}$.

Next we prove the upper bound for $E(t)$. We have $N(t) = I_0(t) + I_1(t) + I_2(t) + I_3(t) \geq 0\ \forall t \geq 0$, hence $I_1(t), I_2(t), I_3(t) \leq N(t)$. We use this to take the equation $\frac{dE}{dt} = \alpha_1 I_1 + \alpha_2 I_2 + \alpha_3 I_3 - \gamma E$ and rewrite it as the inequality $\frac{dE}{dt} \leq (\alpha_1 + \alpha_2 + \alpha_3)N - \gamma E$. Since we have shown $N \leq \frac{\Lambda}{\mu}$, we can write this inequality as $\frac{dE}{dt} \leq (\alpha_1 + \alpha_2 + \alpha_3)\frac{\Lambda}{\mu} - \gamma E$. We also replace $\alpha_1 + \alpha_2 + \alpha_3$ with $\max \alpha_j$, which as per model assumption A.6) is equal to α_3. Thus we have:

$$\frac{dE}{dt} \leq \alpha_3\frac{\Lambda}{\mu} - \gamma E$$

Multiplying both sides of the inequality by $e^{\gamma t}$ gives $\frac{dE}{dt}e^{\gamma t} + \gamma e^{\gamma t}E \leq \alpha_3\frac{\Lambda}{\mu}e^{\gamma t}$. Using the chain rule, we rewrite the left-hand side to get $\frac{d}{dt}\left(e^{\gamma t}E\right) \leq \alpha_3\frac{\Lambda}{\mu}e^{\gamma t}$. Next, we take the definite integral from 0 to t of both sides, using the letter s as a place holder for the integration variable, i.e. we calculate $\int_0^t e^{\gamma s}E\, ds \leq \int_0^t \alpha_3\frac{\Lambda}{\mu}e^{\gamma s}\, ds$. Calculating the integrals results in the inequality $E(t)e^{\gamma t} - E(0) \leq \frac{\Lambda\alpha_3}{\mu\gamma}\left(e^{\gamma t} - 1\right)$, which we then multiply by $e^{-\gamma t}$ to get the inequality $E(t) - e^{-\gamma t}E(0) \leq \frac{\Lambda\alpha_3}{\mu\gamma}\left(1 - e^{-\gamma t}\right)$. Isolating $E(t)$ on the left-hand side results in the final inequality $E(t) \leq \frac{\Lambda\alpha_3}{\mu\gamma} - \left(\frac{\Lambda\alpha_3}{\mu\gamma} - E(0)\right)e^{-\gamma t}$. Hence $E(t) \leq \frac{\Lambda\alpha_3}{\mu\gamma}$ so long as $E(0) \leq \frac{\Lambda\alpha_3}{\mu\gamma}$. □

Remark 1 (Global Uniqueness and Existence)**.** It follows from Theorem 2.3.3 that solutions

of the IVP given by equations (2.1)-(2.5) with initial conditions which are in Ω exist globally.

Knowing the model is globally well-posed, we are able to investigate the DFE.

2.4 Disease Free Equilibrium (DFE)

As in [38], we consider the disease free equilibrium (DFE) to be "the point at which no disease is present in the population", that is, the value of the susceptible population, I_0, when all other compartments $I_{1,2,3}, E$, are equal to zero. First we show the DFE exists for all parameters and is unique.

Theorem 2.4.1. The DFE exists for all parameters and is unique for equations (2.1)-(2.5) with nonegative initial conditions. This DFE is given by:

$$D = (I_0^*, I_1^*, I_2^*, I_3^*, E^*) = \left(\frac{\Lambda}{\mu}, 0, 0, 0, 0\right) \tag{2.6}$$

Proof. Since we are in a disease-free environment, $I_{1,2,3} = 0$ and $E = 0$. Hence the equations (2.2)-(2.5) are trivially satisfied for any parameter values. Thus for equation (2.1) at equilibrium we have that $0 = \Lambda - cEI_0 - \mu I_0$. In the disease-free environment, $E = 0$, therefore $0 = \Lambda - \mu I_0$, from which we obtain the steady state for I_0; $I_0^* := \frac{\Lambda}{\mu}$ for any value(s) of Λ and $\mu > 0$. Thus, the disease free equilibrium in (2.1)-(2.5) is unique. That is, the DFE defined in equation (2.6) is the only DFE. □

Now that we've shown uniqueness and existence, we investigate the stability of the DFE. First, we take the Jacobian matrix, $\mathcal{J}$, of equations (2.1)-(2.5).

$$\mathcal{J}(I_0, I_1, I_2, I_3, E) = \begin{bmatrix} -cE - \mu & 0 & 0 & 0 & -cI_0 \\ cE & -\delta_1 - \mu & 0 & 0 & cI_0 \\ 0 & \delta_1 & -\delta_2 - \mu & 0 & 0 \\ 0 & 0 & \delta_2 & -\delta_3 - \mu & 0 \\ 0 & \alpha_1 & \alpha_2 & \alpha_3 & -\gamma \end{bmatrix} \tag{2.7}$$

Evaluated at the DFE, $(\frac{\Lambda}{\mu}, 0, 0, 0, 0)$, the Jacobian becomes:

$$\mathcal{J}(I_0^*,0,0,0,0) = \begin{bmatrix} -\mu & 0 & 0 & 0 & -c\frac{\Lambda}{\mu} \\ 0 & -\delta_1-\mu & 0 & 0 & c\frac{\Lambda}{\mu} \\ 0 & \delta_1 & -\delta_2-\mu & 0 & 0 \\ 0 & 0 & \delta_2 & -\delta_3-\mu & 0 \\ 0 & \alpha_1 & \alpha_2 & \alpha_3 & -\gamma \end{bmatrix} \tag{2.8}$$

In the following theorem, we derive a sufficient, but not necessary, condition for the stability of the DFE.

Theorem 2.4.2. If $\mu \geq \frac{c\Lambda}{\mu}, \mu+\delta_1 \geq \frac{c\Lambda}{\mu}, \delta_2+\mu \geq \delta_1, \delta_3+\mu \geq \delta_2$, and $\gamma \geq \alpha_1+\alpha_2+\alpha_3$ (we refer to these inequalities collectively as $G1$) or if $\mu \geq \alpha_1,\ \mu \geq \alpha_2,\ \mu+\delta_3 \geq \alpha_3$, and $\gamma \geq \frac{2c\Lambda}{\mu}$ (we refer to these inequalities collectively as $G2$) then the DFE is asymptotically stable.

Proof. We will use Gershgorin's Theorem for estimating eigenvalues [9]. We begin by applying the theorem row-wise, then column-wise.

Row-wise: We being by constructing the Gershgorin discs as defined in [9]. From each row of matrix 2.8 we have 5 discs centered at $-\mu, -\delta_1-\mu, -\delta_2-\mu, -\delta_3-\mu, -\gamma$ with radii $\frac{c\Lambda}{\mu}, \frac{c\Lambda}{\mu}, \delta_1, \delta_2, \alpha_1+\alpha_2+\alpha_3$, respectively. So long as $\mu \geq \dfrac{c\Lambda}{\mu},\ \mu+\delta_1 \geq \dfrac{c\Lambda}{\mu},\ \delta_2+\mu \geq \delta_1,\ \delta_3+\mu \geq \delta_2,\ \gamma \geq \alpha_1+\alpha_2+\alpha_3$ the discs lie completely in the negative half plane. By Gershgorin's theorem all eigenvalues of the Jacobian matrix 2.8 must lie in the Gershgorin discs. Thus, all eigenvalues of 2.8 are negative and the DFE 2.6 is asymptotically stable. Note that this gives our first group of sufficient conditions for DFE stability.

Column-wise: From each column of matrix 2.8 we have 5 Gershgorin discs with the same centers as before but with radii $0, \delta_1+\alpha_1, \delta_2+\alpha_2, \alpha_3, \frac{2c\Lambda}{\mu}$ instead. So long as $\mu \geq \alpha_{1,2},\ \delta_3+\mu \geq \alpha_3,\ \gamma \geq \dfrac{2c\Lambda}{\mu}$ the discs lie completely in the negative half plane. From model assumption A.6, we can write $\mu \geq \alpha_3$ instead of $\mu \geq \alpha_{1,2}$. Furthermore, the inequality $\delta_3+\mu \geq \alpha_3$ is trivially satisfied so long as all parameters are positive. By Gershgorin's theorem all eigenvalues of the Jacobian matrix 2.8 must lie in the intersection in the Gershgorin discs. Thus, all eigenvalues of 2.8 lie in the negative half plane and the DFE 2.6 is asymptotically stable. This gives a second group of sufficient conditions for DFE stability. □

Remark 2 (Biological Interpretation of DFE Stability)**.** We can interpret the conditions in G1 as follows:

1. $\mu \geq \frac{c\Lambda}{\mu}$: This can be interpreted a couple different ways. If we fix μ, then either Λ or c is small *relative to* μ. If we fix Λ, then μ is large or c is small relative to Λ. In either case

of fixing μ in $\mu \geq \frac{c\Lambda}{\mu}$, the infection spreads slowly either because the birth rate is small so there are not enough individuals to spread disease, or because the infection rate is small. In the case of fixing Λ in $\mu \geq \frac{c\Lambda}{\mu}$, either the death rate is so high the disease cannot persist, or the infection rate is not sufficiently high to establish the disease. In this first scenario, individuals die faster than they can infect other individuals. In the second scenario the time scale for the disease to propagate is larger than the life span of the individuals. Essentially, the first and second scenarios are the same, which they must be since they are simply reformulations of one another.

2. $\mu + \delta_1 \geq \frac{c\Lambda}{\mu}$: To interpret this we fix parameters one at a time. First, fixing μ, we find that δ_1 (the rate at which individuals in the first level of infection transfer to the second) is large, c, Λ are small relative to μ. So the disease spreads slowly in the uninfected population. Fixing δ_1, μ is large and c, Λ are small relative to δ_1. This means the disease spreads slowly for the same reasons as before. Fixing Λ, we have that μ, δ_1 are large and c is small relative to Λ. Again the infection spreads slowly in the susceptible compartment for reasons above, and many individuals transfer to the second level of infection. Finally, fixing c we find that μ, δ_1 are large and Λ is small relative to c. Disease spreads slowly in the first compartment due to high death and low birth rates, and individuals transfer from the first to the second level of infection rapidly.

3. $\delta_2 + \mu \geq \delta_1$ and $\delta_3 + \mu \geq \delta_2$: The rate at which individuals are leaving infected compartments I_1, I_2, I_3 is higher than the rate at which individuals are entering them.

4. $\gamma \geq \alpha_1 + \alpha_2 + \alpha_3$: The rate at which pathogens decay in the environment is faster than they are replaced in the environment by infected individuals

We can interpret the conditions in G2 as follows:

1. $\mu \geq \alpha_3$: Individuals in compartments I_1, I_2 die faster than they can deposit spores.

2. $\delta_3 + \mu \geq \alpha_3$: Infected individuals (those in I_3) also die faster than they can deposit spores.

3. $\gamma \geq \frac{2c\Lambda}{\mu}$: Spores decay faster than individuals are able to able to transmit infection.

Now that we have an understanding of the DFE, we can investigate the basic reproduction number, $\mathcal{R}_0$.

2.5 Next Generation Matrix (NGM) and the Basic Reproduction Number

We use the Next Generation Matrix (NGM) to calculate $\mathcal{R}_0$ [57]. Our approach follows the work of [14]. The infectious/disease-related compartments in equations (2.1)-(2.5) are $I_1(t), I_2(t), I_3(t), E(t)$. The rate of appearance of new infections into the infectious compartments (this includes not only the term(s) in equation (2.1) which give rise to new infections, but also the term(s) in equation (2.5) which increase the pathogen responsible for infection), the rate of transfer of individuals into the infectious compartments, and the rate of transfer of individuals out of the infectious compartments are denoted by $\mathcal{F}, \mathcal{V}^+, \mathcal{V}^-$, respectively [14]. Looking at equations (2.1)-(2.5), we have:

$$\mathcal{F} = \begin{pmatrix} cEI_0 \\ 0 \\ 0 \\ \alpha_1 I_1 + \alpha_2 I_2 + \alpha_3 I_3 \end{pmatrix} \tag{2.9}$$

$$\mathcal{V}^+ = \begin{pmatrix} 0 \\ \delta_1 I_1 \\ \delta_2 I_2 \\ 0 \end{pmatrix} \tag{2.10}$$

$$\mathcal{V}^- = \begin{pmatrix} (\delta_1 + \mu) I_1 \\ (\delta_2 + \mu) I_2 \\ (\delta_3 + \mu) I_3 \\ \gamma E \end{pmatrix} \tag{2.11}$$

In the next step of the method, one defines $\mathcal{V}$ as $\mathcal{V} = \mathcal{V}^- - \mathcal{V}^+$ [57]. In our system $\mathcal{V}$ is then:

$$\mathcal{V} = \mathcal{V}^- - \mathcal{V}^+ = \begin{pmatrix} (\delta_1 + \mu) I_1 \\ (\delta_2 + \mu) I_2 - \delta_1 I_1 \\ (\delta_3 + \mu) I_3 - \delta_2 I_2 \\ \gamma E \end{pmatrix} \tag{2.12}$$

One then defines $\mathbf{F}$ as the Jacobian matrix of $\mathcal{F}$, evaluated at the DFE [57]. In our

model, $\mathbf{F}$ is given by:

$$\mathbf{F} = \begin{bmatrix} 0 & 0 & 0 & \frac{c\Lambda}{\mu} \\ 0 & 0 & 0 & 0 \\ 0 & 0 & 0 & 0 \\ \alpha_1 & \alpha_2 & \alpha_3 & 0 \end{bmatrix} \tag{2.13}$$

Similarly, $\mathbf{V}$ is defined as the Jacobian matrix of $\mathcal{V}$ evaluated at the DFE [57]. Thus we have:

$$\mathbf{V} = \begin{bmatrix} \delta_1 + \mu & 0 & 0 & 0 \\ -\delta_1 & \delta_2 + \mu & 0 & 0 \\ 0 & -\delta_2 & \delta_3 + \mu & 0 \\ 0 & 0 & 0 & \gamma \end{bmatrix} \tag{2.14}$$

Finally, the NGM is written as $\mathbf{FV^{-1}}$ [57]. Hence we have:

$$\mathbf{FV^{-1}} = \begin{bmatrix} 0 & 0 & 0 & \frac{c\Lambda}{\mu} \\ 0 & 0 & 0 & 0 \\ 0 & 0 & 0 & 0 \\ \alpha_1 & \alpha_2 & \alpha_3 & 0 \end{bmatrix} \begin{bmatrix} \frac{1}{\delta_1+\mu} & 0 & 0 & 0 \\ \frac{\delta_1}{(\delta_1+\mu)(\delta_2+\mu)} & \frac{1}{\delta_2+\mu} & 0 & 0 \\ \frac{\delta_1\delta_2}{(\delta_1+\mu)(\delta_2+\mu)(\delta_3+\mu)} & \frac{\delta_2}{(\delta_2+\mu)(\delta_3+\mu)} & \frac{1}{\delta_3+\mu} & 0 \\ 0 & 0 & 0 & \frac{1}{\gamma} \end{bmatrix} \tag{2.15}$$

$$\mathbf{FV^{-1}} = \begin{bmatrix} 0 & 0 & 0 & \frac{c\Lambda}{\mu\gamma} \\ 0 & 0 & 0 & 0 \\ 0 & 0 & 0 & 0 \\ \Psi & \Phi & \frac{\alpha_3}{\delta_3+\mu} & 0 \end{bmatrix} \tag{2.16}$$

where

$$\Psi = \frac{\alpha_1}{\delta_1 + \mu} + \frac{\alpha_2\delta_1}{(\delta_1 + \mu)(\delta_2 + \mu)} + \frac{\alpha_3\delta_1\delta_2}{(\delta_1 + \mu)(\delta_2 + \mu)(\delta_3 + \mu)}$$

$$\Phi = \frac{\alpha_2}{\delta_2 + \mu} + \frac{\alpha_3\delta_2}{(\delta_2 + \mu)(\delta_3 + \mu)}.$$

Next, we derive the basic reproduction number, $\mathcal{R}_0$. Recall in section 1.4 we discussed the qualitative definition of $\mathcal{R}_0$. To summarize, $\mathcal{R}_0$ is used to approximate the number of secondary infections caused during disease spread. In an epidemiological context, secondary

infections are defined as "the number of individuals infected by a single infected individual during his or her entire infectious period, in a population which is entirely susceptible" [20]. From this definition it follows that when $\mathcal{R}_0 < 1$ we predict disease will not spread in the population, and when $\mathcal{R}_0 > 1$ we predict disease will spread in the population. Mathematically, $\mathcal{R}_0$ is defined as the spectral radius of the NGM [57]. Thus, we have:

$$\mathcal{R}_0 = \sqrt{\frac{c\Lambda}{\mu\gamma}}\sqrt{\frac{\alpha_1}{\delta_1+\mu} + \frac{\alpha_2\delta_1}{(\delta_1+\mu)(\delta_2+\mu)} + \frac{\alpha_3\delta_1\delta_2}{(\delta_1+\mu)(\delta_2+\mu)(\delta_3+\mu)}} = \sqrt{\frac{c\Lambda}{\mu\gamma}}\sqrt{\Psi} \tag{2.17}$$

In the next section, we will investigate how biological processes affect the value of $\mathcal{R}_0$.

2.6 Local Sensitivity Analysis of $\mathcal{R}_0$

In this Section, we aim to gain a deeper understanding of how biological processes in our model (represented by model parameters) influence the value of $\mathcal{R}_0$. To achieve this we perform local sensitivity analysis. In sensitivity analysis, one is interested in investigating how a particular quantity of interest (such as model solutions or an important scalar value) changes as one or more of the model parameters are changed. Given the importance of $\mathcal{R}_0$ as it relates to disease spread, we use local sensitivity analysis to investigate which parameters from the model equations (2.1)-(2.5) have the greatest influence on the value of $\mathcal{R}_0$.

Currently, there are two main ways to perform local sensitivity analysis: analytically through differentiation, or numerical simulation through a statistical approach. Often, the latter is the approach taken by researchers in the current literature. In this research, we use both approaches. Comparing and contrasting the results found in both provides valuable insight into the disease dynamics described by the model equations. In this section, we perform the analytical approach. We will perform the statistical approach with our numerical simulations in Chapter 3, Section 3.6. As mentioned, the analytical approach is based on derivatives. These derivatives are the partial derivatives of the quantity of interest (in this case $\mathcal{R}_0$) with respect to each parameter that is varied. The model described by equations (2.1)-(2.5) has 10 parameters: $\Lambda, c, \mu, \delta_1, \delta_2, \delta_3, \alpha_1, \alpha_2, \alpha_3, \gamma$. Taking the partial derivatives of equation (2.17) with respect to each parameter results in equations (2.18) to (2.27).

$$\frac{\partial\mathcal{R}_0}{\partial c} = \frac{1}{2}\sqrt{\frac{\Lambda}{c\mu\gamma}}\sqrt{\Psi} \tag{2.18}$$

$$\frac{\partial \mathcal{R}_0}{\partial \Lambda} = \frac{1}{2}\sqrt{\frac{c}{\mu\gamma\Lambda}}\sqrt{\Psi} \tag{2.19}$$

$$\frac{\partial \mathcal{R}_0}{\partial \gamma} = \frac{-1}{2}\sqrt{\frac{c\Lambda}{\mu\gamma^3}}\sqrt{\Psi} \tag{2.20}$$

$$\frac{\partial \mathcal{R}_0}{\partial \alpha_1} = \sqrt{\frac{c\Lambda}{\mu\gamma}}\ \frac{1}{2\sqrt{\Psi}}\ \frac{1}{\delta_1+\mu} \tag{2.21}$$

$$\frac{\partial \mathcal{R}_0}{\partial \alpha_2} = \sqrt{\frac{c\Lambda}{\mu\gamma}}\ \frac{1}{2\sqrt{\Psi}}\ \frac{\delta_1}{(\delta_1+\mu)(\delta_2+\mu)} \tag{2.22}$$

$$\frac{\partial \mathcal{R}_0}{\partial \alpha_3} = \sqrt{\frac{c\Lambda}{\mu\gamma}}\ \frac{1}{2\sqrt{\Psi}}\ \frac{\delta_1\delta_2}{(\delta_1+\mu)(\delta_2+\mu)(\delta_3+\mu)} \tag{2.23}$$

$$\frac{\partial \mathcal{R}_0}{\partial \mu} = \frac{-1}{2}\sqrt{\frac{c\Lambda}{\mu^3\gamma}}\sqrt{\Psi} + \left[\frac{1}{2\sqrt{\Psi}}\,(L+M+P)\right]\sqrt{\frac{c\Lambda}{\mu\gamma}} \tag{2.24}$$

$$L = \frac{-\delta_1\alpha_1}{(\delta_1+\mu)^2}$$
$$M = \frac{-(\delta_1+\delta_2+2\mu)\alpha_2\delta_1}{((\delta_1+\mu)(\delta_2+\mu))^2}$$
$$P = \frac{-(\delta_1\delta_3+\delta_2\delta_3+\delta_1\delta_2+2\delta_1\mu+2\delta_2\mu+2\delta_3\mu+3\mu^2)\alpha_3\delta_1\delta_2}{((\delta_1+\mu)(\delta_2+\mu)(\delta_3+\mu))^2}$$

$$\frac{\partial \mathcal{R}_0}{\partial \delta_1} = \sqrt{\frac{c\Lambda}{\mu\gamma}}\left[\frac{1}{2\sqrt{\Psi}}\,(Q)\right] \tag{2.25}$$

$$Q = \frac{\mu}{(\delta_1+\mu)^2}\left(-\alpha_1 + \frac{\alpha_2}{\delta_2+\mu} + \frac{\alpha_3\delta_2}{(\delta_2+\mu)(\delta_3+\mu)}\right)$$

$$\frac{\partial \mathcal{R}_0}{\partial \delta_2} = \sqrt{\frac{c\Lambda}{\mu\gamma}}\left[\frac{1}{2\sqrt{\Psi}}\left(\frac{\mu}{(\delta_1+\mu)(\delta_2+\mu)^2}\right)\left(-\alpha_2\delta_1 + \frac{\alpha_3\delta_1}{(\delta_3+\mu)}\right)\right] \tag{2.26}$$

$$\frac{\partial \mathcal{R}_0}{\partial \delta_3} = \sqrt{\frac{c\Lambda}{\mu\gamma}}\left[\frac{1}{2\sqrt{\Psi}}\left(\frac{\alpha_3\delta_1\delta_2}{(\delta_1+\mu)(\delta_2+\mu)(\delta_3+\mu)^2}\right)\right] \tag{2.27}$$

Next we evaluate the sign of each partial derivative in equations (2.18)-(2.27). We assume all parameters are positive for this analysis so that any conclusions are biologically relevant. For example, looking at equation (2.18) we see that (all other parameters positive and held constant), $\frac{\partial \mathcal{R}_0}{\partial c} > 0 \ \forall c > 0$. Similarly for equations (2.19)-(2.23) (except equation (2.20)), and (2.27), we find $\frac{\partial \mathcal{R}_0}{\partial \Lambda} > 0 \ \forall \Lambda > 0$, $\frac{\partial \mathcal{R}_0}{\partial \delta_3} > 0 \ \forall \delta_3 > 0$, $\frac{\partial \mathcal{R}_0}{\partial \alpha_i} > 0 \ \forall \alpha_i > 0, i = 1, 2, 3$, when all other parameters are positive and held constant (See Table 2.2). For equations (2.20) and (2.24) we find that $\frac{\partial \mathcal{R}_0}{\partial \gamma} < 0 \ \forall \gamma > 0$, $\frac{\partial \mathcal{R}_0}{\partial \mu} < 0 \ \forall \mu > 0$. Thus for the parameters $c, \Lambda, \delta_3, \alpha_{1,2,3}, \gamma, \mu$ we have the following result:

Remark 3 (Monotonicity of $\mathcal{R}_0$ with respect to parameters)**.** Thinking of $\mathcal{R}_0$ as a function of certain parameters, we have the following monotonicity:

1. $\mathcal{R}_0$ is monotonically increasing with respect to $c, \Lambda, \delta_3, \alpha_{1,2,3}$ as a function of c, Λ, δ_3 or $\alpha_{1,2,3}$, respectively.

2. $\mathcal{R}_0$ is monotonically decreasing with respect to γ, μ as a function of γ or μ, respectively.

However, for $\delta_{1,2}$, such concrete results cannot be derived since the sign of equations (2.25) and (2.26) depends on the values of other parameters. We can summarize these results as in Table 2.2 for quick referencing. These results also lead to the following biological interpretation of $\mathcal{R}_0$:

Remark 4 (Biological Interpretation of $\mathcal{R}_0$)**.** To biologically interpret equation (2.17), we consider varying one parameter while holding all others constant. We can do this for individual or groups of parameters. It is not necessary or even possible to do this investigation for all possible combinations of parameters, so we focus on those present in traditional SIR models.

1. Λ represents the birth rate of the population, i.e. it is the rate at which new susceptible individuals are introduced into the population. Thus, if the population is replenished quickly, there are more individuals available to contract the disease, and the disease establishes itself. Conversely, if there are no or very few new susceptible individuals available to contract the disease, the disease cannot persist.

2. c represents transfer of a susceptible individual into the first infected compartment. As c increases, there is a higher number of infected individuals in the population, and thus the disease establishes itself. Conversely, if c is too low, the disease is unable to persist and the population is left with mostly susceptible, not infected, individuals.

3. μ represents the natural death rate of the population, i.e. it is the rate at which individuals at all levels of infection (no, little, medium, and high) are removed from the population. If μ is high, there are simply not enough individuals in the population for the disease to persist. If natural death is very low, then there are plenty of individuals in the population capable of spreading the pathogen, and thus the disease can persist.

4. γ represents the decay rate of the pathogen, i.e. it is the rate at which pathogens causing the disease lose their infectivity. If γ is high, then the pathogen is not able to effectively infect a host, i.e. there are less susceptible individuals moving into the infected compartment(s), and thus the disease cannot persist. Conversely, if γ is low then the pathogens remain active sources of disease in the environment for longer, and can thus spread infection to more susceptible individuals, allowing the disease to become established.

Table 2.2: The summarized results of the local sensitivity analysis of $\mathcal{R}_0$ performed analytically. For each parameter of the model, the sign of $\mathcal{R}_0$'s partial derivative and corresponding results (or lack thereof) are displayed.

Local Sensitivity Analysis of $\mathcal{R}_0$		
Parameter	Sign of $\frac{\partial \mathcal{R}_0}{\partial}$	Result (w.r.t parameter)
c	> 0	$\mathcal{R}_0$ monotonically increases
Λ	> 0	$\mathcal{R}_0$ monotonically increases
$\alpha_{1,2,3}$	> 0	$\mathcal{R}_0$ monotonically increases
δ_3	> 0	$\mathcal{R}_0$ monotonically increases
μ	< 0	$\mathcal{R}_0$ monotonically decreases
γ	< 0	$\mathcal{R}_0$ monotonically decreases
δ_1	Unclear	depends on other parameters
δ_2	Unclear	depends on other parameters

Chapter 3

Numerical Simulations

The purpose of this chapter is to investigate the disease dynamics of our model, as well as fill in knowledge gaps from our mathematical analysis. The analysis in this chapter will be based on computer simulations of the model.

In order to gain a full picture understanding of our model, we explore several aspects of disease dynamics. We run simulations across different sets of parameters, plotting results and looking for any patterns that may arise. We pay attention to patterns such as convergence to the DFE, convergence to a non-disease-free equilibrium (referred to as endemic from now on and denoted EE), and the overall spread of individuals across compartments. We also explore the transience in disease dynamics of the model. Recall in section 1.4 we defined transience as the short-term behaviour of model solutions that reach equilibrium. We will investigate transience as it relates to $\mathcal{R}_0$ to better understand the disease dynamics at play. We take this approach because (as discussed in section 1.4) researchers tend to use $\mathcal{R}_0$ in relation to the stability of the DFE, not in a context of disease spread or general model behaviour. We aim to gain such knowledge by viewing the transience in our model as dependent on $\mathcal{R}_0$.

To fill in the knowledge gaps from Chapter 2, we investigate multiple topics. We need to investigate the stability of the disease free equilibrium. More specifically, we have sufficient but not necessary conditions for DFE stability. We would like to use computational simulation to see if these conditions are also necessary in our mmodel simulations. To strengthen these results, we calculate the eigenvalues of the Jacobian matrix evaluated at the DFE (equation (2.8) from Section 2.4) for each model simulation and see if they agree with expectations. Another goal is to see how our mathematical sensitivity analysis in Section 2.6 compares to the computational sensitivity analysis in Section 3.6. In the mathematical sensitivity analysis we derived clear results for all parameters except $\delta_{1,2}$. In the computational

sensitivity analysis, we hope to see clear results for these parameters. Finally, we recall that our analytical approach (in Section 2.4) we did not derive $\mathcal{R}_0$ as a sharp criterion for the DFE. Furthermore, we are unable to infer the stability of the DFE solely from the value of $\mathcal{R}_0$, with $\mathcal{R}_0 < 1$ indicating the DFE is stable and $\mathcal{R}_0 > 1$ indicating the DFE is unstable. More generally, $\mathcal{R}_0$ is seen as an indicator of whether or not disease will persist in a system [20]. Hence the aforementioned statement regarding $\mathcal{R}_0$ and DFE stability is equivalent to saying if $\mathcal{R}_0 < 1$ disease persists, and if $\mathcal{R}_0 > 1$ disease persists in the population. Since we could not prove this analytically, we must rely on computational simulations.

These topics will be organized as follows: In Section 3.1 we discuss the programming language and relevant packages used to run model simulations. In Section 3.2 we perform typical model simulations. In Section 3.3 we explore model transience as it relates to $\mathcal{R}_0$. In Section 3.4 we explore whether $\mathcal{R}_0$ is a good indicator of DFE and EE. In Section 3.5 we investigate whether we can derive necessary conditions for DFE stability, paying particular attention to how useful the sufficient conditions are. We conclude with Section 3.6, which explores computational sensitivity analysis and its comparison to the local sensitivity analysis in Section 2.6.

3.1 Simulation Set up

In this section, we will outline what coding language and packages were used for the following simulation experiments. All computational simulations were performed using R Statistical Software, v4.2.1, facilitated with the integrated development environment RStudio [45, 47]. A variety of packages were used for multiple analyses performed in this thesis. We list how and what each package was used for, including citations where appropriate. The package `deSolve` was used to numerically integrate the ODE system [53]. The default solver `lsoda` was used to numerically integrate the model [53]. The package `openxlsx` was used to save generated data from `deSolve` in Excel files, making it easier to access across multiple computers and reproduce analysis. The package `ggplot2` was used in graphing figures in sections, 3.2, 3.3, and 3.4. [64]. The package `sensobol` was used for Sobol sensitivity analysis and related figures in Section 3.6 [44]. The packages `foreach, doParallel` were used to run model simulations in sections 3.4, 3.3, and 3.6 in parallel to reduce computational time. In the following sections we will provide details on what the data generated by these packages contains.

3.2 Model Simulations

In this section we investigate the different types of behaviour exhibited by model simulations. For each simulation performed, the model described by equations (2.1)-(2.5) was numerically integrated using `deSolve`, with the results plotted using `ggplot2`. In this investigation, we tested model behaviour across 5 different parameter sets, listed in Table 3.1. We also recorded the $\mathcal{R}_0$ value for each simulation. Each simulation used a different set of parameter values in order to showcase the model behaviour. These parameter sets were derived by starting with an arbitrarily chosen set of "base" values, $P1$. Then, specific parameters or groups of parameters were varied (with other parameters held constant) to see what the impact was on the model behaviour. This lead to the remaining parameter sets as follows: for $P2$ $\alpha_{1,2,3}$ are increased, for $P3$ $\delta_{1,2,3}$ are increased, for $P4$ γ is increased, and for $P5$ μ is increased. We recorded $\mathcal{R}_0$ to see whether the type of equilibrium established (DFE or EE) agreed with standard results concerning the value of $\mathcal{R}_0$. That is, for simulations with DFE, the standard result from Section 1.4 tells us to expect $\mathcal{R}_0 < 1$, and for simulations with EE we expect $\mathcal{R}_0 > 1$. The last important consideration are the initial conditions. For each model simulation initial conditions are given by $(I_0, I_1, I_2, I_3, E) = (\frac{\Lambda}{\mu}, 0, 0, 0, 10)$. Choosing these initial conditions makes the simulation approximate real-world disease dynamics. These conditions describe a situation in which the susceptible population is established, and a small amount of the pathogen has been introduced in the system. The model behaviour is plotted in Figures 3.1-3.5. The plots are plotted only for the beginning of the run time for each simulation, with time measured in days. For many simulations, the model's behaviour is established very rapidly. As a result, plotting the model for the long run times obscures the disease dynamics. For Figures 3.1-3.4 the time duration is 10 days. For Figure 3.5 the time duration in 3 days. These time intervals were chosen as they resulted in the clearest plots. We plot the compartments containing the population (which measures the number of individuals) and the environmental reservoir (which measures the number of pathogens in the environment) on separate axes. In Figures 3.1-3.5 we refer to model compartments $I_{0,1,2,3}$ collectively as SI compartments, since I_0 represents susceptible individuals, and $I_{1,2,3}$ represents infectious individuals.

We will now go through the results for each Figure/parameter set. Note that any time intervals or state function values are approximations based on the graph axes. In Figure 3.1, the disease does not persist. More specifically, we see that compartment I_0 experiences a brief decrease in the interval $t \in [0, 2.5]$. Compartment I_1 experiences a brief increase in the

same interval. For E, we have what seems like an exponential decrease, with E starting at around 10, and decreasing to zero in (approximately) the interval $t \in [0, 7.5]$, with most of the change happening for $t \in [0, 5]$. The population is comprised of only healthy individuals. Additionally, we note that the standard result regarding $\mathcal{R}_0$ holds, i.e. we have a DFE and $\mathcal{R}_0 = 0.4367458 < 1$

In Figure 3.2 disease does persist. For this graph, it's best to investigate the compartments one at a time. We'll start with E, which overall increases in a log-like fashion. The compartments I_1, I_2, I_3 all seem to increase in a log-like fashion, with $I_1 > I_2 > I_3$. For I_0, we see what looks like an exponential decrease. It is also important to look at the "spread" of individuals in the compartments. As we mentioned, disease does persist in this simulation, however, we have $I_1 > I_2 > I_0 > I_3$ for $t \geq 5$, so the disease does not completely dominate the system. That is, the infectious population is mostly comprised of individuals in the lowest and middle levels of infection. Also, the uninfected population is greater than the number of individuals at the highest level of infection. The environmental reservoir, E, increases in a log-like fashion. The standard result regarding $\mathcal{R}_0$ holds, i.e. we have a EE and $\mathcal{R}_0 = 4.367458 > 1$.

Disease also persists in Figure 3.3. All compartments $I_{1,2,3}$ experience a peak for $t \in [0, 1.25]$, after which their size is essentially constant. Again I_0 decreases in an exponential fashion, but much more sharply than in Figure 3.1. The curve for E looks the same as in Figure 3.2. In this case, disease does dominate the system, with the amount of individuals in I_0 remaining barely above 0, the population is comprised almost entirely of infected individuals, with the infected population satisfying $I_1 > I_2 > I_3$. In contrast to Figure 3.2, the number of susceptible individuals is now smaller than the number of individuals at the highest level of infection. The standard result regarding $\mathcal{R}_0$ holds, i.e. we have a EE and $\mathcal{R}_0 = 7.569749 > 1$.

Moving to Figure 3.4, we see the disease persists. There are many similarities between Figure 3.3 and Figure 3.4 for compartments $I_{0,1,2,3}$. The main difference between the two is that rather than I_0 decreasing exponentially and ending below I_3, I_0 now only decreases for $t \in [0, 1.25]$, after which it has a slight increase before maintaining a constant size. Though disease persists in this simulation, it does not totally dominate the population like in Figure 3.3, instead, we have $I_1 > I_0 > I_2 > I_3$. This is different from both Figures 3.2 and 3.3, with the number of susceptible individuals now being greater than the numbers of individuals in both the middle and highest level of infection. For the environmental reservoir, E, there is an initial sharp decrease followed by a rapid increase which leads to a peak at $t \approx 1.25$,

which then decreases slightly again before levelling out at around $t = 2.5$. The standard result regarding $\mathcal{R}_0$ holds, i.e. we have a EE and $\mathcal{R}_0 = 2.393765 > 1$.

Finally in Figure 3.5, we see the disease does not persist. The appearance of Figure 3.5 is the same as Figure 3.1, but on a much shorter timescale. The standard result regarding $\mathcal{R}_0$ holds, i.e. we have a DFE and $\mathcal{R}_0 = 0.2951388 < 1$.

Preliminary results suggest the standard result regarding $\mathcal{R}_0$ hold for our model. As well, in all simulations where disease persists (Figures 3.2-3.4) the infectious population can be described by the inequality $I_1 > I_2 > I_3$.

Table 3.1: The parameter values used in the model simulations of equations (2.1)-(2.5) with corresponding $\mathcal{R}_0$ for each run.

Parameter	$P1$	$P2$	$P3$	$P4$	$P5$
Λ	495.0	495.0	495.0	495.0	495.0
c	0.020	0.020	0.020	0.020	0.020
μ	2.0	2.0	2.0	2.0	8.0
δ_1	0.4	0.4	4.0	4.0	4.0
δ_2	0.7	0.7	7.0	7.0	7.0
δ_3	1.0	1.0	10.0	10.0	10.0
α_1	0.1	1.0	1.0	1.0	1.0
α_2	0.4	4.0	4.0	4.0	4.0
α_3	0.7	7.0	7.0	7.0	7.0
γ	1.0	1.0	1.0	10.0	10.0
$\mathcal{R}_0$ Value	0.4367458	4.367458	7.569749	2.393765	0.2951388

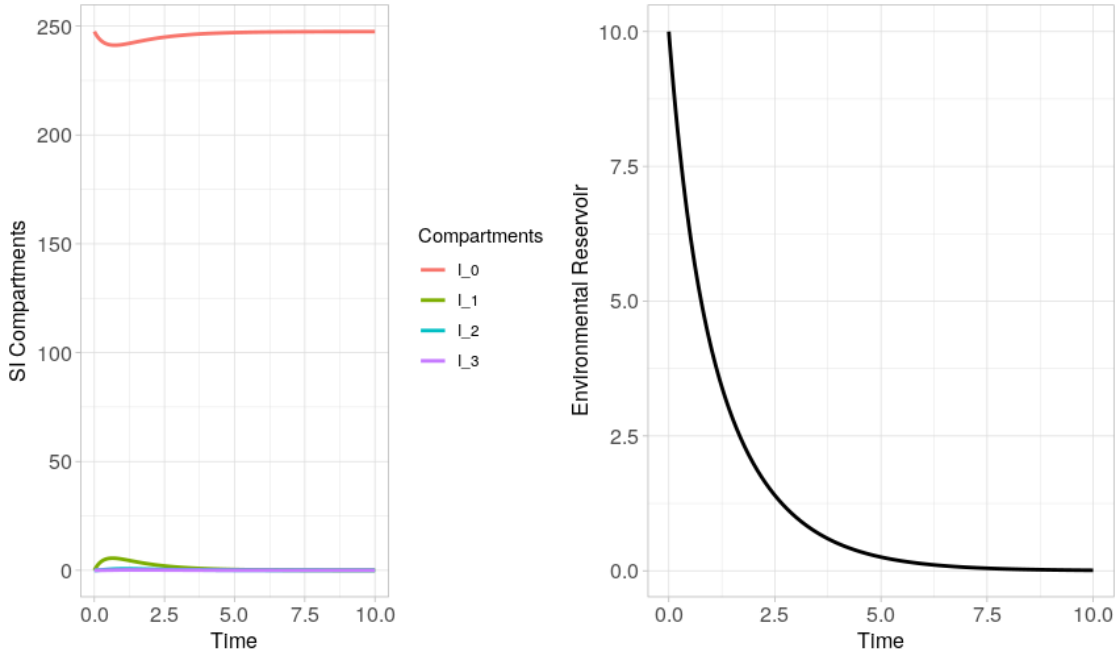

Figure 3.1: Model simulation for parameter set $P1$ for the time interval $t \in [0, 10]$, $\mathcal{R}_0 = 0.4367458$

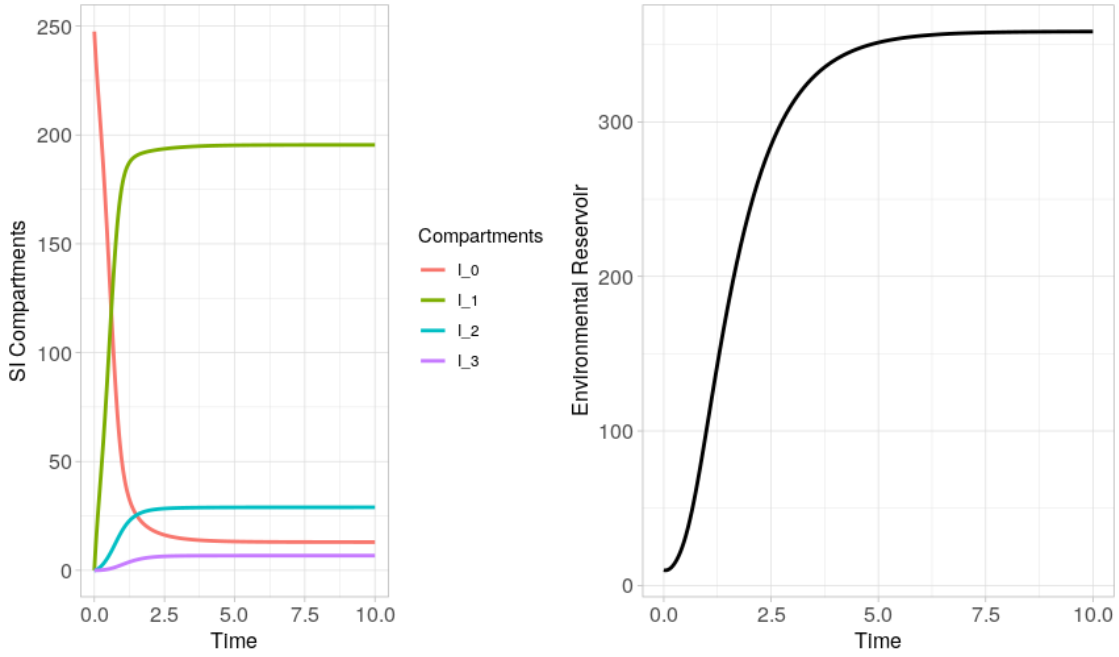

Figure 3.2: Model simulation for parameter set $P2$ for the time interval $t \in [0, 10]$, $\mathcal{R}_0 = 4.367458$.

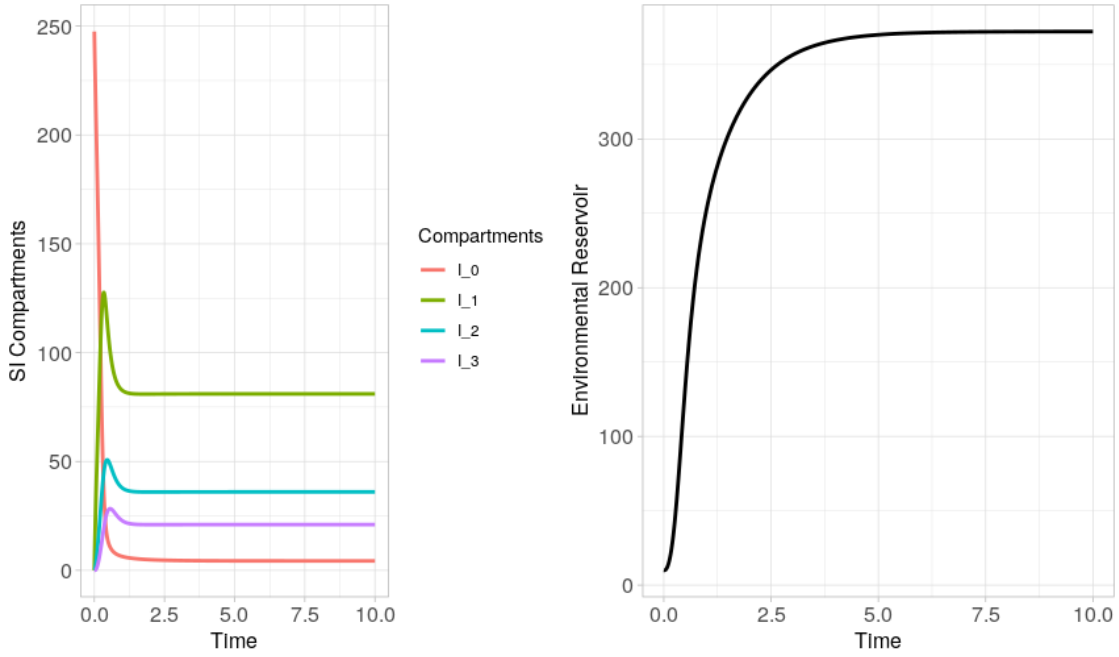

Figure 3.3: Model simulation for parameter set $P3$ for the time interval $t \in [0, 10]$, $\mathcal{R}_0 = 7.569749$.

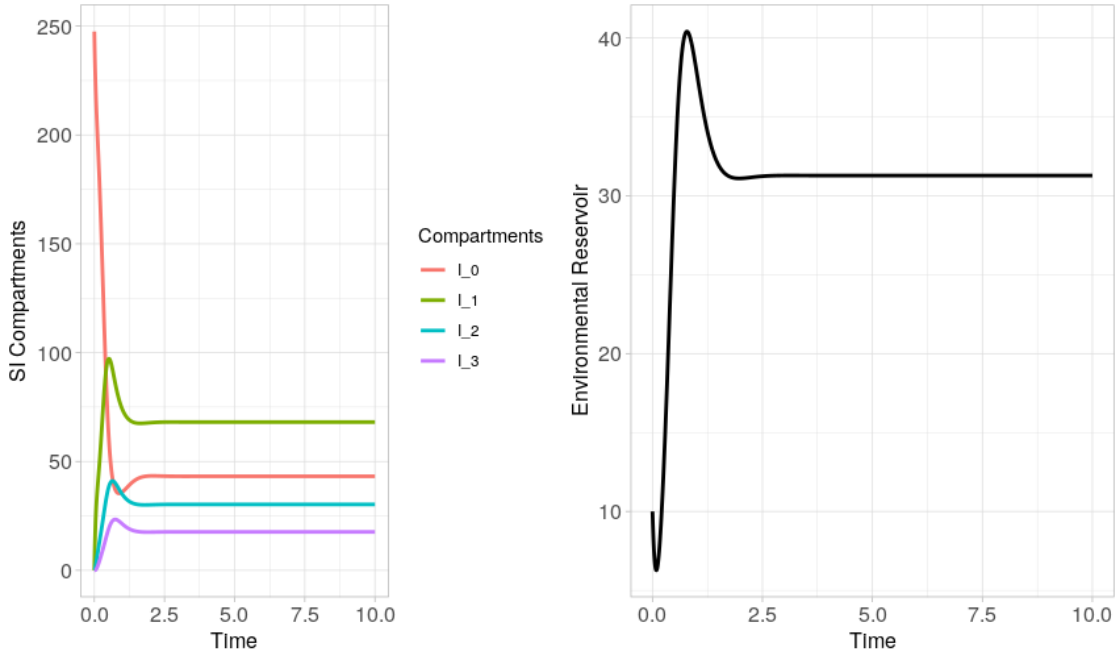

Figure 3.4: Model simulation for parameter set $P4$ for the time interval $t \in [0, 10]$, $\mathcal{R}_0 = 2.393765$.

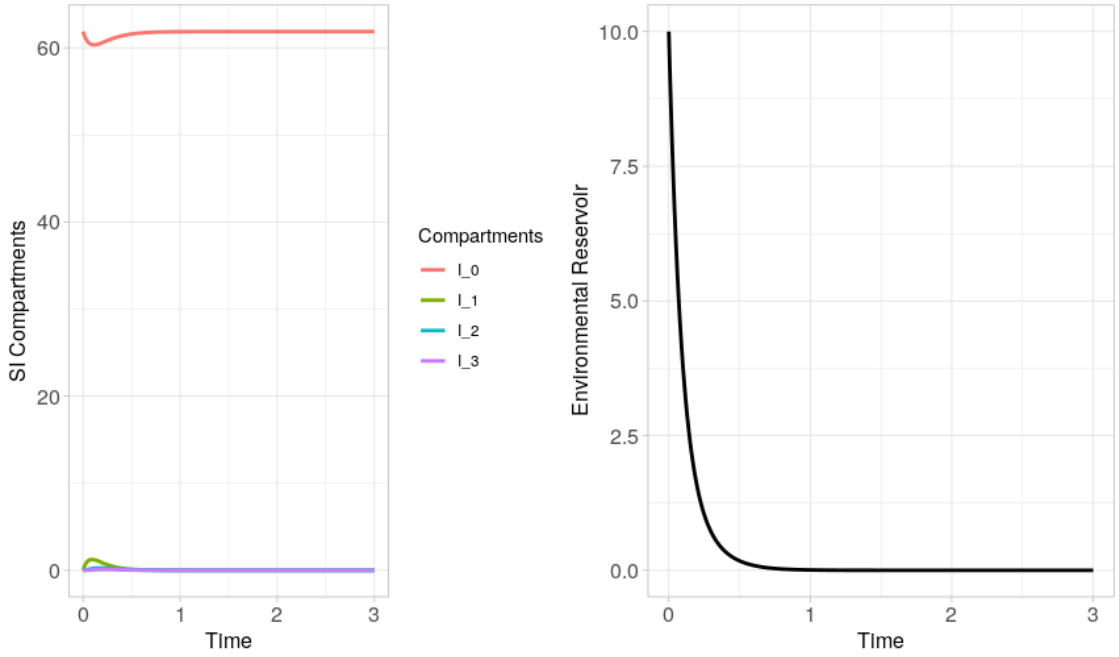

Figure 3.5: Model simulation for parameter set $P5$ for the time interval $t \in [0, 3]$, $\mathcal{R}_0 = 0.2951388$.

3.3 Relationship between Time to Steady State and $\mathcal{R}_0$

In this section, we aim to answer the question "How does the transience in the model relate to $\mathcal{R}_0$?" posed in Section 1.3. Before we can do this, we must introduce a measure of transience for our model. After we define this quantity, we will describe how the data for this analysis was generated. We then perform the statistical analysis used in our investigation.

We define transience as the short-term behaviour of model solutions that reach equilibrium. That is, we wish to measure how slowly or quickly our system reaches long-term behaviour. In this model, long-term behaviour is characterized by the type of equilibrium attained, which is either disease-free or endemic. Thus, our measure of transience is actually a measure of how quickly a disease reaches a state of persistence or dies out. Such information is vital in the context of public health because remedial strategies often need to be implemented in a timely matter to be effective. Thus, the amount of time it takes solutions to reach steady state serves as a measure of transience. However, a steady state is not reached in finite time in an ODE system. Thus, time taken to reach steady state requires a more precise definition.

To aid in notation, we first write an ODE as:

$$\frac{dy}{dt} = f(t, y).$$

Now, when we say time to reach steady state, really what we are doing is establishing a criterion to determine when the derivative of the solution is a good enough approximation of 0. Generally, there are two approaches we can take: we can test whether two subsequent solution values y_n and y_{n-1} are less than some ϵ apart, or we can evaluate if the right hand side of the ODE, is small enough $f(y_n)$. In our model, each $y_n,\ n = 1, 2, 3, 4, 5$ corresponds to the state variables I_0, I_1, I_2, I_3, E, i.e. we define $y_1 := I_0, y_2 := I_1, y_3 := I_2, y_4 := I_3, y_5 := E$. We can use j to denote the current time step. In our simulations we let $t \in [0, 10000], \Delta t = 1$, and in R coding indices start at 1, thus we have $j = 1, 2, \ldots, 10001$. Essentially, in the notation t_j, the subscript j is one value "ahead" of the value of t, so t_1 indicates the first time step, but the value of $t_1 = 0$, as a result of indexing differences in R software. To calculate time taken to reach steady state, called `SStime` for brevity, we assess whether the solution values in two subsequent time steps are close enough together. Thus, we are looking for the smallest t_j such that:

$$\sqrt{(y_n(t_j) - y_n(t_{j-1}))^2} \leq \mathrm{dt} \cdot \epsilon \cdot \sqrt{(f_n(y(t_j)))^2} \tag{3.1}$$

for each $y_n,\ n = 1, 2, 3, 4, 5$. We found that setting $\epsilon = 1 \times 10^{-8}$ allowed a sufficient number of simulations to reach steady state within a reasonable amount of computational time. This is a very tight criterion for steady state, since computationally the values of $y_j - y_{j-1}$ are incredibly small. With time taken to reach steady state defined, we can now describe the data used in this section.

To generate the data used in this section, we first need to integrate our model numerically using the package `deSolve`. This requires choosing model parameters and initial conditions. We will perform multiple simulations, each of which will have a unique set of parameters and initial conditions. Because we will be running multiple simulations, we need a range of values to choose from for each parameter. Since our original motivation was to study the pathogen *Nosema ceranae*, we use (as much as possible) parameters from *N. ceranae* modelling literature [5, 40] to create these ranges. Some parameters, such as the maximum emergence/eclosion rate (emergence of adult insect from its pupal/larval stage from an egg), spore deposition and (viability) decay rates reported in [5, 40] have a clear equivalent in our model ($\Lambda, \alpha_{1,2,3}, \gamma$, respectively). However, in [5] and [40], seasonality was considered,

resulting in multiple different values for each parameter. Another complication is that in [5] and [40], seasonal effects are considered as well as honey bee polyethism, meaning that the same parameters have multiple reported values for different groups of the population. Hence, while our parameters are informed by *N. ceranae* data, they are not an exact representation. We start by mapping as many values from [5, 40] to our parameters as possible. For Λ, we use the maximum eclosion/emergence rate for Spring, for μ, we use the death rate of hive bees in the Winter, for $\alpha_{1,2,3}$ we use the spore deposition rates in Spring, Fall, and Summer (respectively), for γ, we use the spore (viability) decay rate for Fall, rounded to 0.1. For the parameters $\delta_{1,2,3}$, we use the indirect transmission rates for Spring, Summer, and Fall (respectively). For c, we select a parameter range of 0.0020 to 0.25. For Λ, it was best to keep the range fairly tight, so a range encompassing 500 was chosen. However, from assumptions A.6 and A.4 in Section 2.1, we require $\delta_1 \leq \delta_2 \leq \delta_3$ and $\alpha_1 \leq \alpha_2 \leq \alpha_3$ (respectively). For $\delta_{1,2,3}$, we modify the Spring, Summer, and Fall parameters (respectively) in [40] by factors of 10 to ensure the inequality is maintained. Hence for $\alpha_{1,2,3}$, the parameters from [5, 40] are used in the order of least to greatest, resulting in ranges for $\alpha_{1,2,3}$ that include the Spring, Fall, and Summer parameters (respectively). Putting all this together, we arrive at Table 3.2. For initial conditions, we use the same set up as in Section 3.2, i.e. $(I_0, I_1, I_2, I_3, E) = (\frac{\Lambda}{\mu}, 0, 0, 0, 10)$. Before the numerical integration begins, all sets of parameters that will be used are randomly selected from a uniform distribution with range according to Table 3.2, and stored in a matrix. We choose a uniform distribution to ensure parameters are positive and reasonably close to their reported values in the *Nosema* literature. With the values for the parameter sets recorded, we calculate the corresponding sets of initial conditions for each simulation and store it in another matrix.

Next, we need to decide how many simulations to run. In order to draw conclusions about model behaviour, we need a substantial number of simulations. We select 5000 for the number of simulations. To reduce computational time, each of the 5000 simulations are run in parallel using the packages `foreach, doParallel`. For each simulation, we record (in a data frame) the following pieces of information: time taken to reach steady state (which we call `SStime` for brevity), the value of each component of the steady state (of which there are 5), the value of $\mathcal{R}_0$, the iteration number of the simulation, and the parameter values for the simulation (of which there are 10). From our discussion above, we know that in ODE systems, steady state is not reached in finite time. Thus, not all of the 5000 simulations reach steady state. Of the 5000 simulations run, 4381 reached steady state. Hence the resulting data frame contains 4381 rows (one for each simulation that reached steady state) and 18

columns (one for each of the pieces of information listed previously). Looking at the values of the components of the steady states, we can sub-divide this information into simulations which attain DFE and those which attain EE. For the DFE, we would expect to see $I_0 > 0$ and $I_{1,2,3}, E = 0$. However, such criteria is too strict in a computational environment, so we must introduce approximation of zero for the values of $I_{1,2,3}$, and E. Instead of using the strict equality $I_{1,2,3}, E = 0$ we calculate an approximation of 0 which is relative to the size of the population, $N(t)$. This is the same principle used when deriving an approximation of the time taken to reach steady state. Our tolerance is then calculated as $\sigma = 10^{-3} * N(t)$. Thus we define simulations which attain DFE as satisfying $I_0 > 0$, and $I_{1,2,3}, E \leq \sigma$. All other steady states are then EE. Of the 4381 simulations, we have 1290 DFE and 3091 EE. We also recall that in Section 3.2, all simulations with EE satisfied $I_1 > I_2 > I_3$. We confirmed that this inequality is true for all 3091 such simulations in this analysis. Qualitatively this means that in all cases where disease persists, individuals at the lowest level of infection dominate the infectious population.

Table 3.2: The parameter values used for computational model simulations. All parameters are taken from a uniform distribution.

Parameter	Min.	Max.
Λ	495.0	505.0
c	0.0020	0.25
μ	0.6440	6.449
δ_1	0.05	0.55
δ_2	0.12	0.9
δ_3	0.95	2.4
α_1	0.2056	0.2061
α_2	0.2522	0.2830
α_3	0.2835	0.2935
γ	0.1	1.0

With a thorough understanding of the data used in this analysis, we can now set up our investigation. We want to investigate transience in relation to $\mathcal{R}_0$. As a preliminary step of our analysis, we first plot our measure for transience (time taken to reach steady state, denoted `SStime`), as a function of $\mathcal{R}_0$. The result is Figure 3.6.

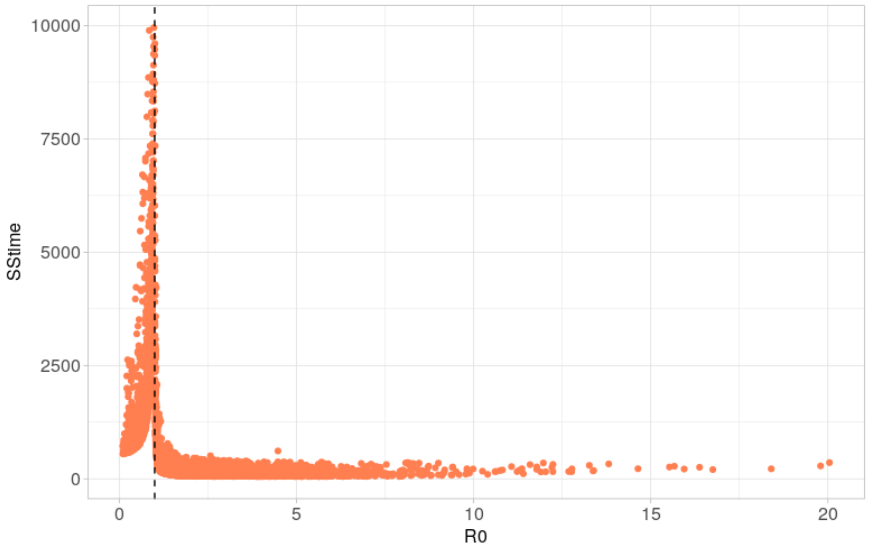

Figure 3.6: A scatter plot comparing the time taken to reach steady state (`SStime` on veritcal axis) against the value of $\mathcal{R}_0$. The value $\mathcal{R}_0 = 1$ is marked with a dashed black line.

.

Figure 3.6 shows that as $\mathcal{R}_0$ approaches 1 (from the left-hand side), time taken to reach steady state increases. As $\mathcal{R}_0 > 1$ increases further, time taken to reach steady state decreases. Excluding points close to $\mathcal{R}_0 = 1$, it seems for $\mathcal{R}_0 < 1$ time taken to reach steady state is higher than when $\mathcal{R}_0 > 1$. Thus, Figure 3.6 implies the following statement is true:

C.1 The value of `SStime` increases and then decreases as $\mathcal{R}_0$ changes from less than to greater than one, respectively.

To evaluate the data in Figure 3.6 we use a piece-wise linear regression model (PWR). Such models can be used to explore linear trends separately for two phases: one before a change/intervention occurs and one during or after the change [58]. The PWR model is written as:

$$y = \beta_0 + \beta_1 x_1 + \beta_2 x_2 + \beta_3 x_2 (x_1 - c) + \rho \text{ [55, 58]}. \tag{3.2}$$

In equation (3.2), y is a vector of length n, with n denoting the total number of observations [55, 58]. The term ρ is a vector with random independent error [55, 58]. x_2 is a dummy variable that distinguishes the data before and after the change has occurred, with $x_2 = 0$ indicating pre-breakpoint data (i.e. no change) and $x_2 = 1$ post-breakpoint data

(i.e. change has occurred) [55, 58]. x_1 represents the independent variable of interest [55]. The value c indicates the final measurement in the pre-breakpoint data [55, 58]. It is chosen such that the values $(x_1 - c)$ start with zero in the post-breakpoint data. The coefficient β_0 is the y-intercept and indicates the start of the regression line in the pre-breakpoint data [55, 58]. The coefficient β_1 represents the trend (of predicted values of y) in the pre-breakpoint data [55, 58]. The coefficient β_2 is interpreted as "the change in level between the [pre-breakpoint data] and the [post-breakpoint data], not confounded with possible trend effects" [58]. Essentially, is it the difference between predicted values of both regression lines at the first measurement of the post-intervention period [58]. The coefficient β_3 represents the trend (of predicted values of y) as the data changes from the pre-breakpoint data to the post-breakpoint data [55, 58].

To set up our PWR model we consider the independent variable y to be `SStime`. We have $n = 4381$ observations. We let x_1 denote the value of the basic reproduction number, $\mathcal{R}_0$. We define the pre-breakpoint data to be data for which $\mathcal{R}_0 \leq 1$, and the post-breakpoint data to be data for which $\mathcal{R}_0 > 1$. Thus the dummy variable x_2 is 0 when $\mathcal{R}_0 \leq 1$ and 1 when $\mathcal{R}_0 > 1$. The value of c is then 1. Our PWR model is then given by equation (3.3).

$$y = \beta_0 + \beta_1 x_1 + \beta_2 x_2 + \beta_3 (x_1 - 1) x_2 + \rho. \tag{3.3}$$

The linear trend for the pre-breakpoint data is then given by the equation (3.4), and the linear trend for the post-breakpoint data is then given by (3.5).

$$y = \beta_0 + \beta_1 x_1 + \rho. \tag{3.4}$$

$$y = (\beta_0 + \beta_2 - \beta_3) + (\beta_1 + \beta_3) x_1 + \rho. \tag{3.5}$$

Using the `lm()` function from the R coding language, we calculate the PWR model, with the resulting output being displayed in Table 3.3.

The value of β_1 shows that with each observation in the pre-intervention period (i.e. data for which $\mathcal{R}_0 \leq 1$), `SStime` increased by 5076.03. That is, the predicted values of `SStime` in the pre-intervention period have a positive slope. The value of β_2 shows for the observation immediately after $\mathcal{R}_0$ became greater than 1, `SStime` decreased by 3540.45. That is, the predicted value of `SStime` for the regression lines $\texttt{SStime} = \beta_0 + \beta_1 t$ (when $\mathcal{R}_0 \leq 1$) and $\texttt{SStime} = \beta_0 + \beta_2 - \beta_3 + (\beta_1 + \beta_3) t$ (when $\mathcal{R}_0 > 1$) differ by 3540.45. The value of β_3 shows in the post-intervention period (i.e. all subsequent observations where $\mathcal{R}_0 > 1$), the slope of

the line is negative. A plot of these results can be seen in figure 3.7. Thus the coefficients from the PWR model agree with statement C.1.

Table 3.3: Coefficients of the linear regression given in equation (3.3)

Dependent variable: SStime			
β_0	β_1	β_2	β_3
-1172.86***	5076.03***	-3540.45***	-5125.93***
Note:	*p< 0.1	**p< 0.05	***p< 0.01

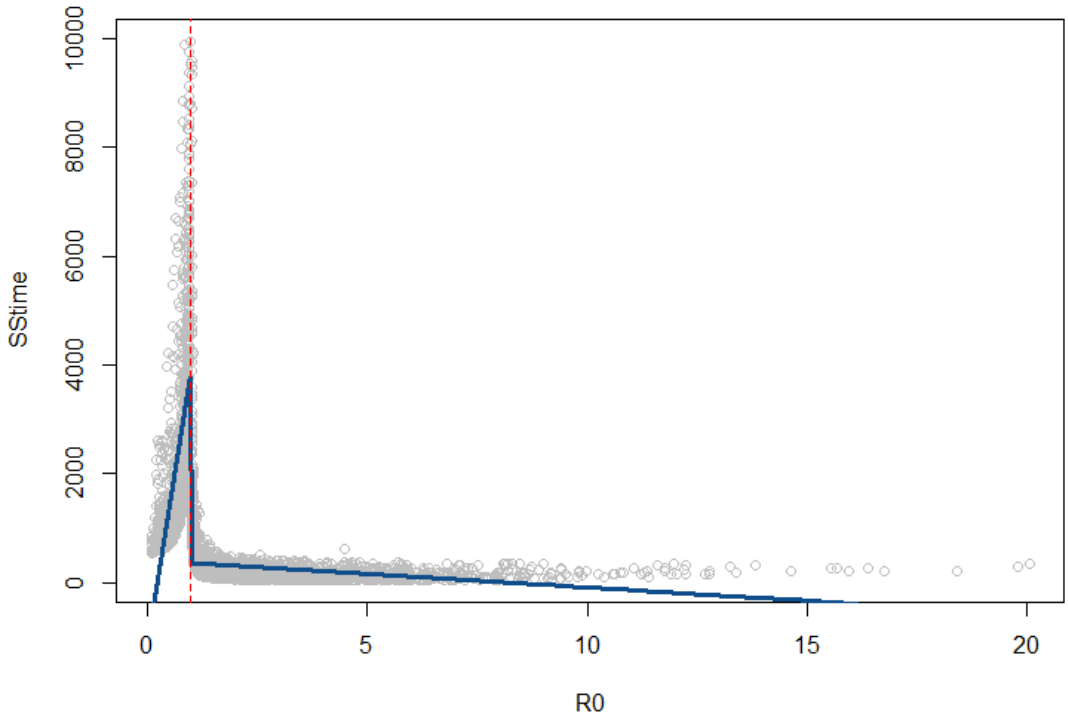

Figure 3.7: A plot of the PWR model. Grey hollow circles denote the data points of the dependent variable, `SStime`, plotted against the observation number. The PWR model is plotted using a dark blue line, which indicates the values of `SStime` predicted by the model. The red dashed line indicates when $\mathcal{R}_0 = 1$.

3.4 $\mathcal{R}_0$ as a sharp criterion for Disease Persistence

In this section we investigate whether $\mathcal{R}_0$ is a good indicator of which equilibrium (DFE vs. EE) will be attained in our model. The data used in the analysis of this section is the same as Section 3.3.

Recall a standard result found in the literature is a statement similar to "if $\mathcal{R}_0 < 1$ the DFE is stable, and if $\mathcal{R}_0 > 1$, the DFE is unstable". More generally, this statement could be viewed as "When $\mathcal{R}_0 < 1$ we predict an infection does not persist in the population, and when $\mathcal{R}_0 > 1$ we predict an infection does persist" [20]. In this section, we will investigate whether such a result holds true in our model through computational analysis. In doing this we aim to answer the question "Is $\mathcal{R}_0$ an appropriate parameter to use as a sharp criterion for persistence of disease?" posed in Section 1.3. Hence, our analysis primarily concerns the following statements:

B.1 If $\mathcal{R}_0 < 1$, then the DFE is attained.

B.2 If $\mathcal{R}_0 > 1$, then the DFE is not attained.

To investigate these statements, we calculate the amount of disease ($|I_1|+|I_2|+|I_3|$), and the population size ($|I_0|+|I_1|+|I_2|+|I_3|$) for each of the 4381 simulations in our data frame. We add these to the data frame discussed in Section 3.3, which had 18 pieces of information for each simulation. Thus for each simulation we now have 20 pieces of information. We then plot the proportion of disease in the population (i.e. disease/population) against the $\mathcal{R}_0$ values for each simulation. This results in Figure 3.8.

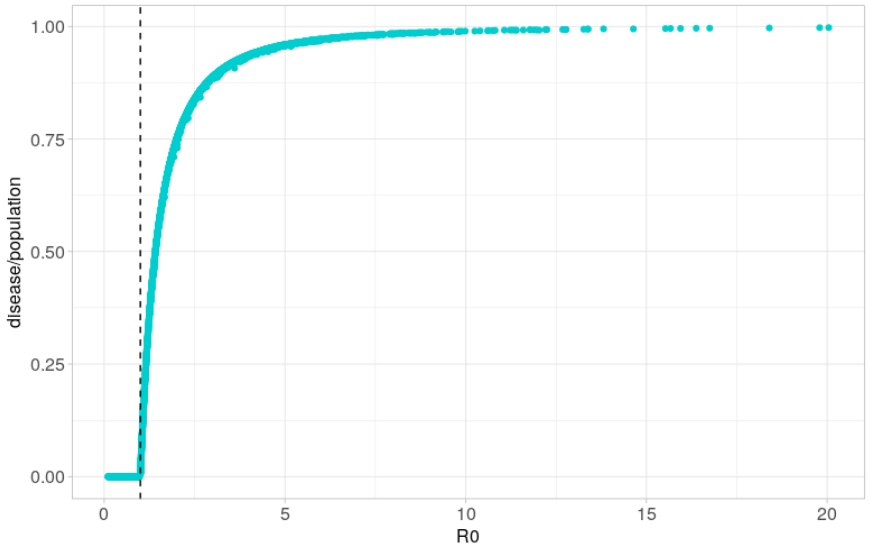

Figure 3.8: A plot comparing the proportion of disease in the population against the value of $\mathcal{R}_0$, for simulations that reached steady state. The value $\mathcal{R}_0 = 1$ is marked with a dashed black line. The y-axis can be interpreted as the percent of the population infected with/carrying disease, ranging from 0% (0.00) to 100% (1.00).

Figure 3.8 shows that for $\mathcal{R}_0 < 1$, the proportion of disease in the population is zero, and for $\mathcal{R}_0 \geq 1$, the proportion of disease in the population is above zero. Thus, it seems that statements B.1 and B.2 are true. To confirm this, we can look at the minimum and maximum values of disease for simulations with $\mathcal{R}_0 < 1$ and $\mathcal{R}_0 \geq 1$. For simulations with $\mathcal{R}_0 < 1$ the minimum and maximum values of the disease ($|I_1|+|I_2|+|I_3|$) are 3.930315e-164 and 4.115687e-161, respectively. For simulations with $\mathcal{R}_0 > 1$ the minimum and maximum values of the disease ($|I_1|+|I_2|+|I_3|$) are 0.6345477 and 741.2678, respectively. Thus for $\mathcal{R}_0 < 1$, the maximum is effectively zero, confirming that the proportion of disease in the system is zero. Therefore, statement B.1 is strictly true. For $\mathcal{R}_0 \geq 1$, the minimum is sufficiently above zero and the maximum is clearly greater than zero. The minimum and maximum values of disease for $\mathcal{R}_0 \geq 1$ are roughly equal to 0.58% of the population carrying infection and 99.7% of the population carrying infection, respectively. Therefore, statement B.2 is strictly true.

3.5 Computational Stability Analysis

In this section, we aim to further explore the stability of the DFE. We use the same data which was generated in Section 3.3. To perform the analysis in this section, we must compute additional data for each simulation. The first pieces of data are related to the inequalities $G1$ and $G2$ from theorem 2.4.1 in Section 2.4. The second piece of data is related to the eigenvalues of the matrix described by equation (2.8) in Section 2.4. We will first describe why and how additional data was calculated. Then, we discuss the results.

Recall in Section 2.4 we were only able to gain partial results for the stability of the disease-free equilibrium. From theorem 2.4.1, we know that if either the inequalities $G1$ or $G2$ are satisfied, then the DFE is asymptotically stable. We use the notation $G1$ to describe the inequalities $\mu \geq \frac{c\Lambda}{\mu}, \mu + \delta_1 \geq \frac{c\Lambda}{\mu}, \delta_2 + \mu \geq \delta_1, \delta_3 + \mu \geq \delta_2, \gamma \geq \alpha_1 + \alpha_2 + \alpha_3$. The notation $G2$ refers to the inequalities $\mu \geq \alpha_1,\ \mu \geq \alpha_2,\ \mu + \delta_3 \geq \alpha_3$, and $\gamma \geq \frac{2c\Lambda}{\mu}$. We can reduce these four inequalities in $G2$ to two by using model assumption A.6 and the fact that all parameters in Table 3.2 are positive. The former allows us to write write $\mu \geq \alpha_3$ instead of $\mu \geq \alpha_{1,2}$. The latter guarantees $\delta_3 + \mu \geq \alpha_3$ is trivially satisfied. Thus to asses whether the inequalities from $G2$ hold, we need only consider whether $\mu \geq \alpha_3$ and $\gamma \geq \frac{2c\Lambda}{\mu}$ are true. For the 4381 simulations that reached steady state, we investigate if $G1$ and/or $G2$ are satisfied.

To investigate $G1$, we use the fact that the first four inequalities all contain μ. We can isolate μ on one side, leading to the inequalities $\mu \geq \sqrt{c\Lambda}, \mu^2 + \delta_1\mu - c\Lambda \geq 0, \mu \geq \delta_1 - \delta_2, \mu \geq \delta_2 - \delta_3$. The quadratic inequality has solutions given by the quadratic formula, i.e. $\mu_{1,2} = \dfrac{-\delta_1 \pm \sqrt{\delta_1^2 + 4c\Lambda}}{2}$. Thus, we can set $M_1 = \max\{\sqrt{c\Lambda}, \mu_1, \mu_2, \delta_1 - \delta_2, \delta_2 - \delta_3\}$. If the first four inequalities in $G1$ are satisfied, we must have $\frac{\mu}{M_1} \geq 1$. We define $\frac{\mu}{M_1}$ as `G1a`, i.e. `G1a` $:= \frac{\mu}{M_1}$. For the last inequality, we can divide both sides by $\alpha_1 + \alpha_2 + \alpha_3$ to get $\frac{\gamma}{\alpha_1+\alpha_2+\alpha_3} \geq 1$. We then define `G1b` as `G1b` $:= \frac{\gamma}{\alpha_1+\alpha_2+\alpha_3}$.

Since all of the inequalities in $G2$ have μ in them, we can isolate μ on one side. From Table leading to the inequalities $\mu \geq \alpha_3$ and $\mu \geq \frac{2c\Lambda}{\gamma}$. Then we can set $M_2 = \max\{\alpha_3, \frac{2c\Lambda}{\gamma}$. If the inequalities in $G2$ are satisfied, we must have $\frac{\mu}{M_2} \geq 1$. We calculate the value $\frac{\mu}{M_2}$ for each simulation that reached steady state, and define `G2` as `G2` $:= \frac{\mu}{M_2}$. Thus the inequalities $G1$ and $G2$ become `G1a,G1b,G2`, where `G1a`≥ 1 and `G1b`≥ 1 indicates $G1$ is satisfied, and `G2`≥ 1 indicates $G2$ is satisfied. We do this calculation for each the 4381 simulations that reached steady state.

We can also use the eigenvalues of the Jacobian matrix evaluated at the DFE (See equation (2.8) in Section 2.4 for the matrix) to investigate the stability of the DFE. Differential

equations theory tells us that if the real components of all eigenvalues are negative, then the DFE is asymptotically stable (See chapter 17 of [59] for reference). For each of the 4381 simulations, we compute the maximum value of the real component of said eigenvalues using using the `eigen()` function in R[45]. We call this quantity `Max_Eval`. When `Max_Eval` is negative, all real components of the eigenvalues are also negative, and we can conclude then that the DFE is asymptotically stable [59]. When `Max_Eval` is positive, then not all real parts of the eigenvalues are negative, and we can conclude the DFE is unstable [59]. We do this calculation for each the 4381 simulations that reached steady state.

We add `Max_Eval` in addition to `G1a, G1b, G2` to the data frame from Section 3.4, which had 20 pieces of information for each simulation. The result is a data frame which now contains 24 pieces of information for each simulation. That is, by adding the calculated quantities from sections 3.4 and 3.5 to the data frame generated in Section 3.3, we have increased the number of columns from 18 to 24. The number of rows in this data frame corresponds to the number of simulations that reached steady state, and thus remains as 4381 for each of sections 3.3, 3.4, 3.5. To summarize, columns 1 to 24 of the data frame contain the time taken to reach steady state, the value of each component of the steady state (of which there are 5), the value of $\mathcal{R}_0$, the iteration number of the simulation, and the parameter values for the simulation (of which there are 10), the amount of disease in the population ($|I_1|+|I_2|+|I_3|$), the population size ($|I_0|+|I_1|+|I_2|+|I_3|$), the quantity `G1a`, the quantity `G1b`, the quantity `G2`, and the quantity `Max_Eval`, respectively.

Now we can report the results obtained by calculating `G1a,G1b,G2` and `Max_Eval`. Of the 4381 simulations that reached steady state, 1290 attained DFE (called DFE simulations) and 3091 achieved an equilibrium with disease being present (referred to as EE simulations). For easier reading, we summarize the data in Table 3.4. From our discussion we know the following statements hold: `G1a`≥ 1 and `G1b`≥ 1 means the inequalities labelled $G1$ are satisfied and the DFE is thus asymptotically stable, `G2`≥ 1 means the inequalities labelled $G2$ are satisfied and the DFE is thus asymptotically stable, `Max_Eval`< 0 implies the DFE is asymptotically stable while `Max_Eval`> 0 implies the DFE is unstable. The result for of the statement `G1a`≥ 1 and `G1b`≥ 1 do not allow us to make conclusions about the stability of the DFE. That is, the inequalities described by $G1$ are far from a necessary conditions. The same is true for `G2`. For all simulations which attain DFE, `Max_Eval` is negative, implying all DFE in these 1290 simulations are asymptotically asymptotically stable. For all simulations which attain EE, `Max_Eval` is positive, implying all DFE in these 3091 simulations are unstable. The computational experiment shows the conditions from theorem 2.4.2 are indeed only

sufficient and not also necessary.

Table 3.4: The truth value of statements, DFE attained, `G1a`≥ 1 and `G1b`≥ 1, `G2`≥ 1, and `Max_Eval` < 0, for all model simulations. Of the 4381 simulations, 1290 attain DFE and 3091 attain EE.

DFE attained	`G1a`≥ 1 and `G1b`≥ 1	`G2`≥ 1	`Max_Eval`< 0
TRUE	FALSE	FALSE	TRUE
FALSE	FALSE	FALSE	FALSE

3.6 Sobol Sensitivity Analysis

Following Section 2.6 we perform local sensitivity analysis (SA) computationally using Sobol Sensitivity Analysis. In contrast to the mathematical SA in Section 2.6 which used partial derivatives, Sobol SA is a statistical based analysis which uses variance-based analysis. We aim to understand what this analysis tells us about the model parameter's affects on $\mathcal{R}_0$ and transience, represented by time taken to reach steady state. We will first provide some background information for the package `sensobol`, then describe how the data was generated, describe the results of the analysis, and conclude by contrasting them against results from our local sensitivity analysis in Section 2.6.

The R package `sensobol` uses variance-based sensitivity analysis to evaluate the sensitivity in model output (with respect to parameters) [44]. In [44], a model is defined as an equation of the from $y = f(\mathbf{x})$, where $\mathbf{x}$ is a vector defined by $\mathbf{x} = (x_1, x_2, \ldots, x_i, \ldots, x_k)$, $x_i \in \mathbb{R}^k$, $i = 1, \ldots, k$, with y being a scalar output and $x_1, \ldots, x_k$ being k uncertain parameters described by probability distributions. In our first SA, y is $\mathcal{R}_0$, and in our second SA, y is `SStime`. In both analyses, the components x_i of the vector $\mathbf{x}$ are the $k = 10$ uncertain parameters, $\Lambda, c, \mu, \delta_{1,2,3}, \alpha_{1,2,3}, \gamma$, each given by a uniform distribution. One way of assessing how sensitive y is to changes in x_i is to investigate how much the variance in y decreases after fixing x_i to its "true" value x_i^*, denoted by $V(y|x_i = x_i^*)$. Often, such a value of x_i is unknown, thus instead the mean of the variance of y is taken after fixing x_i to all possible values over an uncertainty range, whilst all other parameters are varied [44]. This is written as $E_{x_i}[V_{\mathbf{x}\sim i}(y|x_i)]$, with $\mathbf{x} \sim i$ meaning all parameters but x_i, $E(.)$ and $V(.)$ being the mean and the variance operators, respectively [44]. The variance of y is written as $V(y) = V_{x_i}[E_{\mathbf{x}\sim i}(y|x_i)] + E_{x_i}[V_{\mathbf{x}\sim i}(y|x_i)]$ where $V_{x_i}[E_{\mathbf{x}\sim i}(y|x_i)]$ is called the first-order effect of x_i and $E_{x_i}[V_{\mathbf{x}\sim i}(y|x_i)]$ the residual [44]. The importance of a parameter x_i on conditioning

$V(y)$ is demonstrated when its first order effect is high [44]. This property of $V_{x_i}[E_{\mathbf{x}\sim i}(y|x_i)]$ can be demonstrated by plotting the model output y against the range of values in x_i, dividing the latter into n bins and computing the mean y in each bin. The idea is that the parameter whose mean y values are most varied has the highest direct influence in the model output [44]. Repeating this process over subsequently smaller bins (or rather, increasing n) is the conditional variance of x_i on $V(y)$, i.e. $V_{x_i}[E_{\mathbf{x}\sim i}(y|x_i)]$ [44].

If $\mathbf{x} = x_1, x_2, \ldots, x_k$ are independent of each other, $V(y)$ is decomposed as the sum of all partial variances up to the k-th order:

$$V(y) = \sum_{i=1} V_i + \sum_i \sum_{i<j} V_{ij} + \cdots + V_{1,2,\ldots,k}, \tag{3.6}$$

where

$$V_i = V_{x_i}[E_{\mathbf{x}\sim i}(y|x_i)] \tag{3.7}$$

$$V_{ij} = V_{x_i,x_j}[E_{\mathbf{x}\sim i,j}(y|x_i,x_j)] - V_{x_i}[E_{\mathbf{x}\sim i}(y|x_i)] - V_{x_j}[E_{\mathbf{x}\sim j}(y|x_j)]. \tag{3.8}$$

Since 3.6 is similar to the functional decomposition scheme in [52]:

$$f(\mathbf{x}) = f_0 + \sum_i f_i(x_i) + \sum_i \sum_{i<j} f_{ij}(x_i,x_j) + \cdots + f_{1,2,\ldots,k}(x_1,x_2,\ldots,x_k)$$

where

$$f_0 = E(y) \quad f_i = E_{\mathbf{x}\sim i} - f_0 \quad f_{ij} = E_{\mathbf{x}\sim ij} - f_i - f_j - f_0, \ldots,$$

we can write

$$V_i = V[f_i(x_i)] \quad V_{ij} = V[f_{ij}(x_i,x_j)], \ldots \ .$$

So-called Sobol indices (See [52]) are then calculated as

$$S_i = \frac{V_i}{V(y)} \quad S_{ij} = \frac{V_{ij}}{V(y)}, \ldots \tag{3.9}$$

We call S_i the first-order effect of x_i, S_{ij} the second-order effect of (x_i, x_j) (i.e. the effect caused by the first order effect of x_i, x_j and their interaction), and so on [44]. Practically, S_i is used in "factor prioritization", a process where S_i is used to "rank" parameters given their reported contribution to the uncertainty in model output [44]. However, S_i alone is

often insufficient when accounting for all of a model's output variance. Thus, `sensobol` also calculates the total order index T_i, which "measures the first-order effect of x_i jointly with its interactions with all the other parameters" [44]. Thus, T_i includes all terms in equation (3.6) with index i and can be computed as:

$$T_i = 1 - \frac{V_{\mathbf{x}\sim i}[E_{x_i}(y|\mathbf{x}_{\sim i})]}{V(y)} = \frac{E_{\mathbf{x}\sim i}[V_{x_i}(y|\mathbf{x}_{\sim i})]}{V(y)}. \tag{3.10}$$

Now that we understand the sensitivity indices generated in this analysis, let us describe the simulation set up.

The first step of the SA is to choose what parameter range to use for each model parameter in equations (2.1)-(2.5). We use the same set up for parameters as Section 3.3. However, we must note while that the ranges for the distributions from which parameters are selected are the same as Section 3.3, the specific values of parameters for each simulation will differ from those in Section 3.3. This distinction is caused by the different requirements of matrix formatting for computation with the `sensobol` package as compared to the `deSolve` package.

In the next stage of the SA, we set the number of simulations to be performed. For SA, it is important to pick a large number of simulations. In this analysis, we run 4800 simulations for both the SA of $\mathcal{R}_0$ and `SStime`. A single simulation is described as follows: first parameter values are retrieved from the matrix, then the quantity of interest is calculated (in the first SA this quantity is $\mathcal{R}_0$, for the second `SStime`). To reduce computational time, each of these simulations are run in parallel using the packages `foreach, doParallel`. The chosen quantities of interest are then stored in another matrix. In the SA of $\mathcal{R}_0$, we only need to use the packages `sensobol, foreach, doParallel` because we can calculate $\mathcal{R}_0$ directly from model parameters (see equation (2.17)). Thus for each of the 4800 simulations run in the SA of $\mathcal{R}_0$, we have a corresponding $\mathcal{R}_0$ value. However, to compute the quantity of interest in the SA of `SStime`, we first need to numerically integrate the model. Thus, for the SA of `SStime`, we use the package `deSolve` in addition to `sensobol, foreach, doParallel`. We use the same initial conditions and approximation of `SStime` outlined in Section 3.3. Of the 4800 simulations run to perform SA of `SStime`, 4222 reached steady state. After all simulations are performed and data is recorded, we can then use the `sensobol` package to calculate the Sobol sensitivity indices, S_i and T_i.

The computed S_i and T_i of the SA for $\mathcal{R}_0$ are plotted in Figure 3.9. Results for $\mathcal{R}_0$ show that the parameter with the largest first-order effect is μ, with γ, c, having the second and third largest S_i values, respectively. For all other parameters, their S_i values are so low we

say they don't have any first-order effects. The trend for T_i values is the same, that is, μ has the largest T_i value, with γ and c having the second and third largest T_i values, respectively. For each of μ, γ, c, T_i their values are higher than their S_i values, so it is their higher-order effects (i.e. combination with other parameters) that have a greater impact on $\mathcal{R}_0$. For the SA of `SStime` sensitivity indices are not computed for all parameters, meaning the SA is inconclusive.

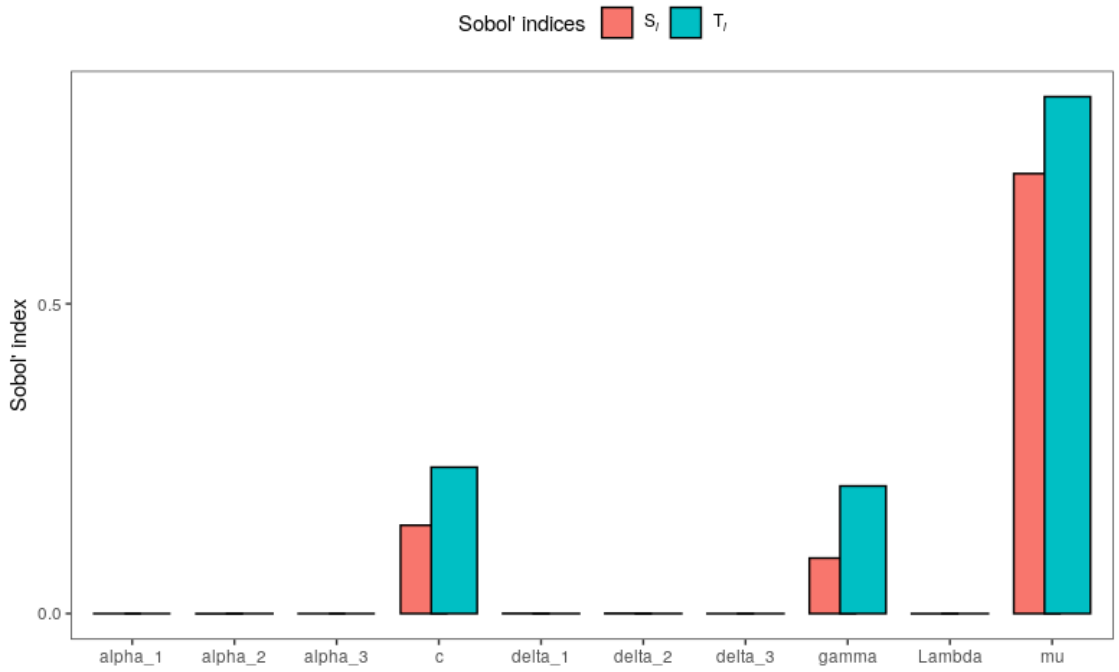

Figure 3.9: A bar plot of the first order Sobol sensitivity indices S_i, and the total order Sobol sensitivity indices T_i of $\mathcal{R}_0$ with respect to each of the model parameters. For each parameter, both S_i and T_i are plotted next to each other, with S_i in red and T_i in blue.

It is important to note that while Sobol sensitivity analysis gives us great insight into parameters affecting $\mathcal{R}_0$, these results are local, and will change for different parameter ranges. Hence, any conclusions we draw from our Sobol sensitivity analysis of $\mathcal{R}_0$ won't necessarily apply to other parameter ranges. To illustrate this, we repeat the Sobol sensitivity analysis for 5 different parameter sets, listed in Tables A.1-A.5, with results plotted in Figures A.1-A.5. Generally, Figures A.1-A.5 show a similar pattern: the parameters $\mu, \gamma, c, \alpha_1, \delta_1$ have sufficiently high S_i and T_i values. In all parameter sets, $S_i < T_i$, implying the combination of these parameters with others is more significant than their first-order (i.e. direct) effects.

Additionally, both the S_i and T_i values are highest for μ across all parameter sets. However, there is much variation between the remaining parameters $(\gamma, c, \alpha_1, \delta_1)$. For the first parameter set (Figure A.1), the indices for γ look slightly higher than those for c, α_1, which look approximately equal, and δ_1's indices are very low. Then in the second parameter set (Figure A.2) the indices for c, γ are highest and approximately equal, meanwhile the indices for α_1, δ_1 are very small. In the third parameter set, (Figure A.3) the pattern remains the same as the second, but with an increase in values for the indices. Results for the third and fourth parameter sets (Figure A.4)-(A.5)) look approximately the same as the third.

To finish this section, we compare the results of the Sobol SA of $\mathcal{R}_0$ with the local sensitivity analysis of $\mathcal{R}_0$ performed in Section 2.6. In Section 2.6, we determined that $\mathcal{R}_0$ was a monotonically increasing function with respect to $\Lambda, c, \mu, \delta_3, \alpha_{1,2,3}$, and a monotonically decreasing function with respect to μ, γ. For $\delta_{1,2}$, results depended on the values of other parameters. The role of $\delta_{1,2}$ was thus left unclear in our local sensitivity analysis. In our computational SA, we find that only the parameters c, γ, μ have an impact on $\mathcal{R}_0$. However, it is the combined affects of c, γ, μ with other parameters that have the most impact on $\mathcal{R}_0$. The Sobol SA indicates that the influence of $\delta_{1,2}$ is only significant when combined with other parameters, thus confirming $\delta_{1,2}$ do not have a clear impact the way the other parameters do. However, we must remain aware that such conclusions are only relevant for the selected parameter ranges, i.e. those in Table 3.2.

With our computational analysis finished, we are ready to discuss the results of this thesis.

Chapter 4

Discussion

This thesis was originally motivated by studying the obligate intracellular spore-forming parasite *Nosema ceranae* which spreads in the Western honey bee, *Apis mellifera*. *N. ceranae* is spread predominantly by indirect transmission, whereby an infected worker bee will deposit spores in the hive through defecation, and an uninfected worker bee will then ingest said spores in the process of comb cleaning, resulting in infection. The hive is thus viewed as the environment in which the *Nosema* spores multiply (as a result of individuals depositing spores into the environment, not as a result of the spores themselves replicating through a biological process). Due to the high variation in spore counts of individual bees, we hypothesized that incorporating discrete stage-structure in infectious compartments could provide new insights. Hence, our aim was to construct a compartmental SIR model for *N. ceranae* which used both indirect transmission and discrete stage structure. However, after performing an adapted scoping literature review, we found that there was very little, if any, research on generic disease models with this structure. Hence, it was necessary to first investigate the dynamics of a generic stage structured model with indirect transmission before adapting it to become a *N. ceranae* model. This review also revealed that many researchers focus on establishing $\mathcal{R}_0$ as a sharp criterion for stability of the disease-free equilibrium by way of a Lyapunov function. While such information is important in understanding the behaviour of a model, it does not give a full picture of how disease spreads in a given system. Thus, we aimed to address disease dynamics in our model both as it relates to both $\mathcal{R}_0$ and transient behaviour.

For easier reading, we will structure each of our discussion points as sections. We begin in Section 4.1 by summarizing the main findings of our research. In Section 4.2 we address the questions posed by the literature review. In Section 4.3 we propose a *N. ceranae* model which incorporates indirect transmission and discrete stage structure. We conclude in Section 4.4

with the limitations of our research.

4.1 Research Summary

In this thesis, we derived a deterministic discrete stage-structured SIR model with indirect transmission. The model has 4 compartments for individuals, with I_0 representing susceptible individuals, I_1 representing individuals in the lowest level of infection, I_2 representing individuals in the middle level of infection, and I_3 representing individuals in the highest level of infection. There is also an environmental reservoir, E, which represents the number of spores in the system. There are also 10 model parameters represented by $\Lambda, c, \mu, \delta_{1,2,3}, \alpha_{1,2,3}$ and γ. The parameter Λ represents the natural birth rate. The parameter c represents the infection rate for susceptible individuals I_0 reaching the lowest level of infection I_1. The parameter μ represents the natural death rate. The parameter δ_1 represents the infection rate for individuals in the lowest level of infection I_1 reaching the middle level of infection I_2. The parameter δ_2 represents the infection rate for individuals in the middle level of infection I_2 reaching the highest level of infection I_3. The parameter δ_3 represents disease related death for individuals in the highest level of infection. The parameters $\alpha_{1,2,3}$ represent the spore deposition from individuals in compartments $I_{1,2,3}$, respectively. Finally, the parameter γ represents the spore decay rate.

We showed this model was well-posed in the sense of [59]; existence, uniqueness, and continuous dependence on data are satisfied globally. In our mathematical approach we were able to derive sufficient but not necessary conditions for the stability of the disease-free equilibrium. These conditions were derived from Gershgorin's Theorem for estimating eigenvalues. The result stated that if the model parameters satisfied either of the inequalities $\mu \geq \frac{c\Lambda}{\mu}, \mu + \delta_1 \geq \frac{c\Lambda}{\mu}, \delta_2 + \mu \geq \delta_1, \delta_3 + \mu \geq \delta_2,$ and $\gamma \geq \alpha_1 + \alpha_2 + \alpha_3,$ or ,$\mu \geq \alpha_1,\ \mu \geq \alpha_2,\ \mu + \delta_3 \geq \alpha_3,$ and $\gamma \geq \frac{2c\Lambda}{\mu}$, then the disease-free equilibrium is asymptotically stable. Each of these inequalities has a biological interpretation. The inequalities $\mu \geq \frac{c\Lambda}{\mu}$ and $\mu + \delta_1 \geq \frac{c\Lambda}{\mu}$ amount to infection is unable to spread at a sufficient rate to cause disease. The inequalities $\delta_2 + \mu \geq \delta_1$ and $\delta_3 + \mu \geq \delta_2$ means infected individuals leave their compartments faster than new individuals are entering them. The inequality $\gamma \geq \alpha_1 + \alpha_2 + \alpha_3$ means spore decay is higher than the rate at which spores are replenished in the environment. The inequalities $\mu \geq \alpha_{1,2},\ \mu + \delta_3 \geq \alpha_3$ indicates that infected individuals die faster than they can deposit spores. The last inequality $\gamma \geq \frac{2c\Lambda}{\mu}$ indicates spores decay at a faster rate than individuals can transmit infection. Across thousands of computational simulations we verified that these

conditions are indeed only sufficient. We also calculated the basic reproduction number, $\mathcal{R}_0$, using the Next Generation Matrix approach. We then studied the influence of parameters on the value of $\mathcal{R}_0$ through local sensitivity analysis. We found that $\mathcal{R}_0$ is a monotonically increasing function with respect to the natural birth rate, Λ. That is, we have "full control" over the value of $\mathcal{R}_0$ by varying Λ. That is, with all other parameters held constant, we can unilaterally vary Λ to get $\mathcal{R}_0 > 1$ or $\mathcal{R}_0 < 1$ independently of all other parameters. The same results hold for the parameter c. We also showed that $\mathcal{R}_0$ is a monotonically increasing function with respect to each of the spore deposition rates $\alpha_{1,2,3}$. However, we do not have unilateral control of the value for $\mathcal{R}_0$ using $\alpha_{1,2,3}$. If $\mathcal{R}_0 < 1$ we can increase either of $\alpha_{1,2,3}$ to get $\mathcal{R}_0 > 1$, but the converse is not necessarily true. The basic reproduction number is also a monotonically increasing function with respect to δ_3. With respect to μ and γ, $\mathcal{R}_0$ is a monotonically decreasing function. We again have full control over the value of $\mathcal{R}_0$ with the parameters μ, γ. For both of δ_1 and δ_2 there was no clear influence on $\mathcal{R}_0$. We then compared the results of our local sensitivity analysis against a computational Sobol sensitivity analysis. The Sobol sensitivity analysis showed that the parameters c, μ, γ had direct influence on $\mathcal{R}_0$. However, their direct impact was not as significant as their impact in combination with other parameters. In our mathematical results we were unable to establish $\mathcal{R}_0$ as a strict criterion for disease persistence using the traditional methods found in the literature. That is, we do not have mathematical proof using a Lyapunov function showing that $\mathcal{R}_0 < 1$ corresponds to DFE stability, and $\mathcal{R}_0 > 1$ corresponds to DFE instability. However, the results of thousands of model simulations indicate that this is true for our model. Thus we conjecture that $\mathcal{R}_0$ is suitable as a sharp criterion for disease persistence. Moreover, the results from the eigenvalues of the Jacobian matrix evaluated at the DFE showed that for simulations that attained DFE (which all have $\mathcal{R}_0 < 1$), the DFE is asymptotically stable, and for simulations that did not attain DFE (which all have $\mathcal{R}_0 \geq 1$), the DFE is unstable. Thus, we conjecture that $\mathcal{R}_0$ also serves as a sharp criterion for the stability of the DFE. The "big picture" interpretation of this material is that if susceptible individuals exit the population (via death) faster than the disease can spread, then the disease will die out.

4.2 Comparison Against the Literature

One of the results from the literature review suggested that there is a lack of knowledge surrounding SIR models with both stage-structure of disease based on viral load and disease spread characterized by indirect transmission. Thus, we must investigate the question,

"What knowledge is gained by incorporating stage-structure?". In this research, stage-structure refers to the multiple infectious compartments I_1, I_2, I_3 through which individuals progress based on the proliferation of the pathogen in their bodies. We will focus on results concerning the stability of the DFE. To compare our results against a SIR model without stage-structure, we first reformulate the model equations in (2.1)-(2.5) to include a single infectious compartment. This results in the following three-dimensional system:

$$\frac{dI_0}{dt} = \Lambda - cEI_0 - \mu I_0 \tag{4.1}$$
$$\frac{dI_1}{dt} = cEI_0 - \delta_3 I_1 - \mu I_1 \tag{4.2}$$
$$\frac{dE}{dt} = \alpha I_1 - \gamma E. \tag{4.3}$$

The DFE of the single-compartment system is given by $(I_0^*, I_1^*, E^*) = (\frac{\Lambda}{\mu}, 0, 0)$ and the corresponding Jacobian matrix evaluated at the DFE is:

$$\mathcal{J}(I_0^*, 0, 0) = \begin{bmatrix} -\mu & 0 & -c\frac{\Lambda}{\mu} \\ 0 & -\delta_3 - \mu & c\frac{\Lambda}{\mu} \\ 0 & \alpha & -\gamma \end{bmatrix}. \tag{4.4}$$

The first eigenvalue of the matrix is $-\mu$. The remaining eigenvalues are given by the eigenvalues of the sub-matrix

$$\mathbf{B} = \begin{bmatrix} -\mu - \delta_3 & c\frac{\Lambda}{\mu} \\ \alpha & -\gamma \end{bmatrix}. \tag{4.5}$$

The trace-determinant classification of stability for planar systems tells us that if $trace(\mathbf{B}) < 0$ and $det(\mathbf{B}) > 0$, the DFE is asymptotically stable. The trace of $\mathbf{B}$ is given by $-(\mu+\delta_3+\gamma)$, hence $trace(\mathbf{B}) < 0$. The determinant of $\mathbf{B}$ is given by $(\mu + \delta_3)\gamma - \frac{c\Lambda\alpha}{\mu}$. We conjectured that $\mathcal{R}_0$ serves as a sharp criterion for the stability of the DFE for the multi-compartmental system (2.1)-(2.5). In order to compare the stability criterion for the DFE of both systems, we will rewrite the determinant of matrix $\mathbf{B}$ so that it parallels the formula for $\mathcal{R}_0$ of the multi-compartmental system. Since we require $det(\mathbf{B}) > 0$, we have $(\mu + \delta_3)\gamma - \frac{c\Lambda\alpha}{\mu} > 0$. Adding $\frac{c\Lambda\alpha}{\mu}$ to both sides gives $(\mu + \delta_3)\gamma > \frac{c\Lambda\alpha}{\mu}$. We then divide both sides of the inequality by $(\mu + \delta_3)\gamma$ and take the square root, which results in the following inequality:

$$1 > \sqrt{\frac{c\Lambda}{\mu\gamma}}\sqrt{\frac{\alpha}{\mu+\delta_3}}. \tag{4.6}$$

This inequality is a much simpler version of the formula for $\mathcal{R}_0$ given in equation (2.17), with the second term $\sqrt{\Psi}$ being replaced with $\sqrt{\frac{\alpha}{(\mu+\delta_3)}}$. Additionally, the inequality in equation (4.6) does not contain either of δ_1 or δ_2 which are present in equation (2.17). So adding multiple compartments to the system described in equations (4.1)-(4.3) gives us a more refined description than what we can obtain without including multiple infectious compartments. This refined information might be beneficial for remedial strategies in a public health context.

Another result from the literature review suggested that researchers tend to focus solely on $\mathcal{R}_0$ as a sharp criterion for DFE stability. Predicting the timescale of a disease, whether a disease is likely to persist or die out, and which factors are most likely to influence its spread are crucial in the context of disease management. That is, by investigating the dynamics of the disease at hand one can gain valuable information about what disease management strategies could be effective. We investigated disease dynamics by investigating the transience of our system. Our investigation of transience concerns model solutions which have already obtained equilibrium. Our equilibria are categorized as those that attain DFE, i.e. solutions in which disease persists, and those that attain EE, i.e. solutions in which disease persists. Since transience measures how quickly (or slowly) something changes in a system, we use the time taken to reach steady state as a measure of transience. Effectively, time taken to reach steady state measures how quickly (or slowly) the disease persists (or establishes) in the system. When comparing time taken to reach steady state against $\mathcal{R}_0$, we found that (generally) it takes a disease longer to die out than to spread (i.e. values of $\mathcal{R}_0$ less than or bigger than 1 but not close to 1). However, when $\mathcal{R}_0$ is close to the threshold value 1, it takes much longer for the disease to establish. We also investigated the relationship between time taken to reach steady state and model parameters via Sobol sensitivity analysis. Unsurprisingly, results showed that it is the combination of model parameters that most impact time taken to reach steady state, rather than direct influence of any particular parameter. We also found that in all simulations where disease persisted, $I_1 > I_2 > I_3$, where each $I_j (j = 1, 2, 3)$ denotes the individuals at the lowest, middle, and highest levels of infection, respectively. Similar results can be seen for diseases such as COVID-19 and influenza (i.e. the common flu). The latest COVID-19 numbers from the Government of Canada report that of the 4,625,842 total confirmed cases 3,474 are

occupying hospital beds [42]. In the FluWatch annual report summary for the 2021-2022 influenza season, the Government of Canada reports that out of 16,126 laboratory-confirmed influenza detection, only 776 are influenza-associated hospitalizations [41].

Other approaches in the literature for investigating disease dynamics can be varied. We will provide three examples of how disease dynamics were investigated in the literature from Section 1.3. Our first example comes from [8]. In [8] a model exploring the impact of climatic factors and human behaviour on the spread of cholera is proposed. The model incorporates both direct and indirect transmission, where indirect transmission is a result of "environmental knowledge", i.e. the level of education on the spread of cholera [8]. To investigate the spread of disease, the authors performed model simulations to analyse the effect of malnourishment, behaviour (respect of hygiene standards) of population, and the recovery rate [8]. For the model simulations, parameters denoting the proportion of undernourished individuals, contact rate of direct transmission, proportion of the people who respect the standards hygiene, and recovery rate of symptomatic infected individuals were varied [8]. The results showed differences between the number of asymptomatic and symptomatic infected individuals as different parameters were varied [8]. The authors conclude that disease spread becomes more important for values corresponding to an increase in $\mathcal{R}_0$, for $\mathcal{R}_0 > 1$ [8]. Importantly, this result establishes a relationship between the value of $\mathcal{R}_0$ and the spread of cholera, just as our investigation establishes a relationship between time taken to reach steady state and transience.

Another example is found in a cholera model by [46], the authors analyse disease dynamics by calculating the "final outbreak size" of the disease [46]. This research proposes a multi-patch model in which direct transmission occurs within each patch and indirect transmission occurs via a single shared water source [46]. In this case, patches are defined by geographical location [46]. Essentially, infected individuals spread cholera within their own patch via direct transmission, and indirectly to other patches by shedding the pathogen *Vibrio cholerae* in a water source shared by all. Considering 2 patches, the authors calculate a final outbreak size for both patch 1 and 2 [46]. The resulting equations show sharing of a water source increases the final outbreak size as compared to when two patches are isolated [46]. That is, the addition of indirect transmission increases the final outbreak size. Importantly, all equations relating to the final outbreak size in [46] include $\mathcal{R}_0$ and assume $\mathcal{R}_0 > 1$. Thus, the final outbreak size is dependent on using $\mathcal{R}_0$ as a criterion for disease persistence.

Our third example comes from HIV models proposed in [22]. In this study, two models were used to study how variations of infectiousness of individuals impact the spread of HIV

[22]. The first model accounts for two things; the different levels of virus between individuals during the chronic phase of infection, and the increase in the average time from infection to AIDS that goes along with a decreased viral load [22]. The second model follows the approach of our model, which assumes "infected individuals progress through a series of infection stages, with the infectiousness of a person depending upon his current disease stage" [22]. The authors investigate disease dynamics by investigating the "relative impact" of the infected groups on the spread of the epidemic [22]. More specifically, their aim is to investigate how the fraction of the infections attributed to each infected compartment is directly related to the assumptions regarding length of time spent in each compartment and each compartment's infectivity [22]. The relative impact is defined as "the fraction of individuals being infected whose infecting partner comes from group i" [22]. In order to compare the relative impact between the two models, the authors first perform numerical simulations of the models (just as [8]) [22]. For the both model simulations, the authors use four infectious compartments [22]. Next, the authors compare how quickly the simulated values of the relative impact converge to their value at steady state specifically for equilibria which are not disease free [22]. Note that the values of the relative impact at steady state explicitly contain $\mathcal{R}_0$ [22]. For the first model, results indicate the first infected group causes the most infections early in the epidemic, but as time passes the second infected group becomes the most important in terms of transmission [22]. For the second model, the first infected group also transmits the bulk of infections early in the epidemic, however, as time passes the fourth infectious group becomes the most significant for transmission [22]. The authors conclude that the differences of internal dynamics of transmission across models have implications for planning intervention strategies [22].

It is impossible to compare all of the numerous approaches to investigating disease dynamics found in the literature. However, exploring these examples shows some commonalities. In two of these examples [8] and [22]), model simulations are run. These model simulations allow researches to visualize the affect of different parameters on disease spread [8], and compare simulated values against those which have explicit formulae [22]. In all three examples, disease dynamics are analyzed in relation to $\mathcal{R}_0$. However, our approach differs from the examples above because we only have one method of transmission, whereas many of the models from the literature incorporate both direct and indirect transmission. Thus, while there are similarities between the approaches, such as performing simulations and relating results to $\mathcal{R}_0$, there are differences in what tests are performed.

4.3 A *Nosema ceranae* Model

We will now explore what a *Nosema ceranae* model with indirect transmission and discrete stage structure could look like. In order to make the model in equations (2.1)-(2.5) an *N. ceranae* model, we look at previous work for inspiration. We will list these considerations as assumptions for easier reading.

D.1 The first assumption of most *N. ceranae* models states that only bees in the worker caste are affected by the disease, that is, the queen and drone castes are not affected by the disease nor do they have any influence on its spread [2, 5, 39, 40, 43].

D.2 In the context of *A. mellifera*, natural birth rate is called the eclosion rate. As in [40, 43], we assume the eclosion rate is determined by the daily maximum potential eclosion rate and a measure of the colony's brood-rearing capacity. The maximum potential eclosion rate is determined by the average number of eggs laid per day by the queen [40, 43]. The colony's brood-rearing capacity is represented by a sigmoidal function [40, 43]. Thus, low levels of worker bees can decrease the eclosion rate [40, 43].

D.3 To simplify the mathematical model, we also assume that bees emerge as adults [5, 40, 43]. As mentioned in [43], making this assumption removes the need to include differential delays in the model.

D.4 This assumption incorporates temporal polyethism into a mathematical model. Recall from our discussion in Section 1.1, temporal polyethism refers to the division of labor among worker bees corresponding to an individuals age, with the eldest bees performing foraging duties, and the middle-aged bees performing within-hive duties [50]. Temporal polyethism manifests in most *N. ceranae* models through the assumption that the worker bee population can be divided into two categories: hive and forager bees, denoted by F and H, respectively [2, 5, 39, 40, 43]. This distinction is important as worker bees are primarily infected as hive bees, yet it is foragers which are more affected by the disease [40, 43].

D.5 We assume hive bees emerge as healthy (i.e. susceptible) individuals but can become infected by ingesting spores from the environmental reservoir [10, 40, 43]. Thus we make the distinction between healthy hive bees and infected hive bees [10, 40, 43]. To incorporate stage-structure in the hive bee population, we further assume the infected hive bees can belong to one of three infectious stages categorized as low, medium, and

high levels of infection. We denote healthy hive bees with H_0, and the three levels of infected hive bees as H_1, H_2, H_3, respectively. In total there are four compartments for hive bees. We assume the progression of infected hive bees is uninfected (H_0) $\rightarrow$ low infection (H_1) $\rightarrow$ medium infection (H_2) $\rightarrow$ high infection (H_3). For nosemosis, the spore counts per bee are $\leq 500,000$ for low infection, $500,000 - 1,000,000$ for medium infection, and $\geq 1,000,000$ for high infection [18]. This mirrors model assumption A.7 from Section 2.1. Just as in model assumption A.7 from Section 2.1, we further assume assume recruitment into a higher level of infection is proportional to each class.

D.6 We assume the infection rate of hive bees moving from compartment H_0 to H_1 increases with the amount of healthy bees and with the strength of the environmental reservoir [43]. As in [43], this relationship is linear for the former, but saturates for the latter when the environmental reservoir is exceedingly large. Essentially, once there are a sufficient number of spores on the combs of the hive, increasing the number of spores does not increase the likelihood of infection [43]. However, the number of infected bees is directly proportional to the number of bees partaking in hive duties [43]. Once in the first infectious compartment, transfer of hive bees to higher levels of infection is a result of the *Nosema* spores replication inside the body, not as a result of ingesting more spores. This movement is proportional to the level of infection. We make this distinction to mirror assumption A.7 from Section 2.1.

D.7 To simplify the model, we assume in-hive acquisition is the primary source of infection. That is, we eliminate the possibility that foragers acquire disease from fields [10, 40, 43]. Effectively this means infected foragers are a result of infected hive bees becoming infected foragers. Similarly, healthy hive bees transition into healthy foragers [40, 43]. For simplicity, the ratios at which healthy and infected bees transition are equal [40, 43]. In combination with assumption D.5 this leads to an additional four compartments for forager bees: healthy foragers, F_0, infected foragers in the lowest level of infection, F_1, infected foragers in the middle level of infection, F_2, and infected foragers in the highest level of infection, F_3. Like infected hive bees, infected forager bees progress to higher levels on infection as a result of the *Nosema* spore's replication inside the body, not the ingestion of more spores. This movement is proportional to the level of infection. We include this assumption to mirror assumption A.7 from Section 2.1.

D.8 We assume the primary route of transmission of *N. ceranae* is ingestion of spores during hive cleaning. That is, we use indirect transmission as the only route of transmission.

As with the proposed model in this thesis, we introduce the environmental reservoir, E, of the disease as a measurement of the number of viable spores on hive combs [5, 40, 43]. We further assume E increases as a result of infected hive bees (not foragers) depositing spores via defecation, and decreases as a result of spores losing viability [5, 40, 43]. To mirror model assumption A.6 in Section 2.1, we assume hive bees deposit spores proportionally to their level of infection.

D.9 In the generic SIR model with stage-structure and indirect transmission, we assumed individuals in all compartments had the same natural death rate, and that only individuals in the highest level of infection experienced disease-related death. For an *N. ceranae* model we instead assume hive bees and foragers experience different death rates (see assumption A.3 in Section 2.1 for comparison). We assume the natural death rate of foragers is higher than the death rate of hive bees [10]. This stems from the idea that foragers are less protected than hive bees as a result of exposure to inclement weather, other stressors that may induce homing failure, and generally are older than hive bees [10]. We also assume the death rate increases as an individual's level of infection increases.

D.10 Since honey bee biology, population dynamics, and nosemosis disease dynamics vary across seasons, we must have time-dependent parameters with periodicity of 1 year [10, 40, 43]. We further assume all parameters are non-negative [43]. For better readability, we do not include t explicitly in model parameters in equations (4.7)-(4.14).

These assumptions result in model equations (4.7)-(4.14). The total population is written as $Z(t) = H(t) + F(t)$ where $H(t) = \sum_{i=0}^{3} H_i$ and $F(t) = \sum_{j=0}^{3} F_j$.

$$\frac{dH_0}{dt} = \beta\frac{Z^n}{\kappa + Z^n} - \sigma_0 H_0 + \eta_0\frac{F}{Z}F_0 - \mu_0 H_0 - \alpha_0 H_0\frac{E}{\lambda + E} \tag{4.7}$$

$$\frac{dH_1}{dt} = \alpha_0 H_0\frac{E}{\lambda + E} - \sigma_1 H_1 + \eta_1\frac{F}{Z}F_1 - \mu_1 H_1 - \alpha_1 H_1 \tag{4.8}$$

$$\frac{dH_2}{dt} = \alpha_1 H_1 - \sigma_2 H_2 + \eta_2\frac{F}{Z}F_2 - \mu_2 H_2 \tag{4.9}$$

$$\frac{dH_3}{dt} = \alpha_2 H_2 - \sigma_3 H_3 + \eta_3\frac{F}{Z}F_3 - \mu_3 H_3 \tag{4.10}$$

$$\frac{dF_0}{dt} = \sigma_0 H_0 - \eta_0\frac{F}{Z}F_0 - \rho_0 F_0 \tag{4.11}$$

$$\frac{dF_1}{dt} = \sigma_1 H_1 - \eta_1\frac{F}{Z}F_1 - \rho_1 F_1 - \delta_1 F_1 \tag{4.12}$$

$$\frac{dF_2}{dt} = \sigma_2 H_2 - \eta_2\frac{F}{Z}F_2 - \rho_2 F_2 - \delta_2 F_2 \tag{4.13}$$

$$\frac{dF_3}{dt} = \sigma_3 H_3 - \eta_3\frac{F}{Z}F_3 - \rho_3 F_3 \tag{4.14}$$

$$\tag{4.15}$$

$$\frac{dE}{dt} = \sum_{j=1}^{3}\omega H_j - \alpha_0 H_0\frac{E}{\lambda + E} - \gamma E \tag{4.16}$$

We will now discuss each of the parameters in equations (4.7)-(4.14). Much of our description is informed by the model in [43]. In equation (4.7) β is the maximum emergence rate of healthy hive adult bees and κ is the brood maintenance coefficient [43]. As in [43], we take the exponent n in $\frac{Z^n}{\kappa+Z^n}$, to be $n = 3$. The term $\alpha_0 H_0(E/(\lambda + E))$ in equations (4.7) and (4.8) describes the acquisition of the disease by healthy hive bees, which then move to the lowest level of infection H_1. From assumption D.6 this acquisition depends on the number of *N. ceranae* spores in the hive, with α_0 being the maximum infection rate and λ being the half-saturation constant for the environmental potential, E [43]. We consider $\alpha_i, i = 1, 2, 3$ in equations (4.8)-(4.10) to denote the transfer of infected hive bees into higher levels of infection, with α_i denoting transfer from compartment $i - 1$ into compartment i. This transfer does not depend on the environmental potential as the individuals progress to higher stages of infection as a result of the pathogen increasing inside the body. From assumption D.6 we have $\alpha_{i-1} \leq \alpha_i$, i.e. the infection rate for infected hive bees increases with one's infectious class. Similarly for equations (4.11)-(4.14) the parameters $\delta_i, i = 1, 2$ denote transfer from infectious compartment i to infectious compartment $i + 1$. As per assumption

D.7, $\delta_{i-1} \leq \delta_i$, i.e. transfer of infected forager bees to to higher infection classes increases with an individual's current level of infection. In all equations, terms with $\sigma_i, i = 0, 1, 2, 3$ denote the transition of hive bees into forager bees, also called recruitment in honey bee modelling literature [43]. Due to the stage-structure of our model, we assume recruitment decreases as infection increases, i.e. $\sigma_{i-1} \geq \sigma_i$. The parameter $\eta_i, i = 0, 1, 2, 3$ denotes the possible back reversion of forager bees into hive bees. Due to the stage-structure of our model, we assume reversion decreases as infection increases, i.e. $\eta_{i-1} \geq \eta_i$. The parameters $\mu_i, i = 0, 1, 2, 3$ and $\rho_i, i = 0, 1, 2, 3$ denote the death rate of hive and forager bees, respectively. As per assumption D.9 we have $\mu \leq \rho$ (hive bees have a lower death rate than forager bees), and $\mu_{i-1} \leq \mu_i$, $\rho_{i-1} \leq \rho_i$ (death increases as infection increases for both hive and forager bees). Finally for equation (4.15) we have two parameters left to define. First, $\omega_j, j = 1, 2, 3$ which denotes the spore deposition rate of hive bees. As per model assumption D.8, $\omega_{i-1} \leq \omega_i$, i.e. spore deposition is proportional to one's infection class. Second, we have γ, which denotes the spore's loss in viability. For ease of reference this information is summarized in Table 4.1.

We can use the dynamics of the generic stage structured model with indirect transmission to conjecture disease management strategies for nosemosis. In the generic model, increasing γ and decreasing $\alpha_{1,2,3}$ corresponded to a decrease in E. To increase γ, one would need to remove spores from the hive. This could be achieved by disinfecting hive combs/equipment with acetic vapors, and/or removing hive frames laden with spores from hives altogether. To decrease $\alpha_{1,2,3}$, one would use the antibiotic Fumidil B. Applying Fumidil B would also likely decrease infection rates, leading to a decrease in $\delta_{1,2}$. In a *Nosema* context, a decrease in $\delta_{1,2}$ indicates bees are infected at a later stage of development. Similar treatment strategies have been found in *Nosema* modelling literature [2, 5].

Table 4.1: A summary of model parameters used in equations (4.7)-(4.15)

Symbol	Name/Interpretation
β	Maximum eclosion rate
κ	Brood maintenance coefficient
λ	Half-saturation constant
σ_i	Recruitment of hive to forager bee
η_i	Reversion from forager to hive bee
μ_i	Death rate of hive bees
ρ_i	Death rate of forager bees
δ_i	Transfer of infectious forager bees
α_i	Transfer of infectious hive bees
ω_i	Spore deposition rate
γ	Spore decay

4.4 Limitations

We will now conclude with discussing the limitations of our work. The main limitations in Chapter 1 come from the literature review in Section 1.3. Recall in Section 1.2 we explored the various meanings of the term "stage-structure" found in various epidemiological models. In many models exploring disease in an ecological system, stage structure referred to the compartmentalization of individuals based on what stage of the life cycle an individual was in, also known as age-structure or age of infection. However, in HIV/AIDS modelling, stage-structure is referred to as staged-progression, and indicates the compartmentalization of individuals based on their infectious stage, and follows the same framework as our research. Thus, with a lack of standardized nomenclature for this type of modelling framework, it is possible that the key words used in our search queries did not encapsulate all relevant research. Related to this, we screened for models which only used discrete stage-structure and indirect transmission, this excludes models with continuous stage-structure and indirect transmission. The continuous counterpart may have some results which overlap with the discrete case. However, a discrete structure more readily lends itself to use in a public health setting, as clearly defined groups are much easier to account for rather than fluent continuous situations without clear boundaries. Additionally, in Section 1.3 we outlined the numerous journals that had limited to no access for search results. With many of the abstracts giving

insufficient detail on model structure, papers from these journals were unable to go through the full screening process. Thus, there may be some papers which were eliminated from the results (due to lack of PDF access) that were relevant to this research. Lastly, the literature review served as a way to gain a big picture understanding of what is known about the model structure proposed in this thesis. As a result, articles were not subjected to a full text PDF review the way they would be in a technically correct/full scoping review. Thus, there may be other results or methodologies outside of those which were deemed standard which could have aided in the analysis of our model.

In Chapter 2, the main limitations surround the model derivation and techniques used to investigate DFE stability. For the former, we do not point out limitations per se, but rather alternative arguments that could have been used in model formulation. In our first assumption, we assumed infected individuals had to progress through the three stages of infection in order (see assumption A.1). That is, individuals followed the pathway $I_0 \to I_1 \to I_2 \to I_3$. One could instead assume that the compartment to which a susceptible individual transfers depends on the amount of pathogen they come into contact with in the environment, with increased exposure corresponding to transfer into a higher level of infection. This would result in the pathways $I_0 \to I_1$, $I_0 \to I_2$, $I_0 \to I_3$, and $I_0 \to I_2 \to I_3$ in addition to $I_0 \to I_1 \to I_2 \to I_3$. For simplicity, we treated all parameters were constants. In particular, a constant birth rate does not accurately reflect real-world populations, thus a logistic birth rate could be used instead. Similarly, we assumed all compartments had the same natural death rate, and disease-related death only occurred in the highest level of infection (see assumptions A.3 and A.7). One could instead assume that each sub-population has a different death rate, with an increase in infection level corresponding to an increase in the death rate. As it relates to stage-structure, we assumed spore uptake only plays a role in moving a susceptible individual into the first compartment (see assumption A.7). This assumption was a consequence of the motivation material, *Nosema ceranae*. However, this may not be true for other diseases. Hence, an alternative assumption could be that both pathogen uptake and the pathogen's germination inside the body affect movement into higher infectious compartments. We also assume that individuals are removed from the population only by death (see assumption A.3). Thus, we do not investigate the affects of temporary immunity or vaccination on the spread of indirectly transmitted disease. For the stability of the DFE, we were only able to derive a sufficient condition using Gershgorin's theorem. Given more time, one could try using a Lyapunov function to prove the stability of the DFE. One could also try to derive a necessary and sufficient condition analytically for

DFE stability through use of the eigenvalues of the Jacobian Matrix evaluated at the DFE.

One limitation common to all sections of Chapter 3 (except for Section 3.6) is that only one set of parameter ranges was used. Thus, while our results make intuitive sense in the context of disease modelling, it would be interesting to see if the same results are obtained across different parameter sets. Additionally, in defining our approximation for the time taken to reach steady state, `SStime`, we used a very tight criterion. It is possible that such a tight criterion causes the calculated `SStime` values to be higher than necessary for practical purposes. Given more time, one could investigate if the relationship between $\mathcal{R}_0$ and time taken to reach steady state remains for a less strict criterion of `SStime`.

Chapter 5

Conclusions And Further Work

From our discussion in Chapter 4 we draw our final conclusions and outline topics for future work.

5.1 Conclusions

This thesis has shown there is very little knowledge surrounding SIR models with discrete stage structure and indirect transmission. Many models in the literature consider just stage structure or indirect transmission but not the combination of these affects. Also, many models include indirect transmission as a secondary route of transmission, and thus cannot make direct conclusions about the impact of this transmission route on disease spread. Our research found that for a general disease model incorporating discrete stage structure and indirect transmission, standard results concerning the basic reproduction number hold. Additionally, we found that when disease persists, the population is mostly comprised of individuals at the lowest level of infection. This phenomenon has been observed in other viral diseases. Most importantly, we saw that the basic reproduction number plays an important role in describing/characterizing the fate of a disease in a population.

Another takeaway from this research is that it is possible to close knowledge gaps in mathematical model analysis through extensive computational work. Such computational work can lead to conjectures surrounding model behaviour. However, one must be aware that simulation results are impacted by choices of model parameters.

5.2 Future Work

The most important topic for future work involves the analysis of the proposed *Nosema ceranae* model. Thus far, most *Nosema* models have not incorporated stage-structure. In this research, stage-structure refers to incorporating multiple infectious compartments in a model, which individuals progress through as a result of the proliferation of a pathogen inside the body. We posit that this assumption could be important for modelling *N. ceranae* since much variation has been observed in spore counts across individual bees, colonies, and apiaries [5]. Incorporating this structure could provide insight on if variations in spore counts across individual bees has an impact on *N. ceranae* spread throughout the colony. When accounting for the biological processes of the model in addition to discrete stage structure, the result is a far more complicated model. As a consequence of this, analysis of the proposed model would rely heavily on numerical simulations.

Another point of interest surrounds the model structure of the general SIR model with indirect transmission and discrete stage-structure. Many of our assumptions surrounding model parameters would not accurately reflect their real-world counter part(s). Additionally, we only considered three infectious compartments which individuals progress through sequentially. One topic for future work could be to extend this model to n infectious compartments with more realistic assumptions concerning model parameters and/or movement across compartments. In doing this, one could try to examine whether the disease dynamics observed in the simplest set up hold for a more complicated, realistic set up. Most notably, we do not consider the affects of immunity (temporary or permanent) on indirectly transmitted diseases. If one incorporated vaccination in this model (with a fixed number of compartments or otherwise), it could provide insight as to what degree vaccination reduces disease spread for indirect transmission. This would be very interesting to compare such against results for models using direct transmission and stage-structure to highlight the differences between these transmission pathways. Understanding these differences could allow us to speculate on what treatment strategies are most effective for containing disease. Analysis of such a model or model(s) however, would involve extensive computational work.

We used computational analysis to gain a deeper understanding of our model. As a result, there is a conjecture that lacks rigorous mathematical proof. This conjecture states that for all model solutions which do not attain a disease-free equilibrium, the inequality $I_1(t) > I_2(t) > I_3(t)$ hold. That is, the number of infectious individuals at the lowest level of infection is greater than that middle of the middle level of infection, which is in turn greater

than the highest level of infection. Mathematical proofs of this conjecture would confirm the validity of these results across all possible values of model parameters.

Bibliography

[1] N. Babakordi and Hamid R. Z. Zangeneh. Multiple bifurcations analysis in a delayed predator–prey system with disease in prey and stage structure for predator. *International journal of dynamics and control*, 8(2):370–385, 2020.

[2] Matt I. Betti, Lindi M. Wahl, and Mair Zamir. Effects of infection on honey bee population dynamics: A model. *PLOS ONE*, 9(10):1–12, 10 2014.

[3] Fred Brauer, Pauline Driessche, and Jianhong Wu. *Compartmental Models in Epidemiology*, page 19–79. Springer Berlin Heidelberg, 2008.

[4] Jun Chen, Gloria DeGrandi-Hoffman, Vardayani Ratti, and Yun Kang. Review on mathematical modeling of honeybee population dynamics. *Mathematical Biosciences and Engineering*, 18(6):9606–9650, 2021.

[5] J. Reilly Comper and Hermann J. Eberl. Mathematical modelling of population and food storage dynamics in a honey bee colony infected with *Nosema ceranae*. *Heliyon*, 6(8):e04599, 2020.

[6] Canadian Honey Council. Bee facts, 2018. Accessed: 07.19.2021).

[7] National Research Council. *Status of Pollinators in North America*. The National Academies Press, Washington, DC, 2007.

[8] Ezekiel Dangbé, Damakoa Irépran, Antoine Perasso, and David Békollé. Mathematical modelling and numerical simulations of the influence of hygiene and seasons on the spread of cholera. *Mathematical biosciences*, 296:60–70, 2018.

[9] Hermann J. Eberl. Math*6020 scientific computing lecture notes, 2021.

[10] Hermann J. Eberl and Nasim Muhammad. Mathematical modelling of between hive transmission of nosemosis by drifting. *Communications in nonlinear science & numerical simulation*, 114:106636–, 2022.

[11] B. Emsen, Ernesto Guzman, Mollah Hamiduzzaman, Les Eccles, Brian Lacey, Rosario Ruiz-Pérez, and Medhat Nasr. Higher prevalence and levels of *Nosema ceranae* than nosema apis infections in canadian honey bee colonies. *Parasitology research*, 115:175–181, 09 2015.

[12] Berna Emsen, Alvaro De la Mora, Brian Lacey, Les Eccles, Paul G. Kelly, Carlos A. Medina-Flores, Tatiana Petukhova, Nuria Morfin, and Ernesto Guzman-Novoa. Seasonality of *Nosema ceranae* infections and their relationship with honey bee populations, food stores, and survivorship in a north american region. *Veterinary Sciences*, 7(3), 2020.

[13] Centers for Disease Control and Prevention (CDC). Lesson 1: Introduction to epidemiology, 2012.

[14] Mugabi Francis, Joseph Mugisha, Betty Nannyonga, Henry Kasumba, and Margaret Tusiime. Parameter-dependent transmission dynamics and optimal control of foot and mouth disease in a contaminated environment. *Journal of the Egyptian Mathematical Society*, 27, 12 2019.

[15] Mike Goblirsch. *Nosema ceranae* disease of the honey bee (*Apis mellifera*). *Apidologie*, 49(1):131–150, 2018.

[16] Hongbin Guo and Michael Y. Li. Global dynamics of a staged-progression model with amelioration for infectious diseases. *Journal of biological dynamics*, 2(2):154–168, 2008.

[17] Hongbin Guo and Michael Yi Li. Global dynamics of a staged progression model for infectious diseases. *Mathematical Biosciences and Engineering*, 3(3):513–525, 2006.

[18] Ernesto Guzman. Interview. Personal Communication, July 2021. Interview performed by Abby Anderson and Hermann J Eberl.

[19] Vita Bee Health. Fumagilin-b: Nosema prevention and treatment, 2023.

[20] Jane Heffernan, R.J. Smith, and L.M. Wahl. Perspectives on the basic reproductive ratio. *Journal of the Royal Society, Interface / the Royal Society*, 2:281–93, 10 2005.

[21] Terry P. Hughes, Cristina Linares, Vasilis Dakos, Ingrid A. van de Leemput, and Egbert H. van Nes. Living dangerously on borrowed time during slow, unrecognized regime shifts. *Trends in Ecology & Evolution*, 28(3):149–155, 2013.

[22] James Hyman, Jia Li, and E. Stanley. The differential infectivity and staged progression models for the transmission of hiv. *Mathematical Biosciences*, 11 2013.

[23] Veritas Health Innovation. Covidence systematic review software.

[24] Sarafa A. Iyaniwura, Musa Rabiu, Jummy F. David, and Jude D. Kong. Assessing the impact of adherence to non-pharmaceutical interventions and indirect transmission on the dynamics of covid-19: a mathematical modelling study. *Mathematical Biosciences and Engineering*, 18(6):8905–8932, 2021.

[25] Katelin C. Jackson, Christopher T. Short, Kellan R. Toman, Matthew S. Mietchen, Eric Lofgren, and for the CDC MInD-Healthcare Program. Transient dynamics of infection transmission in a simulated intensive care unit. *PLOS ONE*, 17(2):1–14, 02 2022.

[26] Jianwen Jia and Bo Wu. The study of a class of pest control pollution model with stage-structure and time delay. *ISRN applied mathematics*, 2012:1–14, 2012.

[27] Paul Kelly. Fumigating with acetic acid to decontaminate brood chambers, 2023.

[28] Peter G. Kevan, Emesto Guzman, Alison Skinner, and Dennis van Englesdorp. Colony collapse disorder in canada: Do we have a problem? *HiveLights*, 5 2007.

[29] Shane S. Klassen, William VanBlyderveen, Les Eccles, Paul G. Kelly, Daniel Borges, Paul H. Goodwin, Tatiana Petukhova, Qiang Wang, and Ernesto Guzman-Novoa. *Nosema ceranae* infections in honey bees (*Apis mellifera*) treated with pre/probiotics and impacts on colonies in the field. *Veterinary Sciences*, 8(6), 2021.

[30] Andrei Korobeinikov. Global properties of sir and seir epidemic models with multiple parallel infectious stages. *Bulletin of Mathematical Biology*, 71:75–83, 2009.

[31] Glenn Lahodny, Raju Gautam, and Renata Ivanek. Understanding the effects of intermittent shedding on the transmission of infectious diseases: example of salmonellosis in pigs. *Journal of Biological Dynamics*, 11:436–460, 12 2017.

[32] Jianquan Li, Zhien Ma, and Fengqin Zhang. Stability analysis for an epidemic model with stage structure. *Nonlinear Analysis: Real World Applications*, 9:1672–1679, 09 2008.

[33] Ming-Tao Li, Gui-Quan Sun, Juan Zhang, and Zhen Jin. Global dynamic behavior of a multigroup cholera model with indirect transmission. *Discrete Dynamics in Nature and Society*, 2013:1–11, 01 2013.

[34] Suli Liu and Michael Y. Li. Epidemic models with discrete state structures. *Physica D: Nonlinear Phenomena*, 422:132903, 2021.

[35] M.A Masud, Md. Hamidul Islam, and Byul Nim Kim. Understanding the role of environmental transmission on covid-19 herd immunity and invasion potential. *Bulletin of mathematical biology*, 84(10):116–116, 2022.

[36] Peters MDJ, Godfrey C, McInerney P, Munn Z, Tricco AC, and H. Khalil. *JBI Manual for Evidence Synthesis: Chapter 11: Scoping Reviews*. JBI, 2020.

[37] Reza Memarbashi and Seyed Mahdi Mahmoudi. A dynamic model for the covid-19 with direct and indirect transmission pathways. *Mathematical Methods in the Applied Sciences*, 44(7):5873–5887, 2021.

[38] Quinn Morris. Analysis of a co-epidemic model. *SIAM Undergraduate Research Online*, 4:121–133, 01 2011.

[39] Nasim Muhammad and Hermann J. Eberl. A simple model of between-hive transmission of nosemosis. In *Recent Advances in Mathematical and Statistical Methods*, Springer Proceedings in Mathematics & Statistics, pages 385–395. Springer International Publishing, Cham, 2018.

[40] Nasim Muhammad and Hermann J Eberl. Two routes of transmission for nosema infections in a honeybee population model with polyethism and time-periodic parameters can lead to drastically different qualitative model behavior. *Communications in nonlinear science & numerical simulation*, 84, 2020.

[41] Government of Canada. Annual influenza reports, 2023.

[42] Government of Canada. Covid-19 epidemiology update: Current situation, 2023.

[43] Alex Petric, Ernesto Guzman-Novoa, and Hermann J. Eberl. A mathematical model for the interplay of nosema infection and forager losses in honey bee colonies. *Journal of Biological Dynamics*, 11(sup2):348–378, 2017.

[44] Arnald Puy, Samuele Lo Piano, Andrea Saltelli, and Simon A. Levin. sensobol: An R package to compute variance-based sensitivity indices. *Journal of Statistical Software*, 102(5):1–37, 2022.

[45] R Core Team. *R: A Language and Environment for Statistical Computing*. R Foundation for Statistical Computing, Vienna, Austria, 2021.

[46] Suzanne L. Robertson, Marisa C. Eisenberg, and Joseph H. Tien. Heterogeneity in multiple transmission pathways: modelling the spread of cholera and other waterborne disease in networks with a common water source. *Journal of biological dynamics*, 7(1):254–275, 2013.

[47] RStudio Team. *RStudio: Integrated Development Environment for R*. RStudio, Inc., Boston, MA, 2015.

[48] Lei Shi, Hongyong Zhao, and Daiyong Wu. Modelling and analysis of hfmd with the effects of vaccination, contaminated environments and quarantine in mainland china. *Mathematical Biosciences and Engineering*, 16(1):474–500, 2019.

[49] Ruiqing Shi, Sanyi Tang, and Wenli Feng. Two generalized predator-prey models for integrated pest management with stage structure and disease in the prey population. *Abstract and applied analysis*, 2013:1–13, 2013.

[50] Adam J. Siegel, M. Kim Fondrk, Gro Amdam, and Robert Page. In-hive patterns of temporal polyethism in strains of honey bees (*Apis mellifera*) with distinct genetic backgrounds. *Behavioral Ecology and Sociobiology*, 67(10):1623–1632, October 2013.

[51] Michael L. Smith. The honey bee parasite *Nosema ceranae*: Transmissible via food exchange? *PLOS ONE*, 7(8):1–6, 08 2012.

[52] I.M. Sobol. Sensitivity analysis for nonlinear mathematical models. *Mathematical Modeling and Computational Experiment*, 1(3):407–414, 1993.

[53] Karline Soetaert, Thomas Petzoldt, and R. Woodrow Setzer. Solving differential equations in R: Package deSolve. *Journal of Statistical Software*, 33(9):1–25, 2010.

[54] Yun Tao, Jessica L. Hite, Kevin D. Lafferty, David J.D. Earn, and Nita Bharti. Transient disease dynamics across ecological scales. *Theoretical Ecology*, 14(4):625–640, 2021.

[55] The Pennsylvania State University. Stat 501: Regression methods course notes, 2023.

[56] Pegah Valizadeh, Ernesto Guzman-Novoa, and Paul H. Goodwin. Effect of immune inducers on *Nosema ceranae* multiplication and their impact on honey bee (*Apis mellifera* l.) survivorship and behaviors. *Insects*, 11(9), 2020.

[57] P. van den Driessche and James Watmough. Reproduction numbers and sub-threshold endemic equilibria for compartmental models of disease transmission. *Mathematical Biosciences*, 180(1):29–48, 2002.

[58] Peter Verboon, Mira Duif, and Piet van Tuij. *Single Case Design Analyses*. 2022.

[59] Wolfgang Walter. *Ordinary differential equations*. Graduate texts in mathematics ; 182. Readings in mathematics. Springer, New York, 1998.

[60] Lingshu Wang and Guanghui Feng. Global stability of an eco-epidemiological predator-prey model with saturation incidence. *Journal of applied mathematics & computing*, 53(1-2):303–319, 2017.

[61] Xueying Wang, Daozhou Gao, and Jin Wang. Influence of human behavior on cholera dynamics. *Mathematical biosciences*, 267:41–52, 2015.

[62] Yi Wang and Jinde Cao. Global dynamics of multi-group sei animal disease models with indirect transmission. *Chaos, Solitons & Fractals*, 69:81–89, 2014.

[63] Curtis L. Wesley, Linda J. S. Allen, and Michel Langlais. Models for the spread and persistence of hantavirus infection in rodents with direct and indirect transmission. *Mathematical Biosciences and Engineering*, 7(1):195–211, 2010.

[64] Hadley Wickham. *Ggplot2: Elegant graphics for data analysis*. Use R! Springer International Publishing, Cham, Switzerland, 2 edition, June 2016.

[65] Ke Zhang, John Dearing, and Jason Sadler. Transient dynamics, 2013.

[66] Tongqian Zhang, Xinzhu Meng, Yi Song, and Tonghua Zhang. A stage-structured predator-prey si model with disease in the prey and impulsive effects. *Mathematical modelling and analysis*, 18(4):505–528, 2013.

[67] Haonan Zhong and Wendi Wang. Mathematical analysis for covid-19 resurgence in the contaminated environment. *Mathematical Biosciences and Engineering*, 17(6):6909–6927, 2020.

Appendix A

Figures & Tables

Table A.1: The first set of parameter values used when testing local results of Sobol sensitivity analysis of $\mathcal{R}_0$ and time to steady state. All parameters are taken from a uniform distribution.

Parameter Set 1		
Parameter	Min.	Max.
Λ	495.0	505.0
c	0.0020	0.025
μ	0.1	2.0
δ_1	0.01	0.4
δ_2	0.45	0.7
δ_3	0.75	1.0
α_1	0.01	0.1
α_2	0.15	0.4
α_3	0.45	0.7
γ	0.1	1.0

Table A.2: The second set of parameter values used when testing local results of Sobol sensitivity analysis of $\mathcal{R}_0$ and time to steady state. All parameters are taken from a uniform distribution.

Parameter Set 2		
Parameter	Min.	Max.
Λ	495.0	505.0
c	0.0020	0.025
μ	0.1	2.0
δ_1	0.01	0.4
δ_2	0.45	0.7
δ_3	0.75	1.0
α_1	0.1	1.0
α_2	1.5	4.0
α_3	4.5	7.0
γ	0.1	1.0

Table A.3: The third set of parameter values used when testing local results of Sobol sensitivity analysis of $\mathcal{R}_0$ and time to steady state. All parameters are taken from a uniform distribution.

Parameter Set 3		
Parameter	Min.	Max.
Λ	495.0	505.0
c	0.0020	0.025
μ	0.1	2.0
δ_1	0.1	4.0
δ_2	4.5	7.0
δ_3	7.5	10.0
α_1	0.1	1.0
α_2	1.5	4.0
α_3	4.5	7.0
γ	0.1	1.0

Table A.4: The fourth set of parameter values used when testing local results of Sobol sensitivity analysis of $\mathcal{R}_0$ and time to steady state. All parameters are taken from a uniform distribution.

Parameter Set 4		
Parameter	Min.	Max.
Λ	495.0	505.0
c	0.0020	0.025
μ	0.1	2.0
δ_1	0.1	4.0
δ_2	4.5	7.0
δ_3	7.5	10.0
α_1	0.1	1.0
α_2	1.5	4.0
α_3	4.5	7.0
γ	1.0	10.0

Table A.5: The fifth set of parameter values used when testing local results of Sobol sensitivity analysis of $\mathcal{R}_0$ and time to steady state. All parameters are taken from a uniform distribution.

Parameter Set 5		
Parameter	Min.	Max.
Λ	495.0	505.0
c	0.0020	0.025
μ	0.1	2.0
δ_1	0.1	4.0
δ_2	4.5	7.0
δ_3	10.0	15.0
α_1	0.1	1.0
α_2	1.5	4.0
α_3	4.5	7.0
γ	1.0	10.0

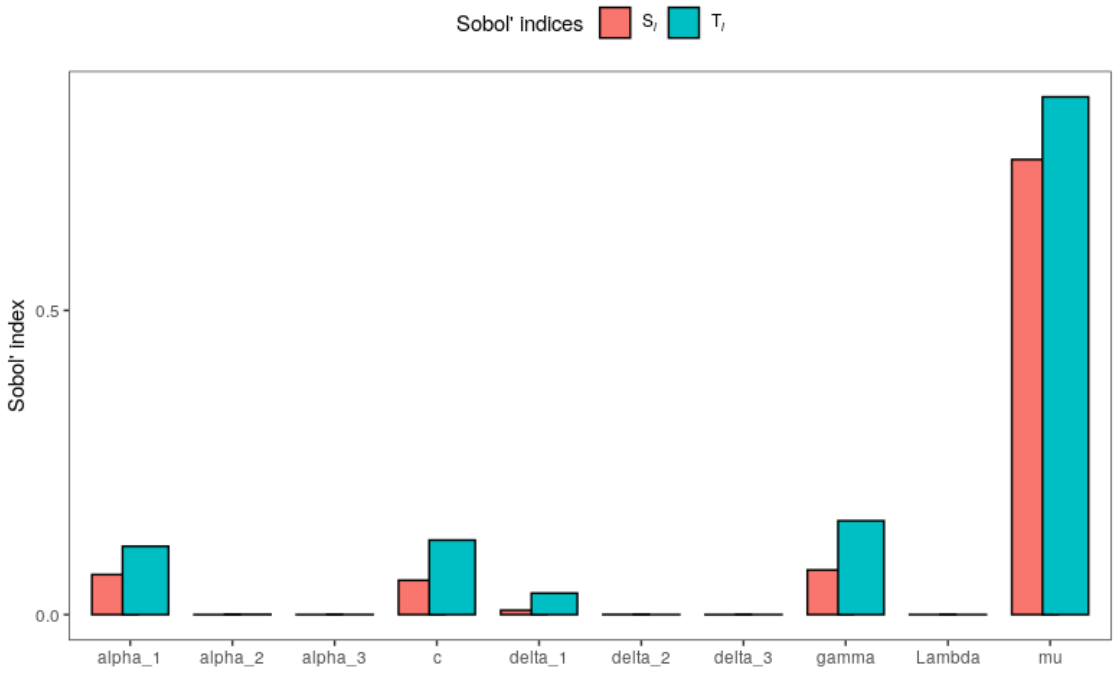

Figure A.1: A bar plot of the first order Sobol sensitivity indices S_i, and the total order Sobol sensitivity indices T_i of $\mathcal{R}_0$ for the first set of parameters.

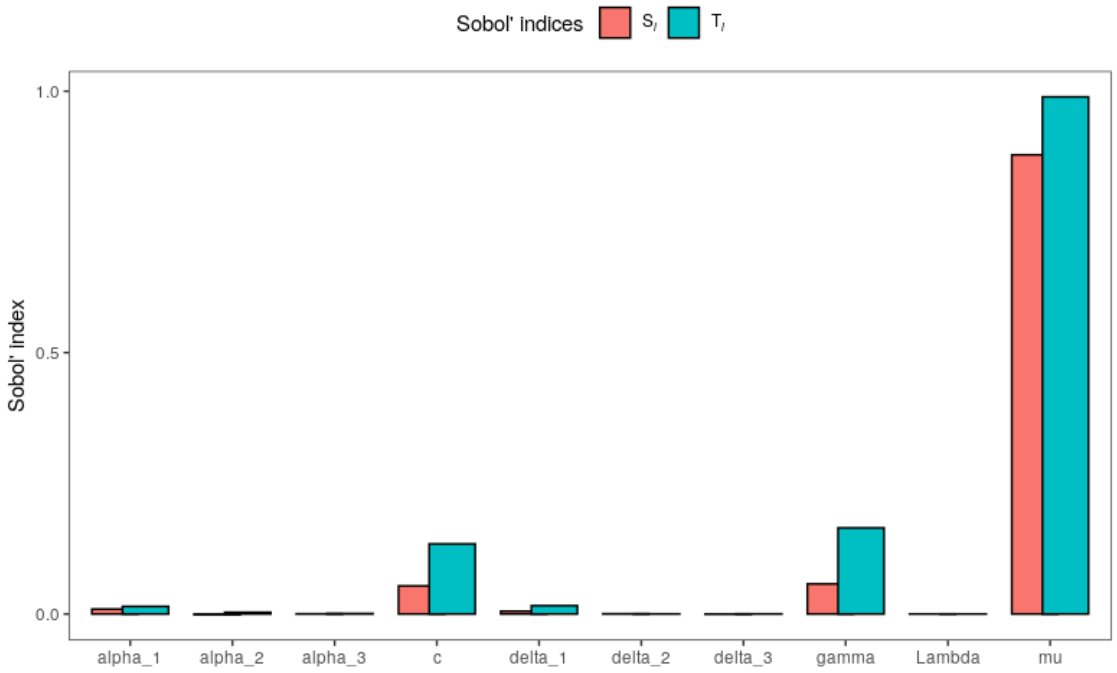

Figure A.2: A bar plot of the first order Sobol sensitivity indices S_i, and the total order Sobol sensitivity indices T_i of $\mathcal{R}_0$ for the second set of parameters.

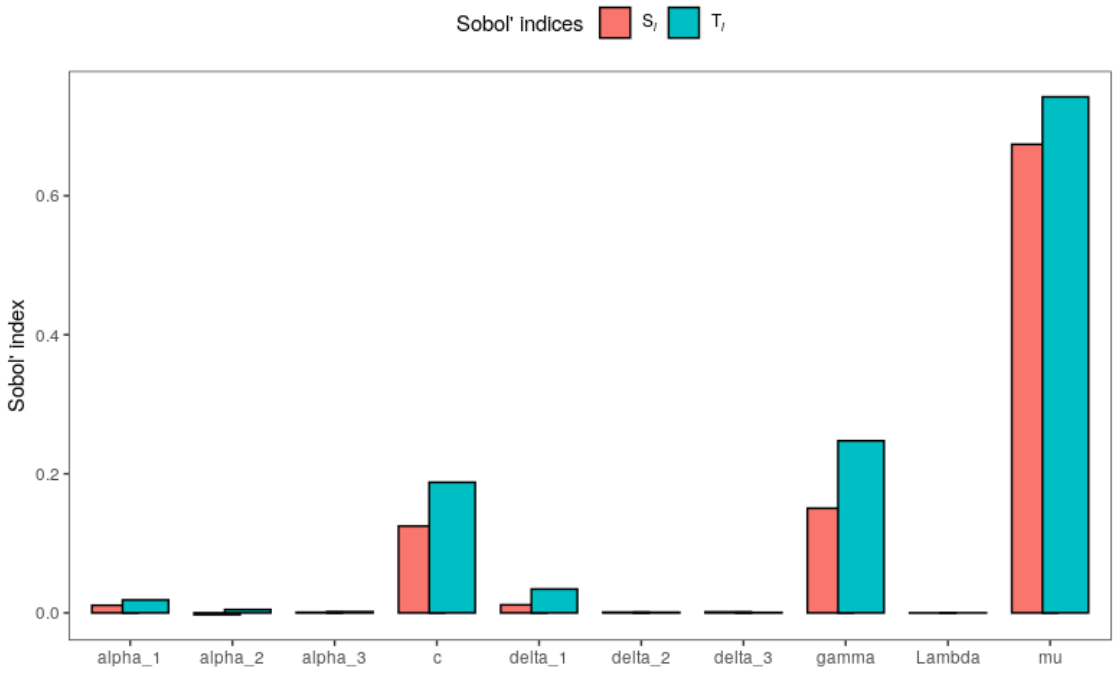

Figure A.3: A bar plot of the first order Sobol sensitivity indices S_i, and the total order Sobol sensitivity indices T_i of $\mathcal{R}_0$ for the third set of parameters.

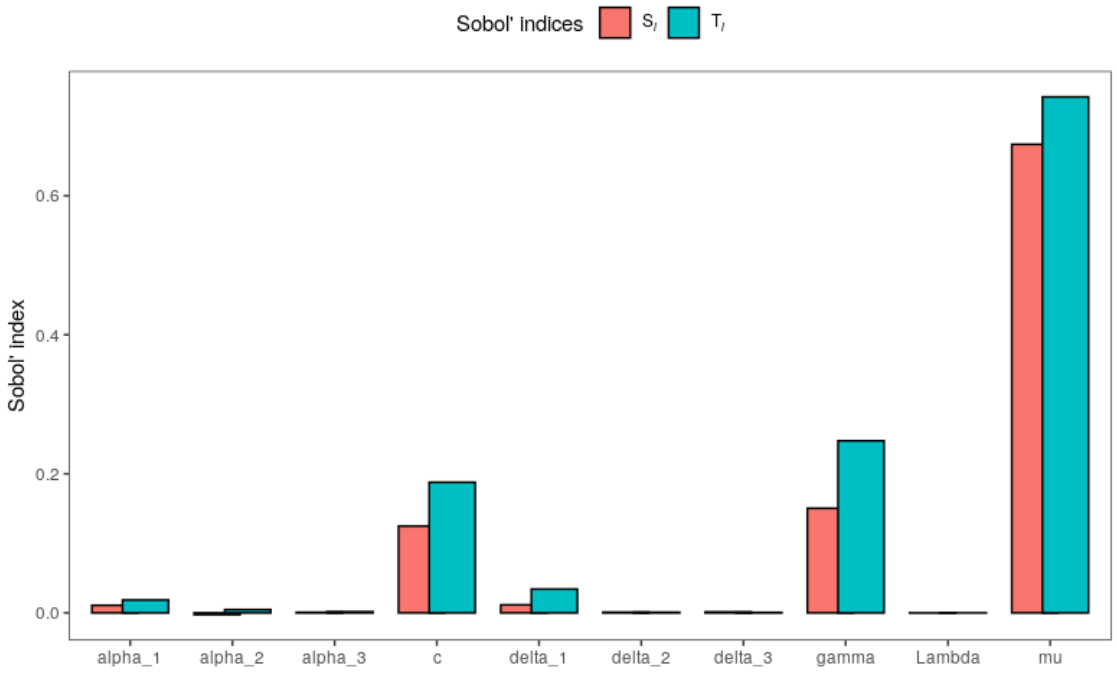

Figure A.4: A bar plot of the first order Sobol sensitivity indices S_i, and the total order Sobol sensitivity indices T_i of $\mathcal{R}_0$ for the fourth set of parameters.

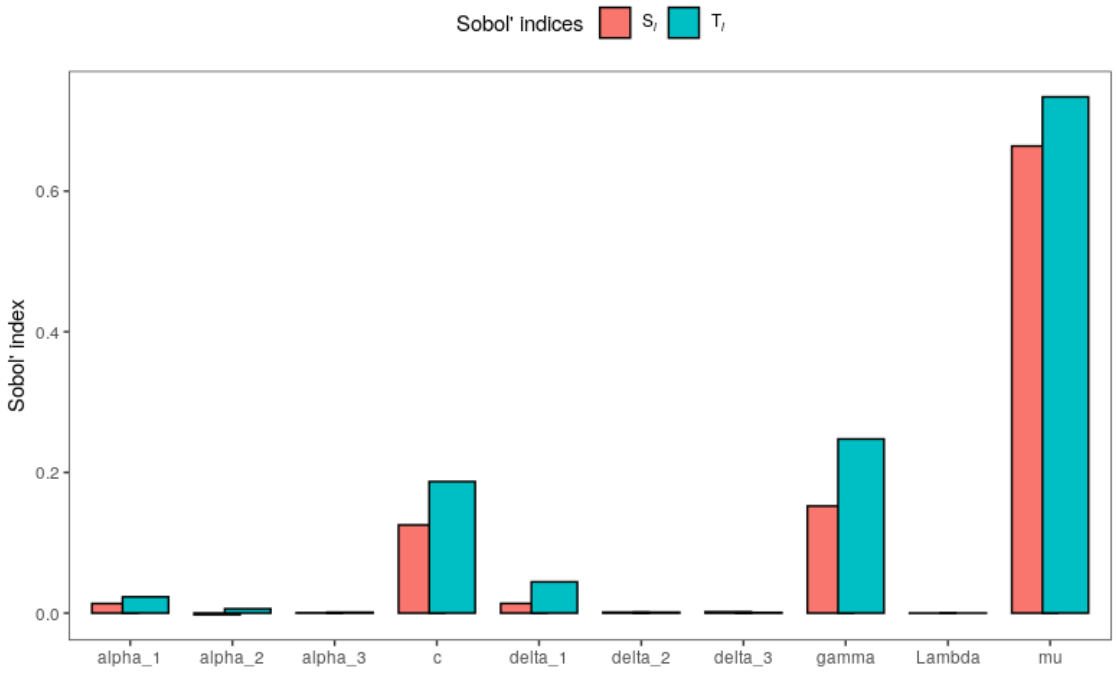

Figure A.5: A bar plot of the first order Sobol sensitivity indices S_i, and the total order Sobol sensitivity indices T_i of $\mathcal{R}_0$ for the fifth set of parameters.